



Norwegian University
of Life Sciences

Master's Thesis 2018 60 ECTS

Department of Animal and Aquaculture Sciences
Dr. Turid Mørkøre

In vivo and in vitro study of dark pigment development in Atlantic salmon using novel methods based on image analysis

Raúl Jiménez-Guerrero

Master of Science in Aquaculture
Norwegian University of Life Science (NMBU)

***IN VIVO AND IN VITRO* STUDY OF DARK PIGMENT
DEVELOPMENT IN ATLANTIC SALMON USING NOVEL
METHODS BASED ON IMAGE ANALYSIS**

Master of Science in Aquaculture

Master thesis

60 credits

By

Raúl Jiménez-Guerrero

Supervisors

Dr. Turid Mørkøre

Dr. Øystein Evensen

Dr. Koestan Gadan

Department of Animal and Aquaculture Sciences
Department of Basic Sciences and Aquatic Medicine
Norwegian University of Life Science (NMBU)
Faculty of Veterinary Medicine

Post Box 5003

1432 Ås

May 2018

ACKNOWLEDGEMENTS

Writing and languages never were my best, but sometimes you have to push forward your limits. Three years ago, I had no idea about fish, English or Norwegian. Today I write the last page of an incredible period of my life (and not in Spanish...). I wanted to write this part the last day for expressing myself as honest as possible. Every word means a lot. Every class and every practice that I had was incredible. I could never imagine how much you can learn in a few years. Sometimes is still hard to believe that I am becoming finally into a fish vet.

I feel very lucky for having Dr. Turid Mørkøre as supervisor, her blind confident and infinite patience in all my crazy ideas has been unimaginable. Without that freedom I would have never been able to build this thesis. Also thanks to my other supervisors; Dr. Øystein Evensen for giving me the possibility of learning about disciplines that I always wanted to do. Their guidance and help have been essential. I want to say thank you to Dr. Koestan Gadan for her kindness, steal-like patience and dedication. You have taught me the best. Moreover, I really felt very blessed and proud to be surrounded by incredible and supportive people as mister Dr. Thomas Larsson (the color master), Dr. Gerrit Timmerhaus, and Dr. Amr Ahmed Abdelrahim. Their unconditional help and gentleness were essential for transforming my ideas into words. Thanks Nofima for shaping all my skills during this period and giving me the possibility to work with big industry players. Thanks BioMar for giving me the possibility of working with their fish and assisting to the sampling at Dønna. It was an enriching experience to be involved in large projects like this, where many fish aspects are studied. I did also learn how much a boat can be moved by the Norwegian waves.

I also want to thank to my friends in Spain and Norway. To my entire family, you have always been there. I think I could never understand how hard can be seeing your son flying that away. Everything that I am, is and will always be because of you, specially one person:

Este año las alas que me ayudaste a construir han sido atravesadas por una lanza. Ahora que el dolor se ha calmado solo me queda una enorme cicatriz que intentaré tapar. Se que ya nunca volveré volar como antes, pero gracias a la fuerza que me has dado seguiré luchando para llegar a lo más alto, como tú tantas veces lo pedías. A mi guitarrista favorito qué decirle, ahora tendrás que tocar la guitarra sin bailaora, pero no te preocupes porque jamás tocarás solo. Todos subiremos al escenario contigo, para seguir juntos. Yo que aún no he actuado, solo espero pisar tan fuerte que allá donde estéis lo podáis escuchar, su mayor deseo.

Gracias por darme los mejores 25 años de mi vida. Este show te lo dedico a ti abuela. Te quiero.

“If you have a dream, a dream that chases you, get out there and follow it. Sacrifice dry land, and expect the unexpected. If you are a warmblood fish living on Nordic conditions, can be challenging, especially if you go counter-current. However, from struggle comes strength, and a strong fish is a healthier fish. Do it with passion, or you will never do it. Do it until your passion becomes flame, and once you are there, don't let go, and keep dreaming...”

Raúl Jiménez-Guerrero

Ås, May 2018

TABLE OF CONTENTS

ABSTRACT	I
ACKNOWLEDGEMENTS	2
1 INTRODUCTION.....	2
2 OBJECTIVES	4
3 THEORETICAL BACKGROUND	5
3.1 Fish immune system	5
3.1.1 Basic fish immunology.....	5
3.1.2 Melano-macrophages centers	7
3.1.3 SHK-1 cells	8
3.2 Melanin and melanogenesis	9
3.3 Melanogenesis regulation	12
3.3.1 Light	12
3.3.2 Stress	13
3.3.3 Diet	14
3.3.4 Others	15
3.4 Chromatophores and skin appearance	15
3.5 Fish fillet quality.....	17
3.6 Salmon topographic anatomy	17
3.7 Color theory	18
4 MATERIAL AND METHODS	22
4.1 In vivo study	22
4.1.1 Fish material and sampling	22
4.1.2 Software for image processing.....	25
4.1.3 Image processing.....	25

4.1.4	Skin measurement	28
4.1.4.1	Threshold calibration.....	28
4.1.4.2	Morphometric analysis	31
4.1.5	Muscle measurement.....	32
4.1.5.1	Anatomical study and “dark spot” characterization	32
4.1.5.2	Threshold calibration.....	32
4.1.5.3	Morphometric analysis	37
4.2	In vitro study.....	38
4.2.1	Fish material and sampling	38
4.2.2	Media preparation and cell culturing	39
4.2.3	Cell stimulation assay.....	39
4.2.4	Microscopy.....	40
4.2.5	Image analysis method	41
4.2.6	Transcriptomics	42
4.2.6.1	RNA isolation.....	42
4.2.6.2	cDNA synthesis	42
4.2.6.3	Real-time polymerase chain reaction (RT-PCR).....	43
4.3	Statistics.....	43
5	RESULTS.....	44
5.1	In vivo.....	44
5.1.1	General	44
5.1.2	Skin.....	45
5.1.3	Muscle	50
5.2	In vitro	58
5.2.1	Microscopy.....	58
5.2.2	Image analysis	59
5.2.3	RT-PCR.....	60

6	DISCUSSION	62
7	CONCLUSION	71
8	REFERENCES	72
9	APPENDICES	90
9.1	Appendix A	90
9.2	Appendix B.....	91
9.3	Appendix C.....	92
9.4	Appendix D	93

ABSTRACT

The appearance of skin and fillet muscle of Atlantic salmon, are the most important quality parameters for consumers. Salmon skin with pearl-shiny, bluish appearance is associated with high quality and freshness while a greener appearance is associated with high sexual maturation signs, which is normally linked to poorer fillet muscle quality. Regarding fillet muscle, consumers consider any dark discoloration with lower quality. Dark pigments are associated with deposition of melanin pigments. The melanin biosynthesis pathway has strong similarities at these two levels on salmon. Melanisation of the skin and skeletal muscle, and *in vitro* through SHK-1 cells, has not been studied simultaneously. The main goal was to study dark pigment development in salmon obtained from feeding trials at three different levels; skin, skeletal muscle and *in vitro* cell culture using SHK-1 cells. The fish were fed either a standard diet or diets added Antarctic krill meal. New objective methods based on image analysis were developed to study skin appearance and dark discoloration of fillets. Additionally, SHK-I cells were conditioned for producing dark pigments *in vitro*, using plasma as growth medium, obtained from post-smolts salmon fed with zero, low or high krill inclusion level.

Results from the image analysis showed that salmon fed low krill meal diet had darker and bluer appearance, while high krill meal resulted in a darker and greener appearance compared with salmon fed the standard diet. The fillets had high prevalence of dark discoloration, but the hyperpigmented areas were generally small in all groups. The inclusion of krill meal had no significant effects on the dark discoloration severity, but the low krill inclusion showed discoloration towards red type. A positive correlation was found between the general b^* value of salmon skin, and the b^* value of the cranio-hypaxial muscle, which suggested a relationship between carotenoids levels in both structures. Additionally, as was hypothesized, a positive correlation between the dark pigmentation of skeletal muscle and skin melanin was found. No significant differences were seen at *in vitro* level in the relative expression of the tyrosinase relate family enzymes under different plasma conditioning from salmon fed graded krill meal levels.

Keywords: *Atlantic salmon, fish quality, skin, muscle, plasma, SHK-1, melanogenesis, melanin, dark spots, method, image analysis, in vivo, in vitro, krill.*

1 INTRODUCTION

Aquaculture is the fastest growing food-producing sector in the world with a growth rate of 4.6% in real value terms. In 2014, the 44.1% of the seafood (excluding aquatic plants) came from the aquaculture industry (although this production is not equally distributed around the world). When it comes to marine fish species, Norway is the largest producer of marine fish species (FAO, 2016). According to the Norwegian Seafood Council, Norway exported 2.6 million tonnes of seafood products with a record value of NOK 94.500 million (USD 11.700 million) in 2017, that tuned the seafood sector in the second largest national industry. 1 million tonnes of this products came from aquaculture with an estimated 72% of the total value. The Atlantic salmon (*Salmo salar* L.) is the dominant farmed species in Norway with 68% of the entire national seafood sector value representing just 38% of the volume. Salmon aquaculture contributes significantly to the development of the national economy, giving job opportunities in rural areas, and offering healthy and quality food resource accessible for the consumers (Børresen, 2008; FAO, 2016).

Salmon farming is a profitable business, although some issues reduce its economic yield as fish mortality, diseases, and poor quality of fillets (Browne & Deegan, 2005; Menzies et al., 1996; Rodger et al., 2005). When it comes to fish quality, the external appearance of the skin (color, the presence of ulcers), and the color of the fillet muscle are the most important parameters for consumers (Anderson, 2001; Giese, 1995; Koteng, 1992). On-growing salmon skin normally has a clean dark blue appearance on the dorsal side of the lateral line and a pearled white appearance on the ventral side. The muscle fillets should have a. When the skin of farmed salmon gets a paler skin color, the difference between the wild and the farmed phenotype increases, and the consumer may lose interest. Skin darkness may be an external stress indicator since it is closely connected to the hypothalamic, pituitary, adrenal axis (Khan et al., 2016; Kittilsen et al., 2009; Smith et al., 2003), but some authors can not describe this relationship (Gesto et al., 2017). Moreover, a greener appearance shows sexual maturation signs which are normally linked to poorer fillet muscle quality. Regarding fillet muscle, besides from sufficient deep orange color between sections and homogeneity, consumers associate to lower quality any dark discoloration of fillets as “dark hyper-pigmented black or red spots”, which are principally represented by pigment-producing granulomatous myopathy (Berg et al., 2012; Koppang et al., 2005; Larsen et al., 2012). Fillets with dark

spots get downgraded from superior or premium quality, and those with large “dark spots” need trimming. If the size of the “dark spot” compromises large fillet areas, they are sent to portion cutting as they cannot be sold as a whole. A recent report suggests that the prevalence of dark spots is ~19% of fillets (Mørkøre et al., 2015). Moreover, the downgrading affects 66.6% of fillets, with a minimum economic loss of 8% that could increase up to 44% the bigger is the size of the discoloration (Färber, 2017). Despite the different embryological origin of cutaneous and the extracutaneous melanin-producing cells, their melanin biosynthesis pathway has strong similarities on salmon. Proved by the isolation and up-regulation of tyrosinase gene family enzymes in dark spots, which were previously described in melanocytes melanogenesis (Arciuli et al., 2012; Haugarvoll et al., 2006; Kelsh et al., 2000; Larsen et al., 2012; Sichel et al., 1997; Slominski et al., 2004; Thorsen et al., 2006). The melanization at the skin and skeletal muscle levels, and *in vitro* through salmon head kidney (SHK-1) cells, has not been studied simultaneously. However, their independent study is well documented, regarding the differences in the expression of the main melanogenesis related enzymes or receptors (Khan et al., 2016; Larsen et al., 2012; Larsen et al., 2013). There is no an objective method for quantifying “dark spots” in salmon fillets, but they may be subjectively evaluated according to a scale from 0 to 8 relate to size and the spatial position in the fillet (Mørkøre, 2012). Other methods as the Computerized Tomography (CT), the Nuclear Magnetic Resonance (NMR) (Rye, 1991; Veliyulin et al., 2005), and the Near-Infra-Red (NIR) spectrophotometry (Isaksson et al., 1995; Wold et al., 1996), offer non-invasive imaging solutions for determination of the gross chemical composition. Another objective solution to this issue would be the use of computer vision for the detection of “dark spots” in salmon fillets simply or combined with hyperspectral imaging (Heia et al., 2009; Mathiassen & Misimi, 2007). In the case of fish skin, it has been described simple visual methods to quantify melanin-based dots per cm² in salmonids (Gesto et al., 2017; Kittilsen et al., 2009). Other methods measure general colorimetric values over specific skin areas (Erikson & Misimi, 2008; Pavlidis et al., 2006) or bigger skin extensions (Marie-Orleach et al., 2014; Saberioon et al., 2018) and segmented color areas (Wedekind et al., 2008). In human medicine, there are methods for analysing morphology, and color of pigmented skin lesions by simple and advanced image processing combined with segmentation techniques (Green et al., 1991; Jain et al., 2015; Mishra & Emre Celebi, 2016).

2 OBJECTIVES

The main goal was to study dark pigment development in salmon obtained from feeding trials at three different levels; skin, skeletal muscle and *in vitro* cell culture using SHK-1 cells. The fish were fed either a standard diet or diets added Antarctic krill meal. New objective methods based on image analysis were developed to study skin appearance and dark discoloration of fillets. Additionally, SHK-I cells were conditioned for producing dark pigments *in vitro*, using plasma as growth medium, obtained from post-smolts salmons fed with zero, low or high krill inclusion level.

3 THEORETICAL BACKGROUND

3.1 Fish immune system

3.1.1 Basic fish immunology

The fish immune system protects organisms from infections or intoxications using several defense levels. In fish, the simplest ones are physical barriers (intestine, scale, skin mucus and gills), which avoid the agent penetration in the organic system (Ellis, 2001; Ingram, 1980; Magnadottir, 2010; Shephard, 1994). Physical barriers and innate immune system offer a preliminary and nonspecific response. They have been considered an essential component in combating pathogens in fish due to limitations of the adaptive immune system with a restricted repertoire of antibodies and the slow proliferation, maturation and memory of their lymphocytes, plus their poikilothermic nature (Alexander & Ingram, 1992; Ellis, 2001; Magnadottir, 2006; Pasquier, 1982; Whyte, 2007).

The innate humoral and cellular response of teleost's, as well higher vertebrates requires a series of mechanisms that comprise cells, principally macrophages, natural killer cells and neutrophils, complement (Harrell et al., 1976; Nonaka et al., 1981), and humoral factors. These may be cellular receptors or molecules as antimicrobial peptides (Hancock & Lehrer, 1998; Jia et al., 2000), lysozymes (Fänge et al., 1976; Fletcher & White, 1976), cytokines as interferons (de Kinkelin & Dorson, 1973), proteolytic enzymes (Hjelmeland et al., 1983), and natural IgM and IgT-type antibodies, that are soluble in plasma and other body fluids (Boes, 2000; Hansen et al., 2005; Magnadottir, 2006; Pasquier, 1982). Natural antibodies can be found in the skin (Hatten et al., 2001), intestine (Rombout et al., 1986), gill mucus (Lumsden et al., 1993), bile (Jenkins et al., 1994), and systemically in plasma (Chantanachookhin et al., 1991; Magnadottir et al., 2005). Natural antibodies are produced in the absence of antigenic stimulation by cells equivalent to B1 type (Boes, 2000).

The acquired response of fish acts by a complex network of proteins and biochemical messages that provide the means to respond specifically to antigens, immunoglobulins, and cells as B and T lymphocytes with high specificity and affinity (Arkoosh & Kaattari, 1991; Whittington et al., 1994). In contrast to higher vertebrates, just three major types of monomer and tetramer form immunoglobulins that are produced in teleost fish: IgM, IgD and IgT/IgZ (unique in teleost's) (Acton et al., 1971; Danilova et al., 2005; Hansen et al., 2005; Hikima et al., 2011; Wilson & Warr, 1992).

While the largest systemic molecule is IgM in salmonids, IgT is mainly located at mucosal level, which supports the local immune response. However, blood monomers of IgT have been observed in salmonids (Hordvik, 2015; Tadiso et al., 2011; Zhang et al., 2010).

One of the most important processes of the immune system in poikilothermic animals as fish is phagocytosis because it is least influenced by temperature compared to other immune tools (Blazer, 1991; Lange & Magnadóttir, 2003; Magnadóttir et al., 2005; Magnadóttir, 2006). Phagocytosing cells are not always effectively eliminating infectious agents, although, they play a crucial role in the initiation and subsequent direction of the adaptative system. In fish, neutrophils and macrophages are the main cells involved in phagocytosis. These cells can eliminate microorganisms by the production of reactive oxygen species, nitric oxide or other antibacterial agents as peroxy-nitrites, hydroxyl groups (Secombes & Fletcher, 1992) and melanin (Ellis & Sousa, 1974; Zuasti et al., 1989; Zuasti et al., 1990).

Commonly among vertebrates, dendritic cells, macrophages, and neutrophils have membrane receptors specialized in the binding with generic pathogen molecules, that activate phagocytic activity and the production and secretion of inflammatory mediators as cytokines or other substances that modulate the behavior of other cells (Janeway et al., 1999; Uribe et al., 2011). Some of this inflammation effects are heat, pain, redness, and swelling, principally as result of vasodilatation and increase of vascular permeability that increases the amount of extracellular protein and liquids as the migration of similar or different inflammatory cells. This process continues in self-limiting control, where it uses to start with neutrophils, followed by macrophages (if they are not tissue-static) which are the principal inflammatory cells, and finally lymphocytes (Janeway et al., 1999; Uribe et al., 2011). In contrast to phagocytes, instead of several different generic membrane receptors, lymphocytes carry specific antigen receptors. After a pathogen is phagocytosed or specific antigens bound by B cell surface receptors, their antigens can be carried and presented over their membranes. Thus, those antigen presenting cells (phagocytes, and B cells but just during adaptatively response) interact with lymphocytes T, and those with lymphocytes B, being parallelly necessary both cells and antigens for the stimulation in lymphoid tissues (Janeway et al., 1999; Uribe et al., 2011).

T cells are specialized to recognize peptide fragments derived from foreign antigens bound to proteins of the major histocompatibility complex (MHC) (Janeway et al., 1999). There are two kinds of MHCs, MHC class I and class II. While class I carry peptides come from endogenous or exogenous (viral) proteins synthesized in the cytosol and recognized by T cytotoxic lymphocytes (Tc), class II binds peptides derived from extracellular antigens integrated by phagocytosis (Janeway et al., 1999).

3.1.2 Melano-macrophages centers

The kidney in teleost fish is the largest site of hematopoiesis, being the equivalent to bone marrow in vertebrates (Zapata et al., 2006). The main cells found in the anterior kidney are macrophages aggregated into structures called melano-macrophage centers (MMCs), and lymphoid cells, which exist mostly as B cells. MMCs can also be found in the spleen, immersed in a reticuloendothelial matrix with thick-walled capillaries that open in the pulp, and its lymphoid tissue (Agius & Roberts, 2003; Ferguson, 1989). Macrophages located along the walls phagocyte and keep antigens, playing an important role in the immunological memory (dos Santos et al., 2000; Uribe et al., 2011). Adventitious MMCs may also develop within maturing chronic inflammatory lesions (Roberts, 1975), as pigment-producing granulomatous myopathies or “dark spots” with MHCs class II positive melano-macrophages cells (Agius, 1985; Larsen et al., 2012; Tews & Pongratz, 1995). This is especially evident in salmonids and cartilaginous fish, being rather randomly distributed throughout the tissues in which they occur, and increasing size and number with fish growth, degeneration of the tissues or chronification of inflammation (Agius, 1979; Agius, 1981; Brown & George, 1985; Roberts, 1975; Roberts, 1976). In this case, MMCs are generally accessible in fish muscle and may be compared using imaging techniques.

Several functions have been related to MMCs. Some authors suggest that they are involved in storing of cell-derived phospholipids and iron because of phagocytosis (Agius, 1979; Agius, 1980; Agius, 1981; Agius & Agbede, 1984), recycling, detoxification and elimination of endogenous or exogenous materials, (Ellis, 1980; Ferguson, 1976; Herraez & Zapata, 1986).

Also, deposition of resistant pathogens or spores (Roberts, 1975), and immunological memory functions by processing and retention of antigens on membranes as MHCs class II or melanosomes (Agius, 1985; Ellis & Sousa, 1974; Lamers & De Haas, 1985; Marks et al., 2003; Press et al., 1996). As a result, MMCs have been suggested for monitoring of health (Wolke et al., 1985), starvation (Agius, 1981), or chemical exposition (Couillard & Hodson, 1996; Long et al., 1995; Meinelt et al., 1997).

3.1.3 SHK-1 cells

One of the most commonly used primary cell lines in fish health research is the SHK-1 (Dannevig et al., 1995; Dannevig et al., 1997; Haugarvoll et al., 2006; Thorsen et al., 2006). These cells are primarily isolated from head kidney and derived from leucocytes with some of the properties of macrophages, as phagocytosis and melanogenic activity (Dannevig et al., 1997; Haugarvoll et al., 2006). SHK-1 cells can be recognized by MAbs specific for Atlantic salmon peripheral blood leukocytes, but not by MAbs specific for polymorphonuclear leukocytes (Dannevig et al., 1997). This cell line has been previously used to get *in vitro* models for indirect quantification of melanin production through tyrosinase family genes transcription, exposing them to different viral or bacterial antigens (Larsen et al., 2013) with not much success. Recently, a research (Skår-Ulvestad, 2017) reported an increase of respiratory burst, when stimulating primarily isolated head kidney cells with well-known immune-stimulants as bacterial lipopolysaccharide (LPS) and β -glucan (Brattgjerd & Evensen, 1996; Dalmo & Seljelid, 1995; Lam et al., 1991; Paulsen et al., 2003; Salinas et al., 2004; Solem et al., 1995).

Fish plasma features as the non-specific immune system may be modified by the diet, for example, the lipid source (Michelsen, 2000). It is also shown how lipid profile of *in vivo* fish cell cultures may be modulated by using plasma as a conditioning incubation environment (Seierstad et al., 2009).

3.2 Melanin and melanogenesis

Melanin is a pigment produced by the oxidation of the amino acid tyrosine followed by polymerization (Figure 3.1). This synthesis process occurs in uvea, retina, meninges, the inner ear, the Harderian gland, and skin from normal mammals (Boissy & Hornyak, 2007). In contrast, some microorganisms and haematopoietic-derived cell lineages of lower vertebrates as fish present extracutaneous melanin production (Agius, 1980; Arciuli et al., 2012; Ellis & Sousa, 1974; Haugarvoll et al., 2006; Roberts, 1975; Thorsen et al., 2006; Zuasti et al., 1989; Zuasti et al., 1990). Melanin pigments are synthesized and placed in melanosomes, which are specific intracellular lysosome-related organelles (Orlow, 1995; Raposo et al., 2002), with a membrane containing lipids, proteins, and melanin pigment. These different fractions in melanosomes depend on the cellular origin (Liu, Yan et al., 2005; Liu, Y. et al., 2005; Ozeki et al., 1997; Ward & Simon, 2007). There are two types of cutaneous melanin; eumelanin, responsible for the dark color, and pheomelanin, with a yellow-red appearance (Ito et al., 2000). While eumelanin (also be sub-divided within black or brown), is presented in many types of living organisms from unicellular to higher vertebrates, pheomelanin has not been found in teleost fish (Burgoyne et al., 2015; Edelstein, 1971; Fujii, 1993a; Kottler et al., 2015; Turner et al., 1975).

The synthesizing process is called melanogenesis, and the produced pigment type depends on their melanogenic enzymes or substrate availability. One of these conditional enzymes is tyrosinase (Tyr) (Hearing, 1993). Mutations disturbing its functionality result in disorder called albinism. In the biosynthesis, the amino acid tyrosine is hydroxylated under the critical rate-limiting activity of Tyr to L-3,4-dihydroxyphenylalanine (DOPA), quickly converted to dopaquinone (Figure 3.1). Under available cysteine molecules, they will react with DOPA, producing cysteinyl-DOPA, that after being oxidized and polymerize will give pheomelanin (Hennessy et al., 2005; Liu, Yan et al., 2005; Yamaguchi et al., 2007). When the intracellular cysteine is depleted, the excess dopaquinone spontaneously gets cycled to dopachrome. While the tyrosinase-related protein 2 (Typr-2) is present (Jackson et al., 1992), the dopachrome will spontaneously lose the carboxylic acid giving 5,6-dihydroxyindole (DHI). Then they are quickly oxidized and polymerized (Ito, 1986; Napolitano et al., 1993; Tsukamoto et al., 1992b), generating the black eumelanin or DHI-melanin, an insoluble polymer with high molecular weight (Figure 3.1) (Tripathi et al., 1992).

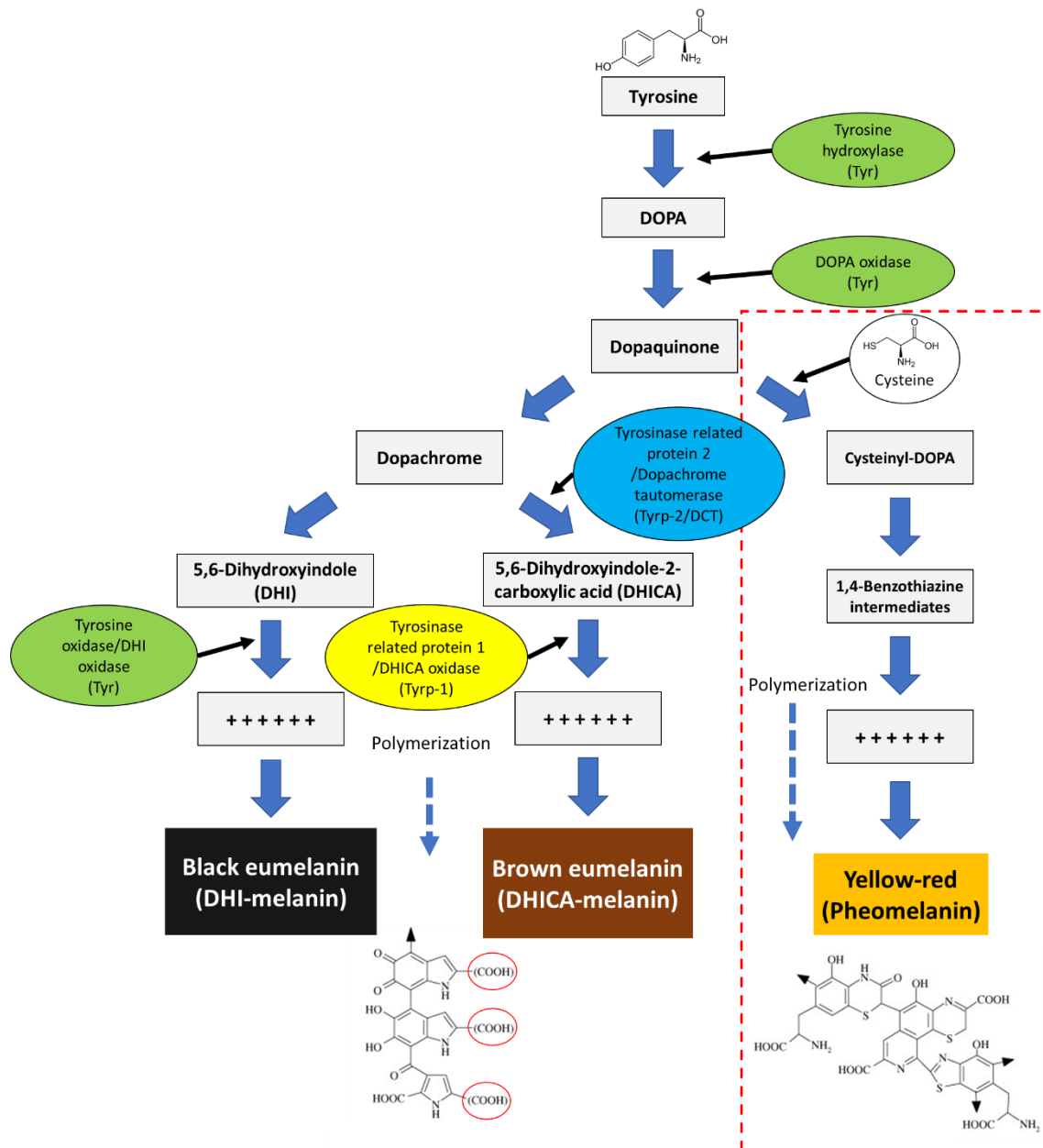


Figure 3.1. DHI and DHICA melanin (black and brown eumelanin) and pheomelanin biosynthesis pathway. Tyrosine amino acid gets converted to dopaquinone by several tyrosinase enzymes. Notice that the pheomelanin pathway (discontinuous red selection) is not presented in fish (Hearing, 1993; Ito, 1986; Jimenez-Cervantes et al., 1994; Kobayashi et al., 1994; Kottler et al., 2015; Kroumpouzou et al., 1994; Napolitano et al., 1993; Tripathi et al., 1992; Tsukamoto et al., 1992a; Tsukamoto et al., 1992b).

Nevertheless, under the presence of Tyrp-2, also called Dopachrome tautomerase (Dct), dopachrome molecules are tautomerized keeping its carboxylic acid group forming 5,6-dihydroxyindole-2-carboxylic acid (DHICA) (Figure 3.1) (Hearing, 1993; Kroumpouzou et al., 1994; Tsukamoto et al., 1992a).

Similarly to DHI, but with the help of the tyrosinase-related protein 1 (Tyrp-1) (Hearing, 1993; Jimenez-Cervantes et al., 1994; Kobayashi et al., 1994), DHICA continues the pathway by getting oxidized and polymerized, which results in the production of the brown eumelanin or DHICA-melanin, a moderately soluble polymer of intermediate size (Ito, 2003; Ozeki et al., 1997; Yamaguchi et al., 2007). It seems that the activity of these three enzymes regulate the ratio between DHI-melanin and DHICA-melanin: Tyr, Tyrp-1 and Tyrp-2 (Figure 3.1) (Aroca et al., 1992). All these enzymes implicated in melanogenesis have been cloned and sequenced in teleost fish like *Fugu rubripes* (Peng et al., 1994), Goldfish (*Carassius auratus*) (Camacho-Hubner et al., 2000; Camacho-Hubner et al., 2002), rainbow trout (*Oncorhynchus mykiss*) (Boonanuntanasarn et al., 2004), and Atlantic salmon (Larsen et al., 2013).

Melanin molecules have a large variety of biological functions. At microbiological level, the pigment has been observed in some unicellular organisms as bacteria's or fungus, conferring resistance to several environmental factors or extreme conditions as UV light, high temperature, desiccation or resistance to polysaccharides lytic enzymes, reinforcing of walls (Hullo et al., 2001; Kollias et al., 1991; Kuo & Alexander, 1967; Kuznetsov et al., 1984). Abilities for encapsulating and isolating oxidizing chemical compounds, pesticides, and infectious organisms, have also been described (Patel et al., 1996).

Eumelanin is considered as an inert, insoluble, resistant and highly stable compound. During its biosynthesis, there is a small and local production of free radicals during polymerization (Sealy, 1984) (Figure 3.1). Moreover, once produced, they are considered as redox polymers with charge transference activity at the intracellular level. Thus, they can absorb and neutralize reactive oxygen species (ROS) (de Cassia & Pombeiro-Sponchiado, 2005; Dunford et al., 1995; Rózanowska et al., 1999; Sarna et al., 1985; Sealy et al., 1984; Wang et al., 2006; Wu et al., 2008). It may sound contradictory that melanin acts as producer and consumer of ROS, with a negative balance since the consumption of oxygen is higher due to several implicated oxidizing steps. However, it could be a way of controlling them in favor of cell functions or needs. Chelating and binding activity of molecules and organic agents have also been observed, sometimes very efficiently, especially with metal ions (Sono et al., 2012), which complements even more its neutralizing capacity (Borovansky, 1994; Bowness et al., 1952; Hill, 1992;

Horcicko et al., 1973). All these make melanin a good candidate for the innate immunological response, especially in lower vertebrates (Blazer, 1991) or poorly vascularised areas as adipose tissue, where acquired immunity is relatively limited (Randhawa et al., 2009). Other properties given macroscopically by its structure in fish can be socially related towards reproduction, hierarchy or camouflage (Crook, 1997; Helen et al., 2013; Korzan & Fernald, 2007).

3.3 Melanogenesis regulation

3.3.1 Light

UV light is segmented into UVA, UVB, and UVC. While atmospheric ozone absorbs UVC, UVA and UVB reach earth surface in a 90-95% and 5-10% of total UV respectively. Longer wavelength types like UVA passes through the skin reaching dermis without difficulties and deeper water layers. On the other hand, the skin epidermis practically entirely absorbs shorter ones as UVB, and just a little fraction get access to dermic levels. That penetration potential determinates their effects in the skin. Thus, UVA generates reactive oxygen molecules that can potentially damage cell DNA as well as other cellular structure. In contrast, UVB may be absorbed by DNA causing damage directly such as mutagenic thymine dimers (Figure 3.2) (de Gruijl, 2000; Kripke, 1984; Orazio et al., 2013; Pfeifer et al., 2005; Tyrrell, 1995). Consequently, there is an induced skin inflammation (Clydesdale et al., 2001), and if the radiation overloads the tolerance damage level, then keratinocytes begin apoptosis, which generates responsive hyperplasia increasing the epidermal thickness (Scott et al., 2012). Therefore, there is an up-regulation of melanogenesis and melanin deposition in melanocytes and keratocytes (Potaman et al., 1993; Rouzaud et al., 2006; Widlund & Fisher, 2003). This up-regulation occurs when keratocytes DNA and cellular damage, activates the transcription of the opiomelanocortin (POMC) gene, which codifies the production of the melanocyte stimulating hormone (α -MSH), MCR agonist (Figure 3.2).

After releasing, α -MSH reaches local melanocortin receptors (MC1R) in melanocytes, activating a molecular chain that ends with the increase of tyrosinase and other melanin biosynthetic enzyme intracellular levels and subsequently melanin production (Figure 3.2) (Bologna et al., 1989; Chakraborty et al., 1995; Corre et al., 2004; Lerner & McGuire, 1961; Levine et al., 1991).

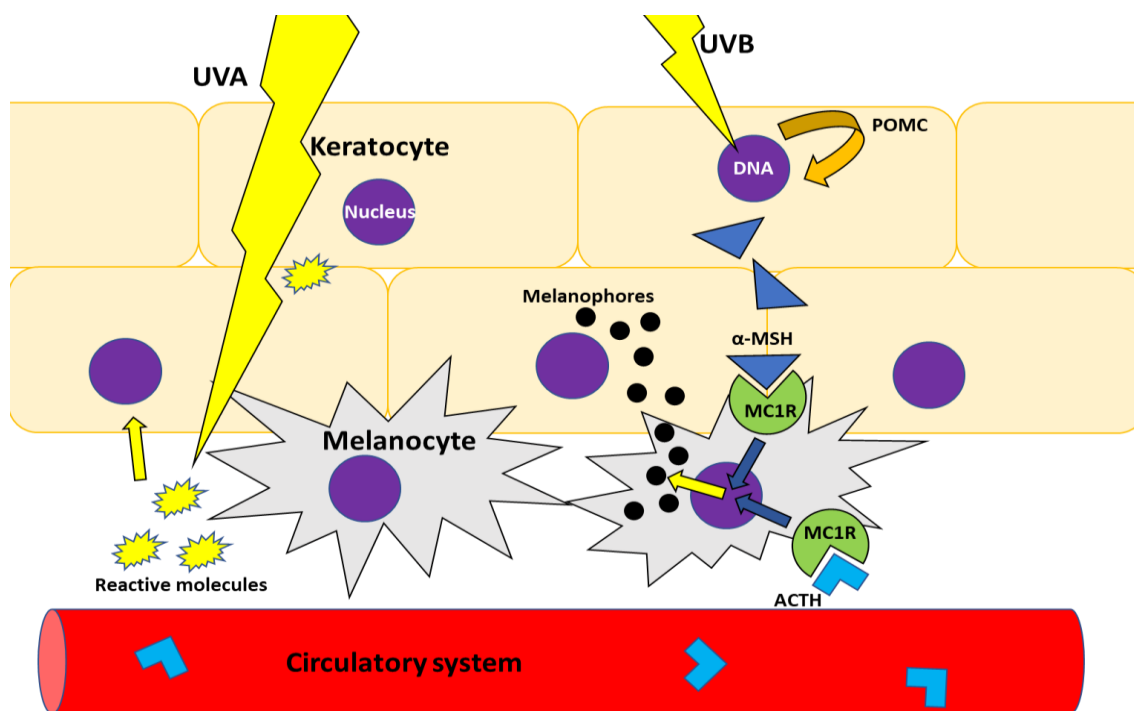


Figure 3.2. Simplified illustration of melanogenesis up-regulation on melanocytes. The melanocortin receptor 1 (MC1R) located on melanocyte membranes may interact with both the melanocyte stimulating hormone (α -MSH) by light/cell inflammation stimuli and the adrenocorticotrophic hormone (ACTH) by the stress pathway (Bolognia et al., 1989; Khan et al., 2016; Lerner & McGuire, 1961; Potaman et al., 1993; Rouzaud et al., 2006; Turan et al., 2012; Widlund & Fisher, 2003).

3.3.2 Stress

Another melanocortin analog to MSH is the adrenocorticotrophic hormone (ACTH, adrenocorticotropin, or corticotropin) (Figure 3.2), a key compound for the hypothalamic-pituitary-adrenal axis generally in response to stress by a cortisol release in negative feedback. Thus, animal stressors response with ACTH and α -MSH may up-regulate expression of the MC2R and MC1R genes respectively (Lerner & McGuire, 1961; Levine et al., 1991). In contrast to MC1R, that is a specific receptor for α -MSH and ACTH, MC2R is just ACTH specific and located at adrenal cortisol-producing tissue (head kidney) (Clark & Weber, 1998; Gallo & Civinini, 2003; Malik et al., 2015).

When a stressor occurs, there is a production of ACTH that upregulates MCRs transcription, binding to MC1R and MC2R receptors, and starting melanin (Figure 3.2) (amount or distribution) and cortisol synthesis respectively (Turan et al., 2012). Cortisol may disperse melanosomes, while melatonin and melanin-concentrating hormone (MCH), results in their concentration (Herrling et al., 2008; Slominski, 2009). Additionally, cortisol increases the production of MC1R antagonists, agouti signaling

protein (ASIP) and agouti-related protein (AGRP) (Cal et al., 2017; Cone et al., 1996). Consequently, the production of melanin can be inhibited by the drop of ACTH, and MC1R antagonists of the adrenal axis (Khan et al., 2016; Kittilsen et al., 2009; Smith et al., 2003). It seems that MC2R has a key role in the melanin production in response to stress, or as it has been described in other studies in rainbow trout skin, individuals with proactive (low cortisol levels), and passive response (high cortisol levels) (Fujii, 1993a; Iger et al., 2001; Khan et al., 2016; Kittilsen et al., 2009). Another study suggests that genes in the melanocortin system impact on the expression of some physiological and behavioral characters (Ducrest et al., 2008), as the link between darker males and higher sexual activity and aggressive character (Horth, 2003). Glucocorticoid hormones as cortisol have shown immunosuppressive effects (Pickering & Pottinger, 1985; Pickering & Pottinger, 1987), inhibiting inflammatory response, leukocyte movement and activity in life fish (Ainsworth et al., 1991; Cato & Wade, 1996; De Bosscher et al., 2000; Engelsma et al., 2003; Maule & Schreck, 1990; Pickering & Pottinger, 1987), and a reduction of lymphocyte survival and cytokine production and response to antigens in *in vitro* lines (Fast et al., 2008).

3.3.3 Diet

There are recent evidences that link “dark spots” in fillet by with dietary effects, where supplementation with antioxidants (vitamin C, E, and selenium) reduced the size and the prevalence by 14% (Rafiq, 2015; Weizhi, 2016). This antioxidant activity may potentially reduce the production of lipid oxidation-induced compounds by free radicals (Lauritzsen et al., 1999; Peng et al., 2009; Sahoo & Mukherjee, 2002), which also directly increase with temperature (Dittmar et al., 2014). Moreover, marine omega-3:6 fatty acids ratio seems to play an important role, since fish fed with less omega-3 have shown higher frequencies of “dark spots” (~7% more), probably related to a larger proinflammatory activity of omega-6, as reported recently (Sissener et al., 2016).

Novel feed ingredients as Antarctic krill (*Euphausia superba*) offers interesting nutritional profile since it is rich in omega-3 lipid and astaxanthin (Xu et al., 2017). It has been used for replacing fish meal partially in salmon diets with no adverse effects (Olsen et al., 2006). In fact, improvements in growth and fillet quality traits have been described (Hatlen et al., 2017; Suontama et al., 2007), principally because of its high palatability,

leading to higher feed intake, and higher growth rates and body weights with lower condition factors. Leaner fish fillets have also been observed with partial inclusion, possibly explained by a larger β -oxidation of fatty acids, which increases their utilization (Hatlen et al., 2017). However, negative effects have been described by using high or total replacement levels with krill in a reduction of lipid digestibility, and growth rate because of the high levels of chitin (Olsen et al., 2006; Tharanathan & Kittur, 2003).

3.3.4 Others

Other stressors as physics (fights, handling or broken bones) (Godoy G, 2015), chemicals (vaccine adjuvants) (Haugarvoll et al., 2010), and biologicals (infectious diseases) (Bjørngen et al., 2015; Nylund et al., 2011) may contribute to the development of “dark spots” (Agius, 1985; Larsen et al., 2012; Roberts, 2012).

3.4 Chromatophores and skin appearance

Pigmentation and color pattern in teleost fish are the have the largest complexity and diversification of all vertebrates (Braasch et al., 2007; Braasch et al., 2008). The implicated cells are called chromatophores, which in teleost structured by an external layer of yellow xanthophores or red erythrophores, both with carotenoid and pteridine pigments (Bagnara & Hadley, 1973). They are followed by a reflecting middle iridophores layer with crystalline platelets reflecting light back through the xanthophores/erythrophores with carotenoids (Herring, 1994; Wedekind et al., 1998). On the base, melanophores or melanocytes area organized as a web (Bagnara & Hadley, 1973), which sometimes can overlay other chromatophores if the thickness of the skin is relatively large. However, in some teleost lineages, other chromatophores can also be found in the basal layer as leucophores (opaque white), and cyanophores (blue) (Bagnara & Matsumoto, 2006; Braasch et al., 2007; Braasch et al., 2008; Mellgren & Johnson, 2002; Takeuchi, 1976).

When light passes through fish skin layers, it interacts first with upper pigmentary cells like xanthophores or erythrophores reflecting their yellow-red pigments color (long-wavelength light), and absorbing violets and blues (short-wavelength light). If partially scatter or direct light reaches the middle stratus, the iridophores reflect light with a color

that depends on the organization and orientation of the reflecting platelets. Thus, when these platelets are disposed to reflect all visible light spectrum, skin appearance will change from yellow to red (passing through xanthophores or erythrophores), or silver (non-upper layer) (Grether et al., 2004; Palazzo et al., 1989). On the other hand, if light reaches the platelets organized to reflect light partially, the long-wavelength are absorbed while short ones are reflected giving an external aspect like blue, or blue-green like if combined with yellow or red pigments from the upper layer when passing through (Fujii, 1993b; Grether et al., 2004; Kelley & Davies, 2016; Palazzo et al., 1989). The skin fish color has a third dimension given by the iridophores aggregative ability and melanocytes for changing the position of their melanin pigment that is synthesized and clustered in melanosomes in the cell body or dendritic processes (Ito et al., 2000). Hence, melanocytes and their dendritic processes can overlay other chromatophores, especially the iridophores (Bagnara & Hadley, 1973). Thus, the more dispersed they are, the more reflecting area or darker the general appearance will be. However, when they are concentrated, other chromatophores are exposed to light reflecting their pigments color, combined or not with iridescence (Bagnara & Hadley, 1973; Kelley & Davies, 2016; Mahalwar et al., 2016; Palazzo et al., 1989). Fish chromatophores, melanosome reorganization, are affected by other factors such as hormones like cortisol, neural control by noradrenaline, and environmental stimuli's like surrounding colors, UV radiation by visible light, temperature, pH, chemicals, etc (Double et al., 2002; Meyskens Jr et al., 2001). For example, melanosomes get aggregated if the animal lives at pale backgrounds, while dispersed over dark backgrounds (Bagnara & Hadley, 1973). Moreover, there is evidence of single or melanosomes globules transference from melanocytes dendrites to surrounding keratocyte perinuclear areas (Ando et al., 2012; Pathak et al., 1980) as well between SHK-I cell (Haugarvoll et al., 2006).

Skin colors are costly to produce and maintain in the animal kingdom, so it may indicate how healthy they are. This fact shows evolutionary advantages as an external signal of internal conditions at reproduction (Griffith et al., 2006). It is known that some darker (more melanin) and redder (more carotenoids) bird males express aggressive and dominant behaviors (Griffith et al., 2006).

3.5 Fish fillet quality

Product quality is the most important aspect for the consumers to consider. Quality can have several approaches; sensory, technological, ethical, nutritional and hygienic, all these connected and related to fish species, farm conditions, handling and storage of the product. However, the basic requirement for food is that the product must be safe to eat (Nortvedt et al., 2007). Regarding the visual aspects of sensory quality, salmon fillet appearance is crucial for consumers (Anderson, 2001; Giese, 1995; Koteng, 1992). The natural color of salmonid fillets is given by the deposition of carotenoid pigments, principally astaxanthin (Nickell & Springate, 2001), which is supplemented by diet. The evaluation of the color appearance of salmon is frequently estimated by comparing the salmon fillet with the *Salmo colourFan*TM (Alfnes et al., 2006; Stien et al., 2006).

It is possible to find alterations of the preferred appearance of salmon fillets, such as dark discoloration problems. Those are represented by melanin hyperpigmentation or dark spots (Berg et al., 2012; Koppang et al., 2005), which may be classified according to their localization (visceral or muscular), area (focal, miliary or diffuse) and depth (superficial or deep).

3.6 Salmon topographic anatomy

The skeleton architecture of the Atlantic salmon follows a common pattern as other bony fish; cranium, jaw, vertebral column, intermural bones, fin bones and rays (proximal or internal and distal or external) (Roberts, 2012).

Vertebra bodies have specific apophysis that in salmon are divided into dorsal with neural spine and pin bone, and ventral with haemal spine and rib bones. However, ribs are not apophysis themselves since they are different bones connected to a joint (Roberts, 2012). These bones provide protection and structural support, but in contrast to higher vertebrates as mammals, they do not have hemopoietic functions (Roberts, 2012). The number of vertebrae (~59) is not constant and may be affected by genetical background or external factors such as the environment during larval development (Fraser et al., 2015).

The skeletal muscle architecture is organized by vertical blocks of red-colored tissue (myomeres) and white stripes of connective tissue (myocommata) that gives a stripe-like appearance. They are organized on both sides of the axial skeleton to bend the body laterally and propelling the fish (Gray, 1968; Videler, 1993). There are four skeletal muscle quadrants in the fish body. They are separated from each other by the median septum and the transverse horizontal septum. The two dorsal blocks of muscles are called epaxial muscles, while those ventrally located are called hypaxial muscles (Gemballa, 1995; Roberts, 2012; Westneat et al., 1993). Both harbor two different types of muscle; the white (anaerobic) for fast and spontaneous movements, and the red (aerobic) muscle for continuous and soft movements, which requires a higher vascularization.

By using the fat content, fillets can be divided it into 3 parts; the fattiest part (20%) from ventral body edge to swim bladder high, followed by the region from the dorsal body edge to the dorsal spine edge (16%), and the less fatty part (11% and 5%) from the dorsal spine edge to the swim bladder high (Aursand et al., 1994; Baeverfjord & Rye, 1994). These sections can be identified by image analysis according to their color (Marty-Mahé et al., 2004), where the caroteind content play also an important role in the general appearance (Bjerkeng et al., 1997a; Bjerkeng et al., 1997b). The fattiest part of the anterior hypaxial fillet sections concentrated the ~94% of melanin problems in previous industry reports (Aursand et al., 1994; Baeverfjord & Rye, 1994; Mørkøre, 2012; Mørkøre, 2017). Prevalence of dark spots in the right and left fillets was also found similar (Mørkøre, 2012).

3.7 Color theory

Albert Einstein described light as radiation of electromagnetic nature. Its waves spread out from any light source and travel at the enormous speed of 300,000 km/s (Einstein, 1905). Its physical properties associated with objects or materials such as light absorption, reflection, or emission light spectra, are called *Color* after being visually perceived (Nassau, 1998). This perception is subjectively done at the central nervous system level that receives the light stimuli through highly specialized cells with photosensitive activity located at the eyes.

Since it is a measure interpreted by the brain, the physical or physiological quantification of color does not totally explain the psychophysical perception of color, so it cannot be quantified by just the degree of stimulation of these photoreceptors (Nassau, 1998). The science of color is termed colorimetry and was firstly described by Sir Isaac Newton. This discipline includes the physics of electromagnetic radiation in the visible range (commonly referred to simply as light), the origin of color in materials, and the color perception in the brain through the human eye. Different visual spectrum colors have different wave lengths. The longest wavelength of light that humans can see is red, while the shortest is violet (Nassau, 1998; Newton, 1672).

Colors can be organized by color spaces, which are represented by three values or dimensions since human vision is trichromatic. There are several color spaces as the RGB, the hue, saturation, and brightness (HSB), and the CIE Lab (Nassau, 1998). RGB is the most commonly-used color space. However, other alternatives such as HSB and Lab provide significant advantages regarding digital imaging processing (Nassau, 1998; Wootton et al., 1995). Hue describes the attribute of pure color (type) by angles in a continuous color-wheel (Figure 3.3), initiating on the right side and moving towards counter-clockwise, where the primary colors; red, green and blue, are placed on the circumference at 0° , 120° , and 240° respectively (Figure 3.3) (Nassau, 1998).

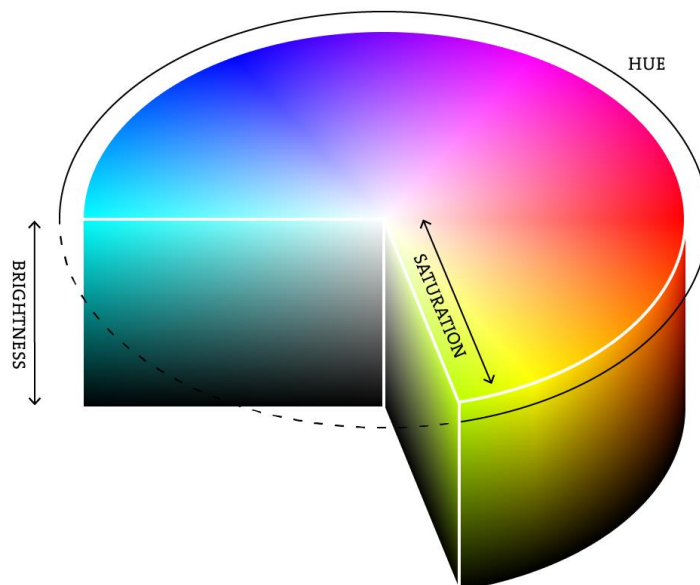


Figure 3.3. HBS color space with hue, saturation and brightness dimensions. The primary colors; red, green and blue, are placed on the circumference at 0° , 120° , and 240° respectively (15/04/2018).

The radius of the circumference is known as the saturation (tone, purity or intensity of the color) and indicates the absence of white, grey, or black, where the center equals white, which is completely desaturated. On the other hand, colors with 100% saturation are considered as pure (Figure 3.3). The height of the wheel corresponds to brightness lightness or luminance, which describes if an area emits more or less light (Figure 3.3) (Nassau, 1998).

When it comes to the Lab color space, the dimension L^* represents lightness in the vertical axis. The perfect white appearance would have an L^* of 100 units, while a perfect black would have an L^* of 0 units (Figure 3.4). The dimension a^* represents greenness for negative or redness for positive values, while b^* represents blueness for negative and yellowness for positive values (Figure 3.4) (Nassau, 1998).

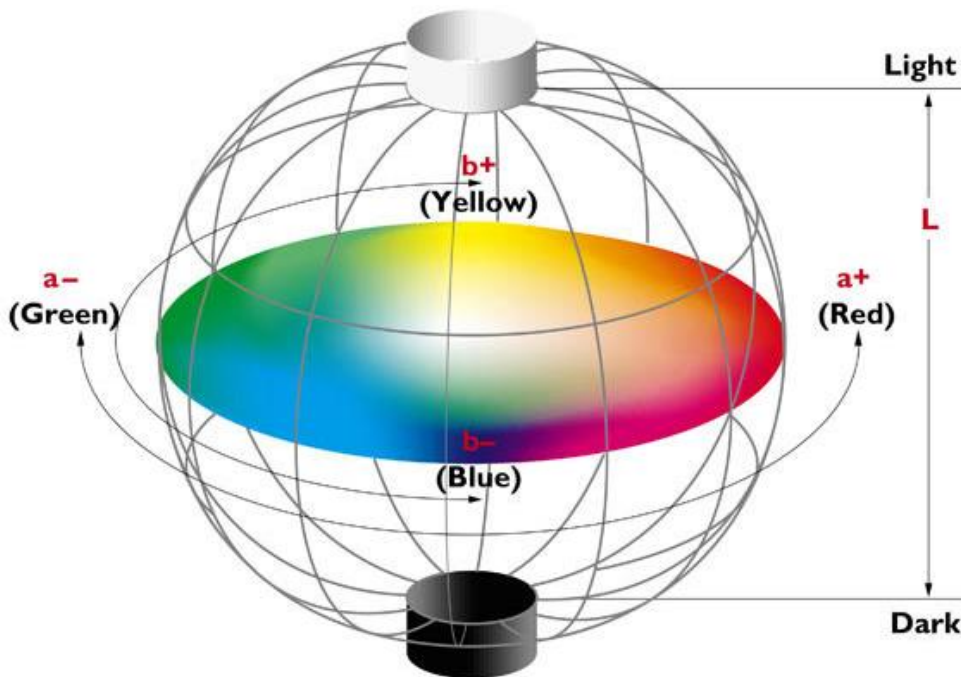


Figure 3.4. CIE Lab color space. Chroma is represented by two dimensions, a^* (negative green to positive red) and b^* (negative blue to positive yellow), while lightness is shown by the vertical axis from white (100) to black (0). The a^* and b^* channels represent true neutral gray values when equaling to 0 units (15/04/2018).

Color appearance may be influenced by external circumstances (Albers, 1963); the reflection of light from an object in a normal environment (object mode), visualisation of the light source directly (illuminant mode), and the distortion of perception by close comparison of two different colors (aperture mode) (Nassau, 1998).

Lab color is designed to approximate human vision, since it includes all perceivable colors and perceptual uniformity (the same amount in a color value should produce a change of about the same visual importance to the human eye or linear effect), in contrast to other color models. Moreover, its L^* axis corresponds with the human perception of lightness and can be modified without alterations on the other axis, while brightness is significantly affected by the light source. Therefore, the Lab model is device independence and standard (CIE, 1976; Ilie & Welch, 2005; Nassau, 1998; Perceptually uniform color spaces, 17/04/2018; Poynton & Funt, 2014).

4 MATERIAL AND METHODS

4.1 In vivo study

4.1.1 Fish material and sampling

A population of Atlantic salmon from a commercial breeder was farmed in closed cages at Sæterosen for 7 months (from the first week of April to late October 2016) and transferred to open sea cages from LetSea research facilities at Slapøya Nord, Dønna for 10 months (from the first week of November to October). When fish were transferred, they were randomly divided into 6 cages/groups (M1, M2, M3, M4, M5, and M6). During on-growing, fish were fed three different diets from BioMar Group. Those dietary groups were D0 (M3, M4), DL (M5, M6) and DH (M1, M2), with none, low or high inclusion of krill meal.

The sampling was divided into 2 main phases: at Dønna open sea cage station and Nofima Ås laboratory. Thus, 15 fish were randomly selected by the plan operators from every cage (90 fish in total) during August 29th - 30th of August 2017. Fish were anesthetized and euthanized by a high MS-222 dose bath. Just after fish euthanasia, a general external examination was performed, and body weight and length of fish were taken before and after evisceration (Figure 4.1).

Fish previously analyzed at Dønna, were transported by a refrigerated truck in Styrofoam boxes with ice to Nofima Ås laboratory was the second part of the analysis was performed during 5th-7th of September 2017. Fish were taken out from their boxes and were prepared to fit into the filleting machine to get two fillets without ribs, vertebral column, neural and haemal spine. This preparation consisted of a transversal cut by the dorsal border of opercula to cut the head off, and a curved one following the caudal border of the fin bones (Figure 4.1). Gutted fish were processed by using a filleting machine Carnitech© model CT 2630.00 (MAREL FOOD SYSTEMS, Gardabaer, Iceland). Then, fillets were separated, checked, and weight from both sides was taken having them ready for the next step. Then, both fillet sides were weighed before visual inspection. Fillet color was analyzed under standardized condition (Salmon color box, Skretting, Stavanger, Norway), by DSM SalmoColour Fan™ (F. Hoffmann-La Roche AG, Basel, Switzerland). Number and position of abnormal vertebrae were recorded (Figure 4.1).

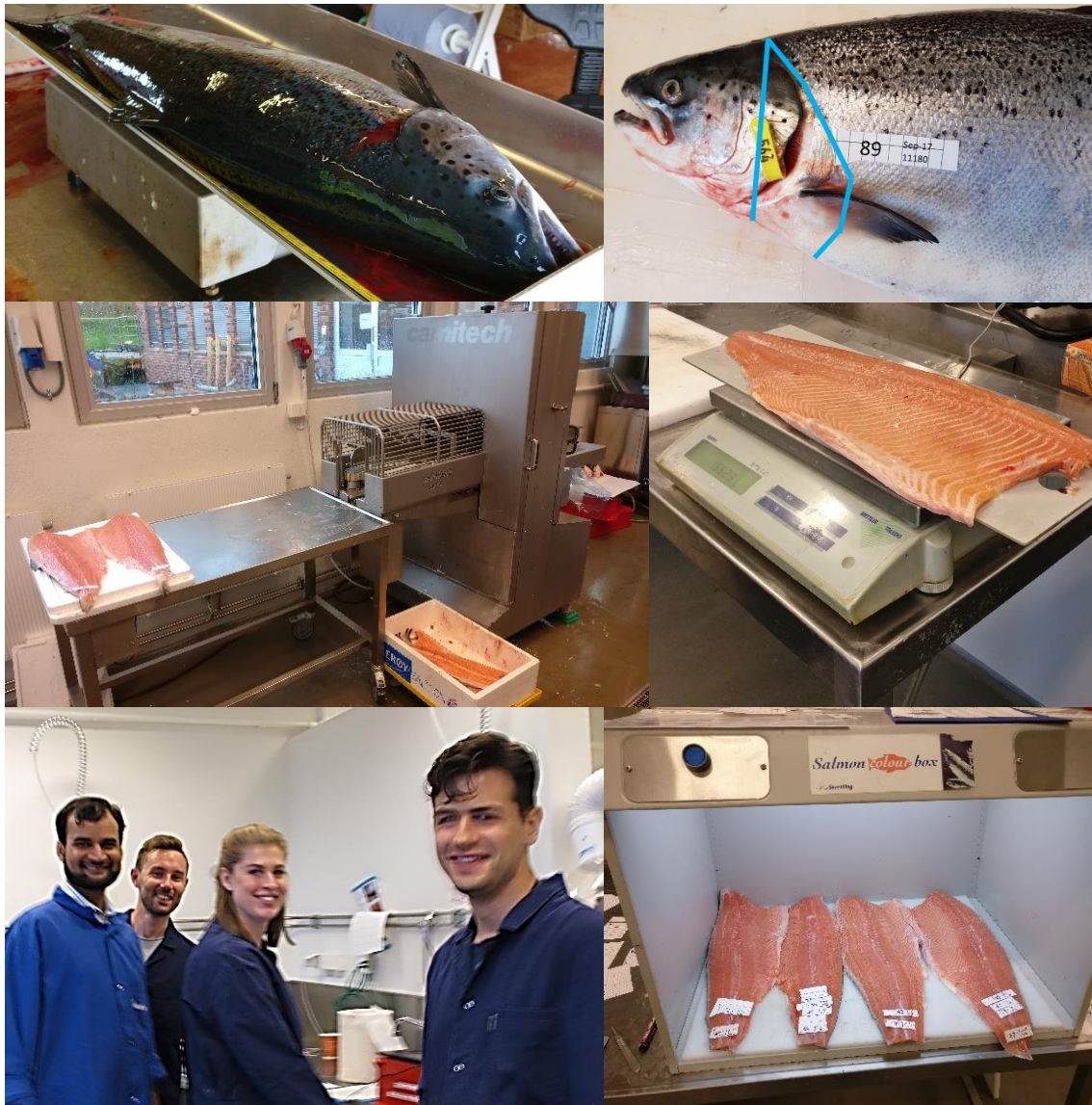


Figure 4.1. Illustration of the sampling at Dønna open cage station, and Nofima Ås laboratory. The blue lines represent cutting lines fish preparation for filleting machine.

Since, there is no differences between right and left skin or fillet side (Erikson & Misimi, 2008; Mørkøre, 2012; Mørkøre et al., 2015), the right side with the most perfect cut was chosen (essential for image techniques). Thus, the dorsal (DC) and ventral (VC) section from each right fillet side were used for image analyses of skin and skeletal muscle, respectively (between vertebra #7 and #29) (Figure 4.2).

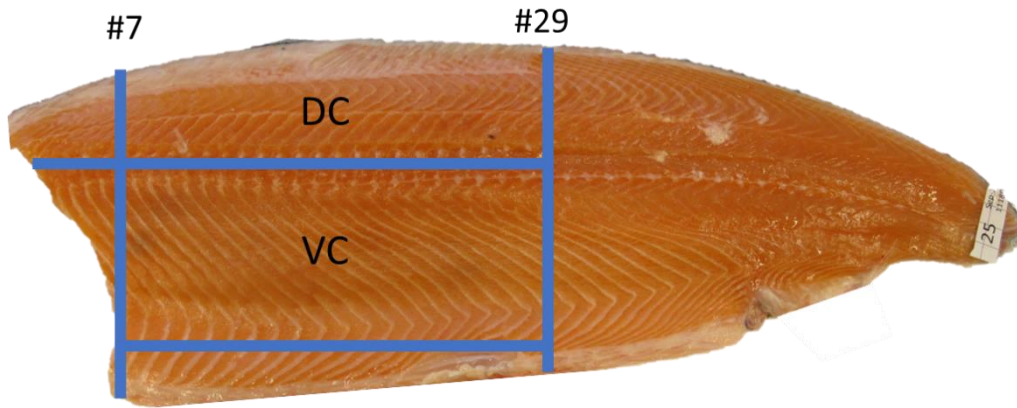


Figure 4.2. Image analyses were performed on the skin (DC section) and fillet (VC section) between vertebra #7 and #29

The DC and VC section were wiped and placed on a black tray and inserted carefully into the inlet box window of PhotoFish© (AKVA group Software AS, Bryne, Norway) (Figure 4.3). Then, pictures from DC skin side and VC muscle were taken by using this light box with standardized conditions previously used in other experiments (Folkestad et al., 2008). Images were also standardized by the grey uniformity using a grey scale card (Figure 4.3 and Figure 4.6). Thus, any variation in light or sensors during the process could be corrected.

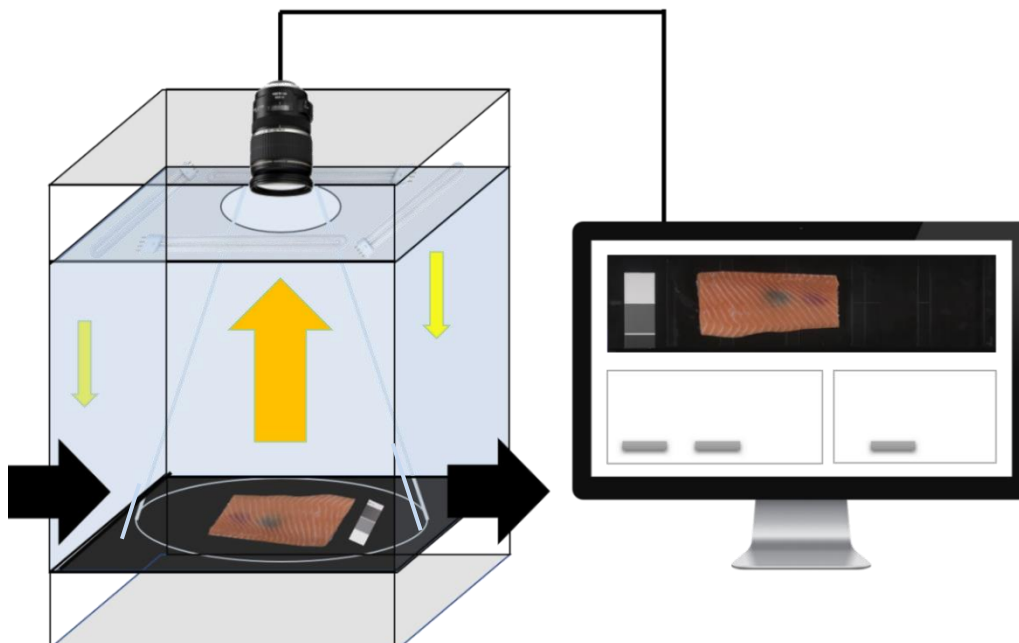


Figure 4.3. Schematic illustration of the system used for image analyses (PhotoFish© system). Black arrows represent inlet and outlet box windows, while yellow and orange show the standardized afferent light source, and the efferent information to the camera sensor respectively. The grey scale for color calibration may be observed in every picture taken.

4.1.2 Software for image processing

The software used for image analysis was Image J (Rasband, 1997), which is an image processing program covered by the General Public License (GPL), based on Java developed at the National Institutes of Health. This software was designed with an open architecture that provides extensibility via Java plug-in and recordable macros, that were used for coding most of the steps building simple programs for every analysis.

4.1.3 Image processing

A selection of the dorsal skin area was created by keeping the borders as close as possible to the cut edges (Figure 4.6). The skin pictures were taken after one week of ice-box storing, which avoided possible initial changes (Erikson & Misimi, 2008). Nevertheless, a visible side-effect of the ice over the skin during refrigeration was observed at filleting, getting a paler color. Consequently, to exclude most of the potentially disturbing areas, a selection was created in every picture from the cranio-ventral corner (quarter A) after dividing the picture into 4 equal quarters (Figure 4.4. 3° picture). This quarter was more protected against ice exposure and was similar to what was used in other studies (Gesto et al., 2017; Kittilsen et al., 2009; Pavlidis et al., 2006).

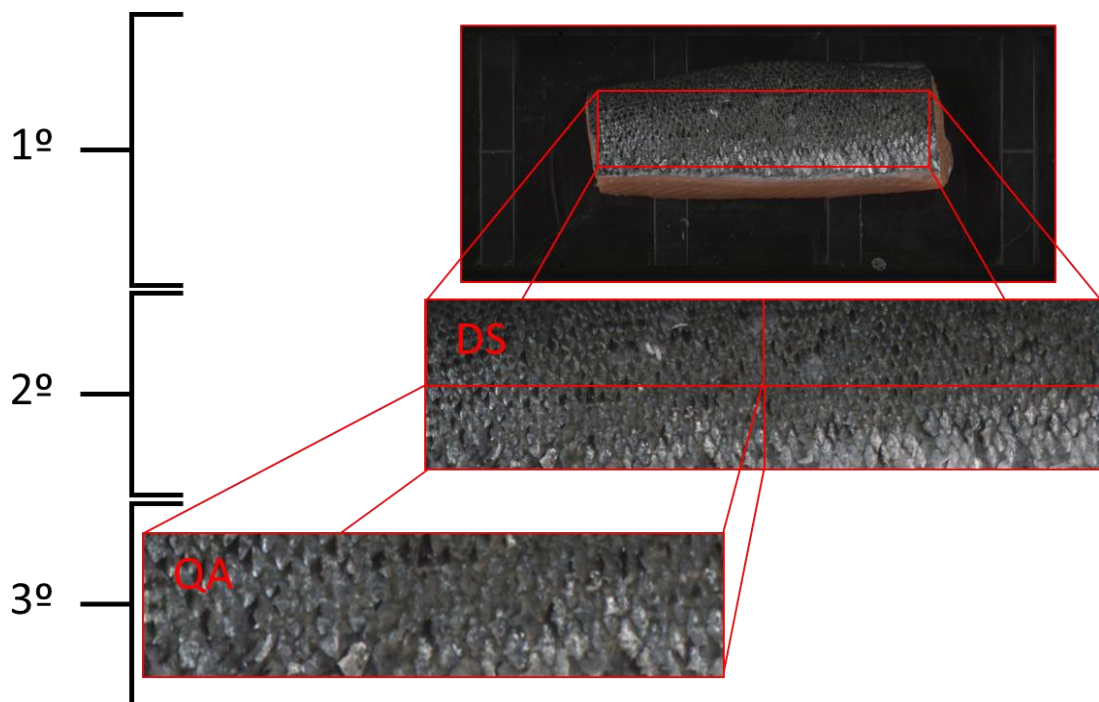


Figure 4.4. Image processing of the dorsal selections (DS) in the 2°, and quarter A (QA) in the 3° picture by using a standardized system (PhotoFish©). Image J software was used for processing and performing the colorimetric and morphological analysis of pictures.

Regarding to ventral muscle selection (Figure 4.6), taking the dorsal and caudal border of the ventral cut (Figure 4.5. 1° picture), a 20 myomeres width selection was created fitting its edges to the top and bottom of ventral cut limits, using the transverse horizontal septum as reference for counting. When the first myomere was not completed because of cutting, the next one took its place as reference (Figure 4.5).

Another processing was performed to remove top-dark and bottom-light problematic areas, to concentrate the selection to the region of the fillets with the highest “dark spot” prevalence (Mørkøre, 2012; Mørkøre, 2017). That process consisted of cutting a selection with a width equals picture length (Figure 4.5. 2° picture), and height 0.25 times that length, located 0.1 times picture length to the bottom of the picture from the transverse horizontal septum as a reference (Figure 4.5. 3° picture).

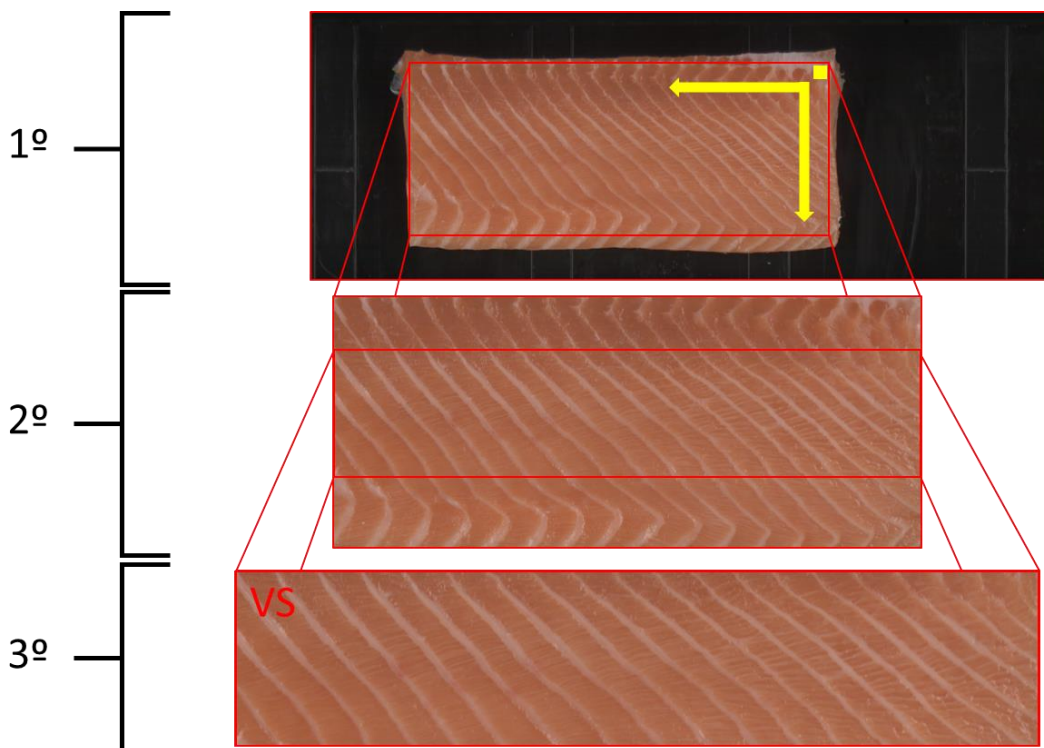


Figure 4.5. Image processing for the ventral selection (VS). In the 3° picture by using a standardized system (PhotoFish©). Image J software was used for processing and performing the colorimetric and morphological analysis of pictures. Yellow arrows show the reference corner and the direction of the selection until covering 20 myomeres using the transverse horizontal septum for counting.

After picture collection, images were stored in the computer for further processing without compression as a bitmap file format (.bmp). Later processing was carried under a tagged image file format (.tif) (Figure 4.6). The color calibration for these segmentations was carried using the HSB color space, while colorimetric values were taken as RGB color space. After that, those colorimetric RGB parameters were transformed into XYZ by means of a linear regression model and then to Lab color space that is more perceptually linear, standard and close to the human vision than other color spaces. This system for color space transformation has been used previously in other studies (Marie-Orleach et al., 2014; Marty-Mahé et al., 2004).

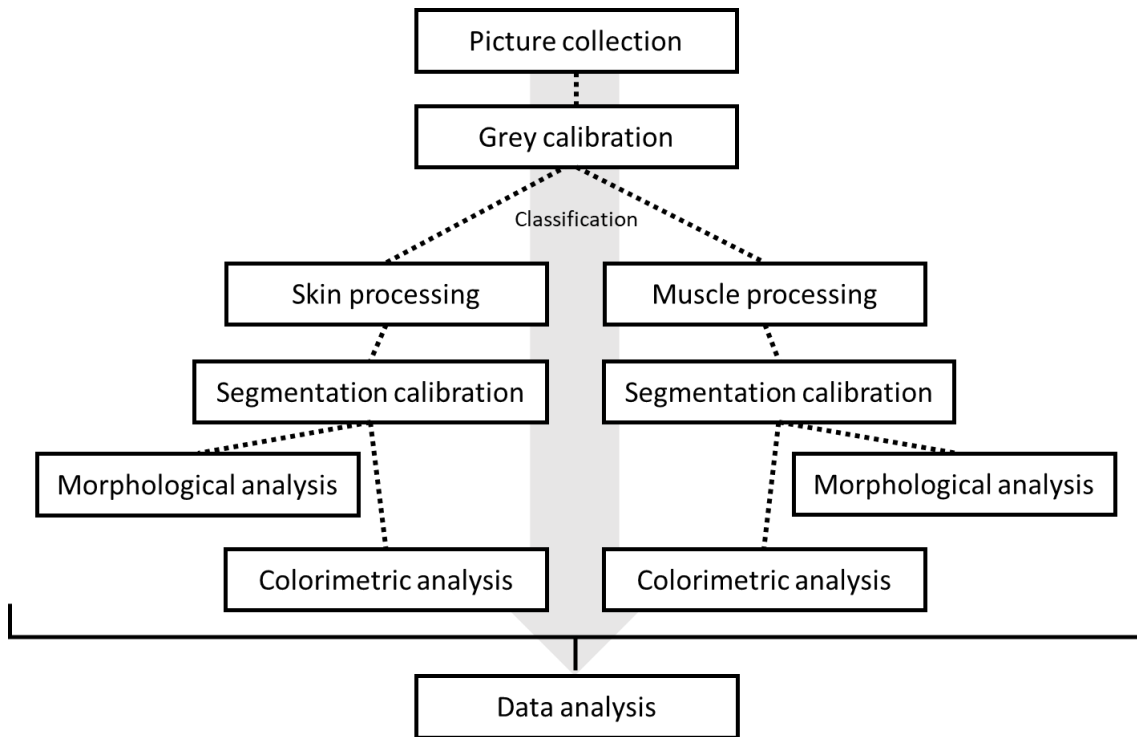


Figure 4.6. Flow diagram for image analysis, from picture collection of fish fillets to data analysis.

4.1.4 Skin measurement

4.1.4.1 Threshold calibration

A segmentation process was carried based on (Marie-Orleach et al., 2014; Wedekind et al., 2008) to define different skin structures for the colorimetric and morphological analysis (Figure 4.6). For calibrating each partition, 8 fish representing all cages were randomly selected, and values were calibrated in dorsal selections to use them after in quarter A`s.

Using Image J, every dorsal selection was segmented into 3 different areas using the brightness channel based on specific reference points. The references were the maximum separated dots delimitation or super-dark pixels, dark pixels in melanin dots, and light pixels belonging to reflective scales, leaving a remaining fraction called background dark pixels. The super-dark pixels area was defined as the area that belonging to visual melanin dots, did not create connections between different well-defined skin dots, selecting defined melanin dots able to be delimited and identified (Figure 4.7. B and Figure 4.8. B). In contrast to the super-dark pixels area, the dark pixels area was defined as the increment of black pixels until all dense black dots in the picture were selected. Theoretically, the super-dark pixels plus the dark pixels area represented the total melanin dots area or the total darkest pixels area (Figure 4.7. B.C and Figure 4.8. B.C). Then, those pixels with high reflectivity located over scales, compared with the rest of the picture were used for defining the light pixels area (Figure 4.7. D and Figure 4.8. D). The fraction area between the dark pixels area limit and the light pixels area was defined as the background dark pixels or those pixels that without being melanin dots did not express any reflective appearance (Figure 4.7. E and Figure 4.8. E). Once individual brightness values were taken for all fish, standard deviations to find outliers, and averages for the whole segmentation were calculated (Table 4.1).

Table 4.1. Reference calibration values for dorsal and ventral skin segmentation.

	Brightness		Saturation		Hue	
	From	To	From	To	From	To
Super-dark pixels area	0	42	0	255	0	255
Dark pixels area	43	58	0	255	0	255
Background dark pixels area	59	114	0	255	0	255
Light pixels area	115	255	0	255	0	255

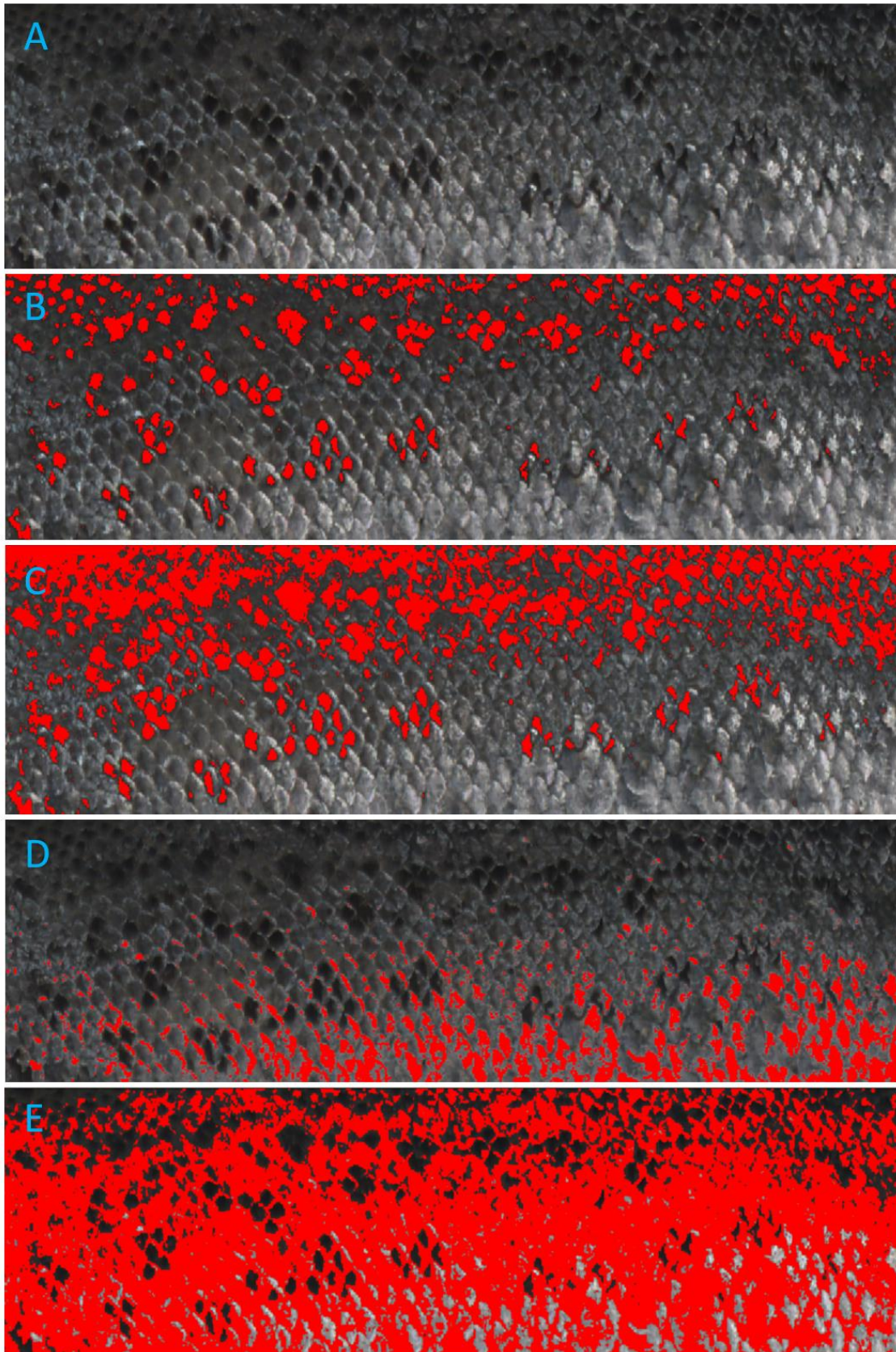


Figure 4.7. Illustration of color calibration of segmented areas (red) in dorsal skin selections. The original picture (A) and segmentations were represented; the super-dark pixels (B), the total darkest pixels area (C), the light pixels (D), and the background dark pixels (E). Notice that the difference between the total darkest pixels area in the C picture, and the super-dark pixels from the B picture, equaled to the dark pixels.

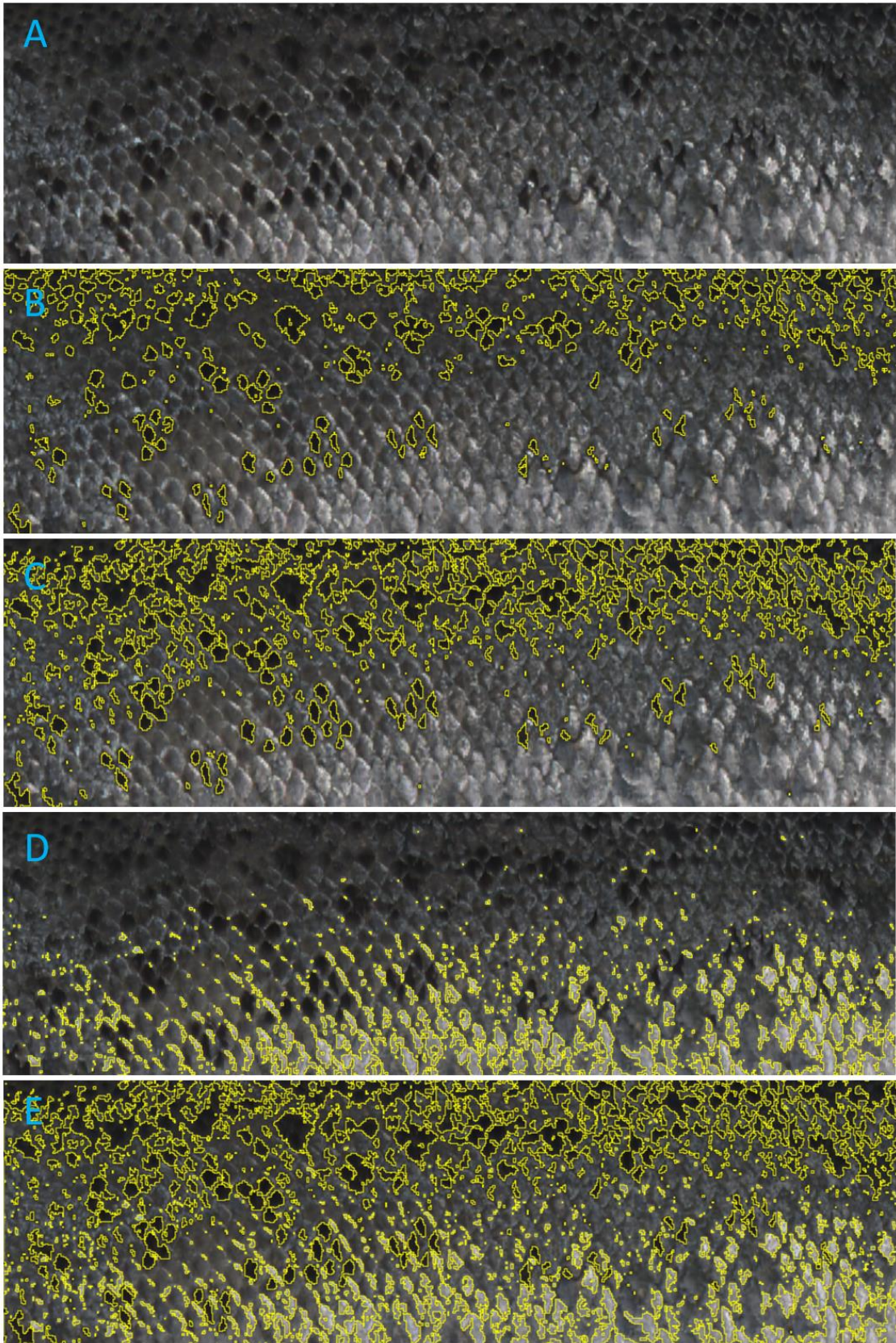


Figure 4.8. Illustration of segmentations (yellow) in dorsal skin selections. The original picture (A) and segmentations were represented; the super-dark pixels (B), the total darkest pixels area (C), the light pixels (D), and the background dark pixels (E). Notice that the difference between the total darkest pixels area in the C picture, and the super-dark pixels from the B picture, equaled to the dark pixels.

The calibration of the morphometric analysis of dots had a different approach. By using the super-dark pixels area brightness threshold (Table 4.1), the dorsal selection had a broad variation regarding dot shape and intensity, showing up potential difficulties to perform a morphological analysis (Figure 4.7. B and Figure 4.8. B). On the other hand, by narrowing down the selection to the quarter A (Figure 4.4. 3° picture), most of the problematic dorsal areas and the variation in the dot morphometry was removed. Thus, most of the spots were located but not completely selected, or in other words, given the difference in the melanin intensity among dots, not all of them were completely delimited, which could be a problem for the morphometric parameters. Increasing brightness limits up to 58, including the dark pixels area (Table 4.1, Figure 4.7. C and Figure 4.8. C), most of the dots merge, something that generates bigger melanin dots than normal sizes, giving enough reasons for using, the super-dark pixels. Additionally, another level of discrimination was performed based on dot size with the quarter A's of 8 fish representing all cages to exclude extreme values. Moreover, the representative normal dot size and belonging scale area was taken manually in every quarter A, establishing the maximum value for scale area as maximum discrimination limit (in this case 541 pixels²). Then, a visual dot counting was performed in every quarter A selection to have a value for testing the estimation by the program. Different types of automatic dot counting's were run to see which minimum discrimination values fitted well with real visual measurements. Those tested values were 0, 2, 4, 8 and 10 to 541 pixels². From that part, the discrimination windows of 2 to 541 resulted in the best indicator for dot number with a determination coefficient equals 83% and a regression equation of $y = 1.0738x + 9.8192$, where "y" and "x" represented estimated and real dot number respectively. To be able to consider just well-defined dots, the same maximum size of 541 pixels² was tested with another minimum discrimination sizes of 50, 60, 70, 80, 90 and 100 pixels² in the same test fish. The bigger value just before finding no dots by the system was selected as a limit (in this case 70 pixels²).

4.1.4.2 Morphometric analysis

The morphometric study of skin dots was performed in quarter A's using Image J, A, where the conditions were better for the automatic counting, in contrast to the dorsal selection where the size, shape and background color might disturb these values.

Thus, using the super-dark pixels area brightness threshold (Table 4.1), and a dot discrimination size between 2 and 541 pixels², dot number in every quarter A was calculated. On the other hand, for knowing the general spot morphological features (circularity and solidity) in the quarter A, using the super-dark pixels area brightness window (Table 4.1), plus a discrimination dot size was taken between 70 and 541 pixels².

4.1.5 Muscle measurement

4.1.5.1 Anatomical study and “dark spot” characterization

Based on experience at sampling and references, an anatomical study of salmon skeletal muscle and main bone structures was carried out. Those structures were connected to the fillet areas with the highest prevalence of melanin dots (ventral selection) by illustrations. The L^* , a^* , and b^* color profiles from the main spot types were characterized. Representative fish for small, medium, large black spots, and red spot were taken. Then, colorimetric values were determined from the selections, excluding their diffuse borders, and from their corresponding parallel areas with normal tissue as control for comparing. All “dark spots” from ventral selection were visually quantified and their maximum length was taken for hybridizing visual values with image analysis techniques.

4.1.5.2 Threshold calibration

Calibration of different “dark spots” fragmentations (“black spots” and “red spots”), was done based on the Figure 4.9 with the help of Image J. Using the HSB color space, it was structured into two main brands defined by their brightness level, being dark or light discolored pixels area. Non-dark discolored pixels were composed of 2 sections; light discolored pixels area, and super-light red discolored pixels area, differenced by brightness, saturation and hue channels. However, the dark discolored pixels area followed a more complex segmentation. Thus, 4 selections were defined; 3 summative (conforming 100% of the dark discolored pixels area), and an independent one called the dark cloudy discolored pixels area. The summative fractional selections were named as the low-dark discolored pixels, medium-dark discolored pixels, and high-dark discolored pixels. Every segmentation kept their complete hue channel except for the super-light red discolored pixels area that was designed as a “red” partition (Figure 4.9).

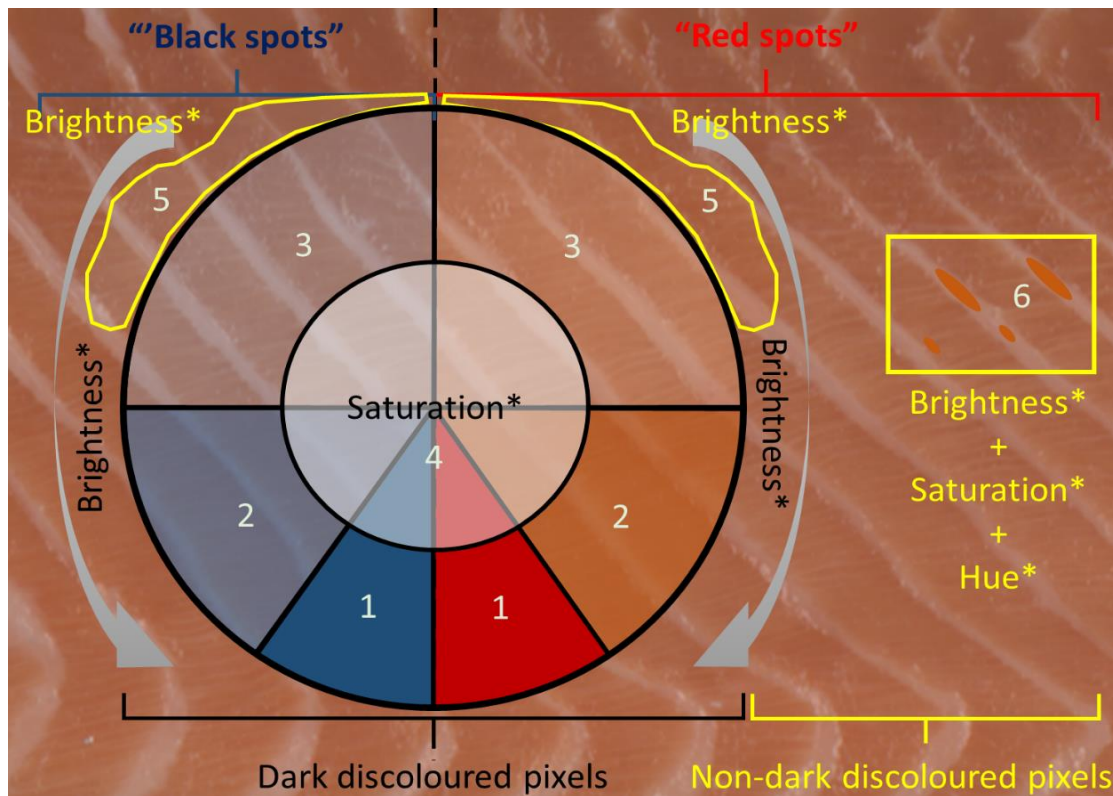


Figure 4.9. Illustration of muscle ventral selection segmentation in salmon fillet “dark spots”. Two different levels of discoloration to focus can be observed; the dark discoloured pixels with its 4 partitions; the high-dark discoloured pixels area (1), the medium-dark discoloured pixels area (2), the low-dark discoloration area (3), and dark cloudy discoloured pixels (4). The non-dark discoloured pixels can be fragmented into the light discoloured pixels (5), and the super-dark discoloured pixels area (6). *HSB color space.

When the segmentation was defined, 5 representative fish with discoloration problems plus 1 control were selected for simultaneous calibration of the dark and non-dark discoloured pixels area (including its partitions) (Figure 4.9), having the possibility to control the selection in several samples at the same time under equal threshold limits. Thus, by the brightness channel, the less bright areas were discriminated progressively until selecting most of the “dark spots” or dark discoloured pixels areas (Figure 4.10). In addition to discolorations, some area of fish fillets uses to be included in this segmentation since they normally have a darker appearance. The threshold limit was established just before false positives on the top of the ventral selections were detected (Figure 4.10). Then, another brightness threshold was created from the dark discoloured pixels threshold to a value able to select every remaining light discolored pixels belonging to “dark spots” (Figure 4.9, Figure 4.11). With the remaining part of brightness spectrum open, hue and saturation were contracted until selecting just the “micro red dots” which were defined as the super-light red discolored pixels (Figure 4.12 and Table 4.2).

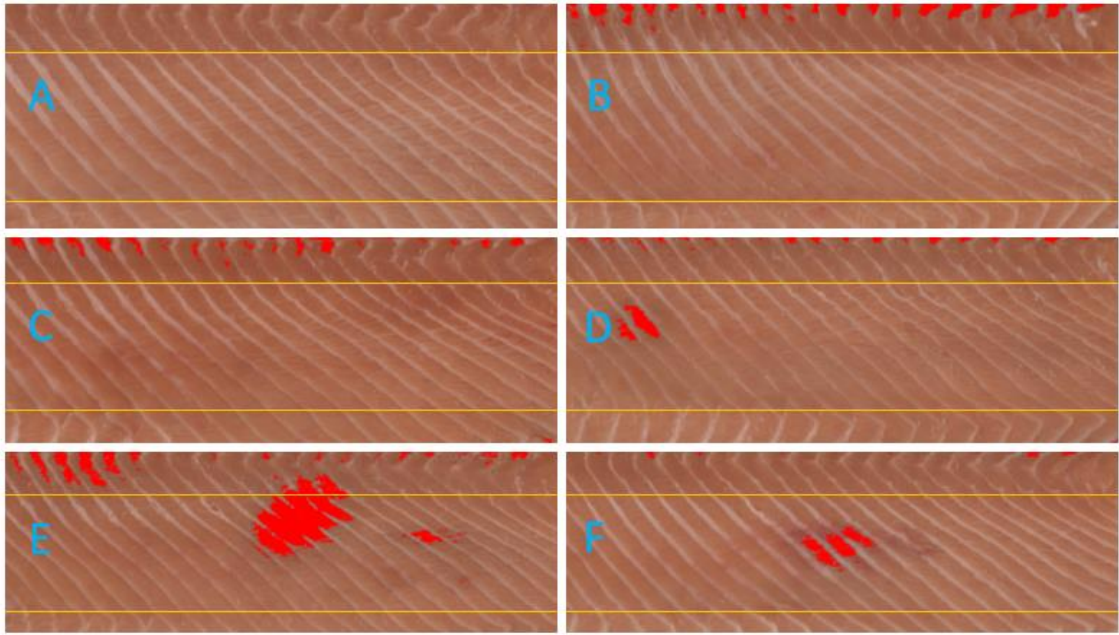


Figure 4.10. Illustration of the dark discolored pixels area calibration on 6 representative fish, where from B to F showed dark discolored pixels area (red) under the same color threshold. Notice that this step was done on ventral selection. However, excluded areas from ventral cuts with false positives (top and bottom division lines) were kept to see their effect. Notice that pictures length and width were modified to fit in the illustration, resulting in non-real processing.

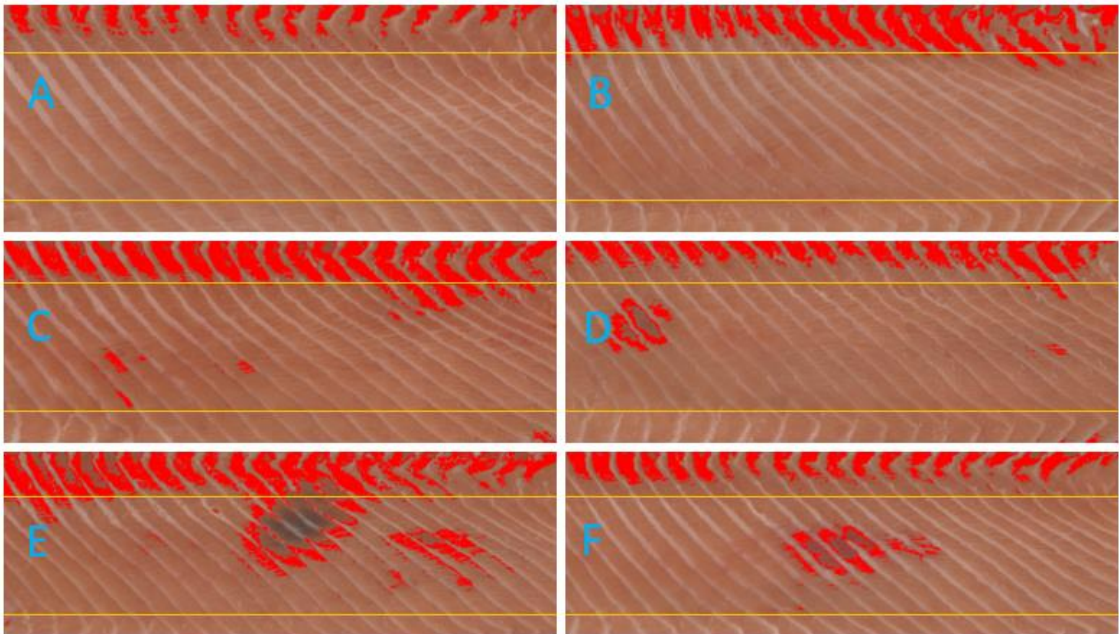


Figure 4.11. Illustration of the dark discolored pixels area calibration on 6 representative fish, where from B to F showed the light discolored pixels area (red) under the same color threshold. Notice that this step was done on ventral selection. However, excluded areas from ventral cuts with false positives (top and bottom division lines) were kept to see their effect. Notice that pictures length and width were modified to fit in the illustration, resulting in non-real processing.

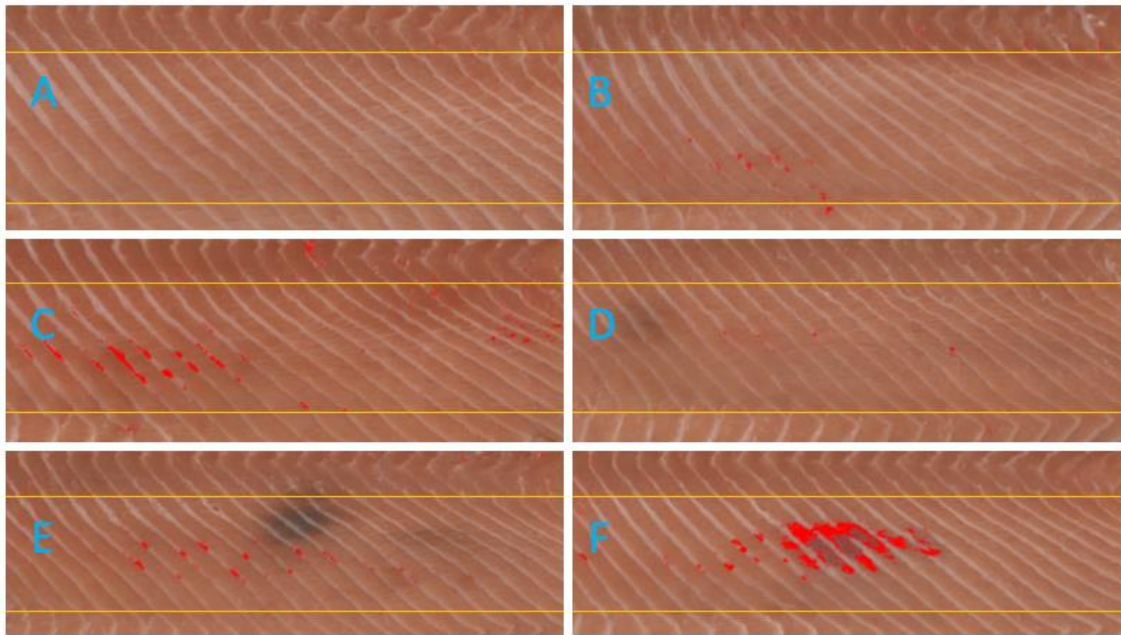


Figure 4.12. Illustration of the dark discolored pixels area calibration on 6 representative fish, where from B to F showed the super-light red discolored pixels area (red) under the same color threshold. Notice that this step was done on the ventral selection. However, excluded areas from ventral cuts with false positives (top and bottom division lines) were kept to see their effect. Notice that picture lengths and width were modified to fit in the illustration, resulting in non-real processing.

If we look at the calibration of the dark discolored pixels segmentation, their thresholds were defined by observing 6 different spots types in color, density, and size at the same time (Figure 4.13). To define the dark cloudy discolored pixels area (the only non-summative fraction), using the dark discolored pixels area brightness, the saturation windows was progressively increased until covering what is normally identified as “scar tissue” in all “dark spots”. Regarding the summative partitions of the dark discolored pixels area, its brightness window was contracted until fitting color selection with brightest parts of discoloration in every spot, also called the low-dark discolored area. The high-dark discolored pixels area was also defined by closing the brightness channel until selecting those very high-density dark micro-dots in the discoloration. The remaining fraction of the dark discolored pixels area segmentation was defined as the medium-dark discolored pixels area (Table 4.2).



Figure 4.13. Illustration of simultaneous threshold calibration for the dark discolored pixels area (1) fragmentation. The original (A), threshold area (B) and selection (C) were shown for every partition; the dark cloudy discolored pixels area (2), the low-dark discolored pixels area (3), the medium-dark discolored pixels area (4) and the high-dark discolored pixels area (5).

Table 4.2. Calibration values for muscle discoloration analysis.

	Brightness		Saturation		Hue	
	From	To	From	To	From	To
Light discolored pixels	147	155	0	255	0	255
Super-light red discolored pixels area	156	255	113	255	0	8
Dark discolored pixels area	0	146	0	255	0	255
Dark cloudy discolored pixels area	0	146	0	96	0	255
Low-dark discolored pixels area	123	146	0	255	0	255
Medium-dark discolored pixels area	86	122	0	255	0	255
High-dark discolored pixels area	0	85	0	255	0	255

4.1.5.3 Morphometric analysis

Estimation of visual numbers and average size of red dots in the ventral selections was performed by using the super-light discolored pixels area threshold from Table 4.2, combined with a filter for dot size, where those dots ≤ 8 pixels² were considered as difficult to recognise by human vision at normal inspection speed (Figure 4.12).

When it comes to the morphology of the dark discolored pixels area, their thresholds were used to estimate parameters as position of the centre of mass, estimated length, width, height, and circularity automatically (Figure 4.14 and Table 4.2). This estimation was done by creating a proportional but smaller ellipse based on the selection center of mass, where its centroid determined the center of the ellipse (Figure 4.14). As was observed, there were two main types of discoloration shapes, with higher or lower circularity. The less rounded and circular was the dark discolored pixels area, the higher was the risk to have excluded parts far from its original center of mass (Figure 4.14).

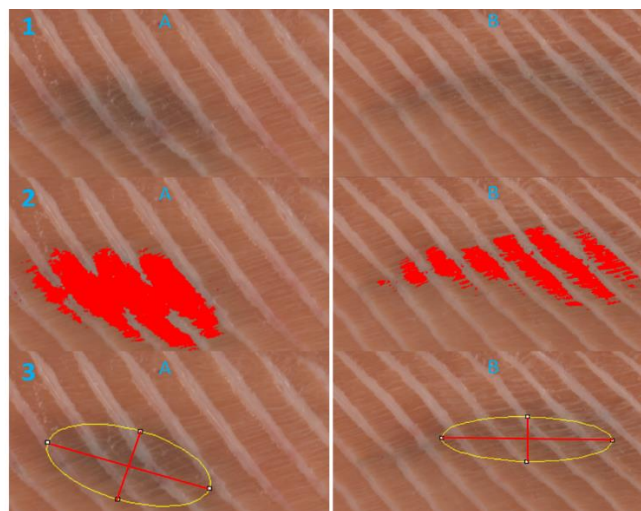


Figure 4.14. Morphologic analysis in discolored areas of ventral selection from two fish (A and B). Red areas represented the dark discolored pixels area (2), while red lines maximum length and width of the virtual ellipses (3).

4.2 In vitro study

4.2.1 Fish material and sampling

A 150-fish population of 100-120g Atlantic salmon post-smolts from Nofima, Sunndalsøra (Norway) were transported to VESO, Vikan (Norway) facilities, where they were divided into three equal groups in tanks and fed with three different diets for 10 weeks, from 31st of August to 9th of November to 500g.

The trial was performed with a stock density <math><40 \text{ Kg/m}^3</math> in seawater conditions at

In the end of the experiment, healthy fish were sedated in the tank with AQUI-S® (AQUI-S New Zealand Ltd., Lower Hutt, New Zealand), collected, and euthanised with benzocaine in a bath. Blood samples were taken from the caudal vein by using VACUTANINER® tubes with heparin. After inverting the tube five times for mixing both fractions, they were centrifuged at 3000 rpm for 10 minutes. Their supernatants were pooled together per treatment group and split by 1ml per Nunc™ tube (Thermo Fisher Scientific Inc., Waltham, United States) using sterile filter-tip pipettes, and placed immediately into liquid nitrogen at in vitro experiment (Table 4.3). Additionally, standard fetal bovine plasma (FBS) for *in vitro* cell lines was used for comparing.

Table 4.3. Setup for the *in vivo* and *in vitro* identification system. D0 and SSO used standard commercial diets.

		Test groups		
Diets (<i>In vivo</i>)		D0 (No krill inclusion)	DL (Low krill inclusion)	DH (High krill inclusion)
Plasmas (<i>In vitro</i>)	FBS (Fetal bovine serum)	SP0 (Salmon plasma with none krill inclusion)	SPL (Salmon plasma with low krill inclusion)	SPH (Salmon plasma with high krill inclusion)

4.2.2 Media preparation and cell culturing

SHK-1 cells (catalogue number 97111106 from the European Collection of Authenticated Cell Cultures), were cultivated following similar methods previously described (Dannevig et al., 1997), using the L-15 Medium (1X)+GlutaMAX™ -1 manufactured by Gibco™ (Thermo Fisher Scientific Inc., Waltham, Massachusetts, United States) supplemented with FBS (5%).

When cell cultures in Corning® flasks (Merck KGaA, Darmstadt, Germany) reached confluency (Figure 4.15. C), the splitting was performed according to the experiment set up. Then, by using a vacuum pipette, old medium was carefully extracted from the bottom of the initial growing container. Once the liquid content was drained, cells were washed with phosphate-buffered saline (PBS). It was important to insert the washing liquid carefully right over some inert sides to minimize cells removal. The liquid was aspirated just after washing steps, with special emphasis on the last one to avoid dilution effects of the trypsination with Trypsin-EDTA in a volume enough for covering the whole flask surface. After the reaction, new media was added to the flask for inhibiting the process. Media, FBS, PBS and other compounds as Trypsin-EDTA, were taken out before using them for several minutes, to get room temperatures avoiding thermic shock in cells.

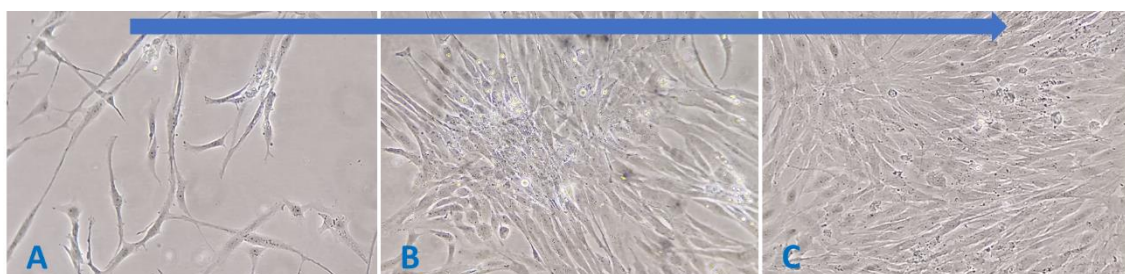


Figure 4.15. Evolution of the growing SHK-1 cell culture one day after splitting at 1:3 ratio with low cell confluency (A), at 4 days post-splitting with medium confluency (B), and 8 days post-splitting (C) with total confluency. The splitting ratio and the initial confluency level determined the number of days for next confluency level on the flask. The magnified images were taken at 10x with an inverted microscope.

4.2.3 Cell stimulation assay

Based on an *in vitro* plasma incubation model (Seierstad et al., 2009), each well of 2x 24 well-plates was filled up of new media with different serum or plasma supplementations; FBS at 5%, SP0, SPL, and SPH at 2%. Once plates were completed, they were kept at incubation temperature at 20°C for 48 hours (until confluency) (Figure 4.16).

Then, as basic immunomodulators, 16x 20 μ l of lipopolysaccharides from *Escherichia coli* (LPS) (L4391-1MG) (20 μ g/ml), and β -1,3-Glucan from *Euglena gracilis* (89862-1G-F) (20 μ g/ml) (Merck KGaA, Darmstadt, Germany) were added to their specific well per serum/plasma plate conditioning (Figure 4.16). After stimulation, the plates were incubated at 20°C for 73 days (until 75 days post-splitting). Pictures were taken at 8, 11, 21, 41 and 75 days post-splitting. Additionally, at 41 days the cells from one plate were harvested for transcriptomics.

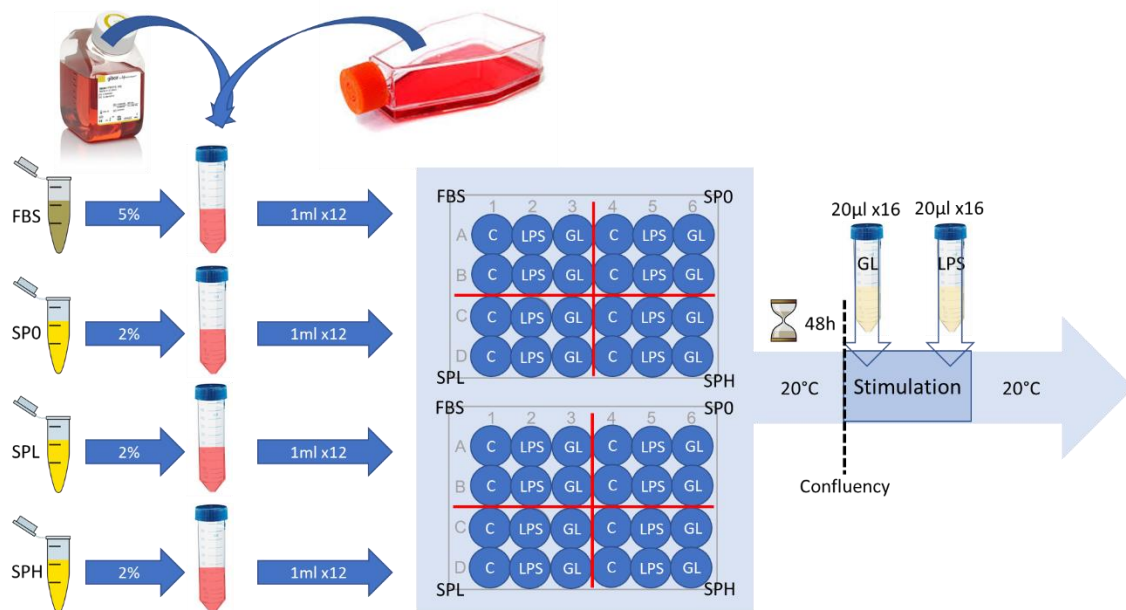


Figure 4.16. Illustration of the *in vitro* assay for all serum/plasma conditioning: FBS, SP0, SPL and SPH. The stimulation with lipopolysaccharides (LPS), and β -glucans (GL) were also represented after 48 hours post-splitting. The blue wells represented the position of none stimulant (C), LPS and GL and their parallels on the 24 well plates. Notice that all plates followed the incubation temperature after the stimulation.

4.2.4 Microscopy

Two inverted microscopes were used; the optical Elipse[®] model TS100 (Nikon Corporation, Tokyo, Japan) for culture controlling and the digital OLYMPUS[®] model IX81 (Olympus Corporation, Shinjuku, Japan) with a digital camera ColorView[®] model U-CMAD3 (Olympus Corporation, Shinjuku, Japan). The chosen conditions for the digital pictures were 10.6 zoom, 55.58ms of exposure time, with 7.2db of grain and PH as observation method with 7.6V of light intensity.

4.2.5 Image analysis method

A simple image analysis method was developed for replicating the visual quantification of melanin pigment clustered as melanosomes (Haugarvoll et al., 2006). The fact that the FBS conditioning presented aberrant cell morphologies, most of the visual melanosomes differences were at plasma level, and the stimulation with lipopolysaccharides and specially β -glucans showed floating material that could potentially disturb the measurements, gave reasons to exclude those pictures from the method. Additionally, the highly crowded were the cells, the more difficult was to quantify those structures. Thus, the visual quantification was carried at day 8 post-splitting when cell confluency was not extremely high. Thus, every picture was divided into 25 equal partitions, and melanosomes (Figure 4.17. Black arrow) from 6 constant selections (Figure 4.17. White squares) were visually counted, excluding big size particles (Figure 4.17. Blue cross).

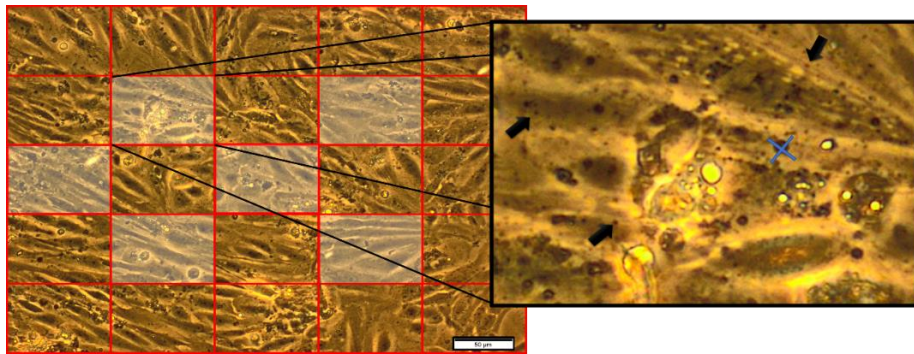


Figure 4.17. Picture processing for melanosome quantification in SHK-1 cell cultures at day 8 post-splitting. To the left, an original picture (taken at 10x with an inverted microscope) divided into 25 equal sections, which 6 constant white rectangles were selected. To the right, zoom on one of white selection where true (black arrows) and false melanosomes (blue cross) can be observed.

To get the automatic approximation for quantifying melanosomes in pictures partitions (Figure 4.17. White squares), the extracted values from visual countings were compared with respective maximum dark values at different levels of noise tolerance until matching each other. Thus number 15 got the best approximation to the manually calculated values (Figure 4.18. Blue dots) from the 6 partitions of every cell conditioning type at day 8 post-splitting. Once, the tolerance value was defined, the method was also tested in partitions for every treatment at day 11, and 21. Given the large amount of floating material on pictures at 41 days post-splitting, they were excluded from the automated measurements.

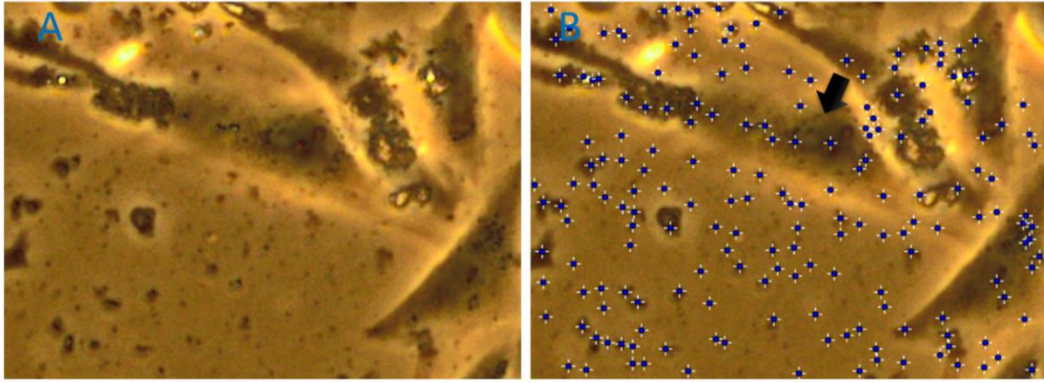


Figure 4.18. Illustration of automated dot counting in SHK-1 cell cultures. (A) represented a normal partition using the post-processing from Figure 4.17. (B) Picture selection after maxima detection (blue dots) treatment at number 15 of noise tolerance. Some dots may not be detected by the system given by their local environment of low contrast (black arrow), but generally, they match with visually counted dots considered as melanosomes. The magnified images were taken at 10x with an inverted microscope.

4.2.6 Transcriptomics

4.2.6.1 RNA isolation

At day 41 post-splitting, every well from the 4 different plasmas (FBS, SP0, SPL and SPH) was washed twice with a PBS solution, harvested with a cell scraper and stored into Eppendorf tubes with 350µl Reverse Transcriptase Lysis (RTL) buffer containing β -2-mercaptoethanol from RNeasy[®] Mini Kit (Qiagen, Hilden, Germany) at -80°C until analysed according to the manufacturer protocol. Total RNA was isolated from all samples by using the RNeasy[®] Mini Kit according to the manufacturer protocol.

4.2.6.2 cDNA synthesis

After RNA isolation and genomic DNA elimination from our samples, the synthesis of complementary DNA (cDNA) or reverse transcription was carried by using 600ng of total RNA per sample utilising the Transcriptor First Strand cDNA Synthesis Kit (Roche Molecular Systems, Inc., Pleasanton, United States) according to the protocol for random hexamer primed cDNA synthesis.

Firstly, prior using the kit components, they were denatured at 65°C for 5 minutes. After that, the program for the reverse transcription PCR consisted in 1 hour at 50°C followed by final heating of 15 minutes at 70°C using the Peltier Thermal Cycler DNA Engine[®] (Bio-Rad Laboratories, Inc., Hercules, United States,).

4.2.6.3 Real-time polymerase chain reaction (RT-PCR)

The RT-PCR was carried out by using the Tyr and Dct primers (Table 4.4) and LightCycler[®] 480 SYBR Green I master (Roche Molecular Systems, Inc., Pleasanton, United States), on the LightCycler[®] 96 (Roche Molecular Systems, Inc., Pleasanton, United States). All amplifications were performed in duplicate 10 reactions using 5 μ l SYBR Green, 2 μ l water, 0.5 μ l of each primer, 2 μ l enzyme mix and 2 μ l of cDNA template. The chosen program for the RT-PCR was 95 °C for 10 minutes followed by 40 cycles of 95 °C for 10 seconds and 72 °C for 10 seconds. The results were extracted from the LightCycler[®] 96 as cyclic threshold (Ct). The relative quantification of those Ct was carried by using the $\Delta\Delta$ Ct method (Livak & Schmittgen, 2001), using β -actin as endogenous control, and untreated control cells from the PBS conditioning as a regulation reference.

Table 4.4. Used real-time PCR primers for the relative gene expression of tyrosinase (Tyr), dopachrome tautomerase (Dct) on SHK-1 cells from FBS, SP0, SPL and SPH groups.

Genes	Forward primer (5'-3')	Reverse primer (5'-3')	GeneBank N ^o
β -actin ^a	CCAGTCCTGCTCACTGAGGC	GGTCTCAAACATGATCTGGGTCA	AF012125
Tyr ^a	CTGGGCTACGAATACTCCTACCT	TGCATGTAGGGAGTCAGGAACT	DQ408549
Dct ^a	TCTCACTCTGCAGCCAATGAC	CAGACTTCCTCATCCACTCATCAA	DQ339140

^aPrimers were supplied by Assays-by-DesignSM service (Thermo Fisher Scientific Inc., Waltham, Massachusetts, United States) (Larsen et al., 2013).

4.3 Statistics

Normally distributed data was statistically analyzed by the one-way analysis of variance (ANOVA) and two tails t-test for unpaired comparisons among three groups (D0/SP0, DL/SPL, DH/SPH). Chi-square test was used for categorical variables. In case of non-normally distributed data or those skewed values above the ± 2 limit (George and Mallery, 2010), the Kruskal-Wallis test and Mann-Whitney U-test were used. The alpha level was set to 5% ($P \leq 0.05$).

The elected software's for this data analysis and calculations were Microsoft[®] Excel[®] (16.0.8431.2110, Microsoft Corporation, Redmond, United States), Statistical Analysis Software (SAS[®]) (version, SAS Institute Inc., Cary, United States), Python[®] (3.6.4, Python Software Foundation, Delaware, United States), and RStudio[®] (3.4.4, RStudio, Boston, United States), under Anaconda[®] navigator (5.1, Anaconda, Inc, Austin, United States).

5 RESULTS

5.1 In vivo

5.1.1 General

The body weight of salmon fed with the DL diet was significantly higher (5000g) compared with those fed using the D0 (4402g; $P=0.0023$) or DH (4032g; $P<0.0001$) treatment. The body weight of the D0 and DH groups did not differ significantly ($P=0.0559$) (Table 5.1). The variation among fish within dietary groups corresponded with a coefficient of variation of 13%, 17% and 20% for the D0, DL, and DH diets, respectively. The body length showed similar variation among the dietary groups as the body weight (Table 5.1).

Abnormal vertebrae were observed for all dietary fish groups; D0 17%, DL 13%, and DH 31% of the fish sampled with non-significant differences ($P=0.2289$) (Table 5.1). The position of the abnormal vertebrae was consistent from vertebra #11–26, counted from the cranial part of the fillet. The highest prevalence was observed from vertebra #20–22.

Table 5.1. Mean values \pm standard errors for body weight, length, and affected fish with abnormal vertebrae in D0, DL and DH groups.

Parameters	D0	DL	DH	P-value	R ²
Body weight (g)*	4402 \pm 137 ^b	5000 \pm 117 ^a	4032 \pm 149 ^b	<0.0001	0.2316
Body length (cm)	69 \pm 0.6 ^b	73 \pm 0.8 ^a	68 \pm 0.8 ^b	<0.0001	0.2289
Affected fish (%)	17 ^a	13 ^a	31 ^a	0.2289	.

P-values shows significant levels ($P\leq 0.05$). Different superscripts represent significant differences ($P\leq 0.05$) between dietary groups. Variation described by the dietary treatment model as the coefficient of determination (R^2). *Body weight equals fish round weight (whole fish).

The general muscle L^* value (lightness) was significantly higher of the DL (53.81 \pm 0.23) compared with the D0 (53.09 \pm 0.24; $P=0.0489$) and DH (52.99 \pm 0.30; $P=0.0387$) that were similar ($P=0.6880$) (Table 5.2). The general a^* value (redness) was not significantly different among the groups ($P=0.6415$). The general b^* value (yellowness) of the DL group (22.24 \pm 0.15) was significantly lower compared with the D0 (22.79 \pm 0.18; $P=0.0271$), while the DH group (22.71 \pm 0.20) did not statistically differ from D0 ($P=0.7789$) or DL ($P=0.0683$) (Table 5.2).

The statistical model including the dietary treatment, body weight, and abnormal vertebras, showed significant differences in parameters as the condition factor ($P=0.0051$), and general b^* value ($P=0.0180$).

Significant correlations were found between the values from SalmoColour Fan™ and general L^* value (-0.40 ; $P<0.0001$), general a^* value (0.56 ; $P<0.0001$), and general b^* value (0.43 ; $P<0.0001$).

Table 5.2. Means and standard errors of D0, DL and DH groups over slaughter and general image analysis parameters.

Parameters		D0	DL	DH	P-value	R ²
Slaughter	Condition factor ¹	1.30±0.02 ^a	1.29±0.03 ^a	1.28±0.02 ^a	0.5827	0.1673
	SalmoColour Fan	25.0±0.2 ^a	25.2±0.2 ^a	25.5±0.2 ^a	0.4924	0.0804
General image analysis	General L^* value	53.1±0.2 ^b	53.8±0.2 ^a	53.0±0.3 ^b	0.0526	0.0711
	General a^* value	20.8±0.2 ^a	20.6±0.2 ^a	20.5±0.3 ^a	0.6415	0.0322
	General b^* value	22.8±0.2 ^a	22.2±0.2 ^b	22.7±0.2 ^{ab}	0.0753	0.1368

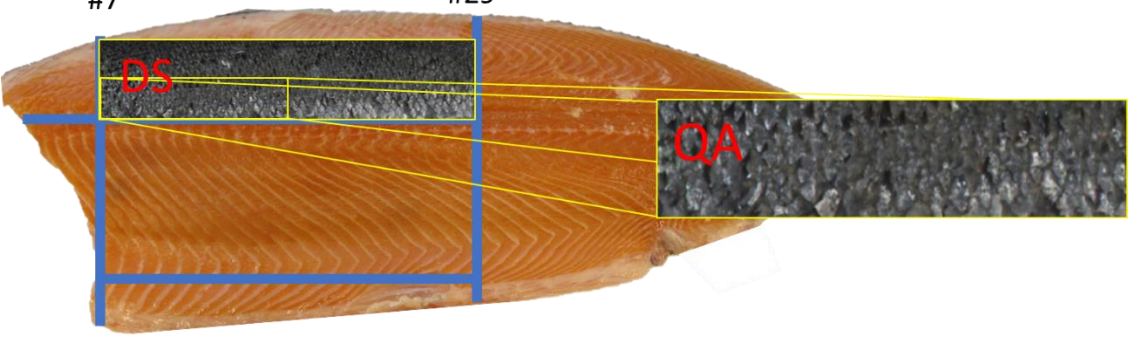
P-values shows significant levels ($P\leq 0.05$). Different superscripts represent significant differences ($P\leq 0.05$) between groups. Variation described by the dietary treatment model as the coefficient of determination (R^2). ¹ Condition factor = $\frac{\text{Round body weight (g)} \times 100}{(\text{Fish length (cm)})^3}$

5.1.2 Skin

In the dorsal skin cut, the general L^* value was statistically lower in the DL (33.2 ± 0.4 ; $P=0.0414$) and DH (33.2 ± 0.5 ; $P=0.0484$) groups compared to D0 (34.4 ± 0.4). The DL and DH did not statistically differ from each other ($P=0.9599$) (Table 5.3) The general a^* value of the DH group (-0.3 ± 0.0) was significantly lower compared with the D0 (-0.1 ± 0.0 ; $P=0.0022$) and DL (-0.1 ± 0.0 ; $P=0.0423$) groups. Statistical differences between D0 and DL were not observed ($P=0.1706$) (Table 5.3 and Figure 5.1). The general b^* value was significantly lower of the DL group (0.1 ± 0.2) than D0 (0.6 ± 0.1 ; $P=0.0056$) and DH (0.4 ± 0.1 ; $P=0.0365$), but no significant differences were found between the D0 and DH groups, ($P=0.4916$) (Table 5.3 and Figure 5.1).

Regarding the quarter A parameters, the general a^* value was significantly higher in D0 (-0.0 ± 0.0 ; $P=0.0057$) and DL groups (-0.1 ± 0.1 ; $P=0.012$) compared to DH (-0.2 ± 0.1). The D0 and DL groups did not statistically differ ($P=0.6243$) (Table 5.3 and Figure 5.2). Therefore, the general b^* value was significantly higher in D0 group (0.4 ± 0.1) than DL (-0.0 ± 0.2 ; $P=0.0354$). However, DH (0.4 ± 0.2) group did not significantly differ from D0 ($P=0.7233$) and DL ($P=0.0814$) (Table 5.3 and Figure 5.2).

Table 5.3. Means and standard errors for colorimetric and morphometric parameters of the dorsal selections (DS) and quarter A (QA) depending on dietary groups: D0, DL, and DH.



	Parameters	D0	DL	DH	P-value	R ²	
DS	Colorimetric values						
	General L* value	34.4±0.4 ^a	33.2±0.4 ^b	33.2±0.5 ^b	0.0679	0.061	
	General a* value	-0.1±0.0 ^a	-0.1±0.0 ^a	-0.3±0.0 ^b	0.0078	0.107	
	General b* value	0.6±0.1 ^a	0.1±0.2 ^b	0.4±0.1 ^a	0.0155	0.092	
QA	Colorimetric values						
	General L* value	37.2±0.3 ^a	36.6±0.5 ^a	36.3±0.5 ^a	0.3522	0.024	
	General a* value	-0.0±0.0 ^a	-0.1±0.1 ^a	-0.2±0.1 ^b	0.013	0.096	
	General b* value	0.4±0.1 ^a	-0.0±0.2 ^b	0.4±0.2 ^{ab}	0.0792	0.057	
	Super-dark pixels L* value	13.5±0.1 ^{ab}	13.4±0.1 ^b	13.7±0.1 ^a	0.0537	0.066	
	Super-dark pixels a* value	1.1±0.0 ^a	1.0±0.0 ^b	0.9±0.0 ^b	0.0043	0.119	
	Super-dark pixels b* value	-0.4±0.1 ^a	-0.5±0.1 ^a	-0.3±0.1 ^a	0.19	0.038	
	Dark pixels L* value	20.6±0.1 ^a	20.6±0.1 ^a	20.6±0.1 ^a	0.798	0.005	
	Dark pixels a* value	0.6±0.1 ^a	0.5±0.1 ^{ab}	0.4±0.1 ^b	0.0825	0.056	
	Dark pixels b* value	0.6±0.1 ^a	0.4±0.1 ^a	0.6±0.9 ^a	0.1326	0.046	
	Background dark pixels L* value	35.3±0.2 ^a	34.9±0.2 ^a	35.2±0.2 ^a	0.1823	0.039	
	Background dark pixels a* value	-0.0±0.0 ^a	-0.0±0.0 ^a	-0.2±0.1 ^b	0.0058	0.113	
	Background dark pixels b* value	0.5±0.1 ^a	-0.1±0.2 ^b	0.4±0.2 ^a	0.0391	0.073	
	Light pixels L* value	54.6±0.3 ^a	54.3±0.4 ^a	53.9±0.3 ^a	0.2467	0.032	
	Light pixels a* value	-0.4±0.1 ^a	-0.6±0.1 ^{ab}	-0.7±0.1 ^b	0.0983	0.053	
	Light pixels b* value	0.3±0.1 ^a	-0.1±0.3 ^a	-0.9±0.2 ^a	0.4427	0.019	
		Morphometric values					
		Super-dark pixels area (%)	2.8±0.3 ^a	3.5±0.3 ^a	3.4±0.4 ^a	0.1991	0.037
		Visual dot number	38±3 ^a	44±3 ^a	40±3 ^a	0.1447	0.044
		Approximated dot number	45±3 ^b	57±4 ^a	49±3 ^{ab}	0.0476	0.068
		Dot average size (%)	89±2.2 ^a	89.6±2.2 ^a	94.3±5.5 ^a	0.5367	0.019
	Dot circularity ¹	0.5±0.0 ^a	0.5±0.0 ^a	0.5±0.0 ^a	0.71	0.01	
	Dot solidity ²	0.8±0.0 ^a	0.8±0.0 ^a	0.8±0.0 ^a	0.4327	0.025	
	Dark pixels area (%)	7.3±0.6 ^b	8.4±0.5 ^{ab}	9.1±0.7 ^a	0.133	0.045	
	Total darkest pixels area (%)	10±0.8 ^a	11.9±0.8 ^a	12.4±1 ^a	0.1256	0.047	
	Background dark pixels area (%)	72.7±0.9 ^a	70.7±1 ^a	71.7±1.1 ^a	0.3367	0.025	
	Total dark pixels area (%)	82.8±0.8 ^a	82.6±1.3 ^a	84.1±1.3 ^a	0.575	0.013	
	Light pixels area (%)	17.2±0.8 ^a	17.4±1.3 ^a	15.9±1.3 ^a	0.575	0.013	

P-values shows significant levels (P≤0.05). Different superscripts represent significant differences (P≤0.05) between groups. Variation described by the dietary treatment model as the coefficient of determination (R²). ¹ $Circularity = \frac{4 \cdot \pi \cdot Area}{(Perimeter)^2}$ ² $Solidity = \frac{Area}{Convex\ area}$

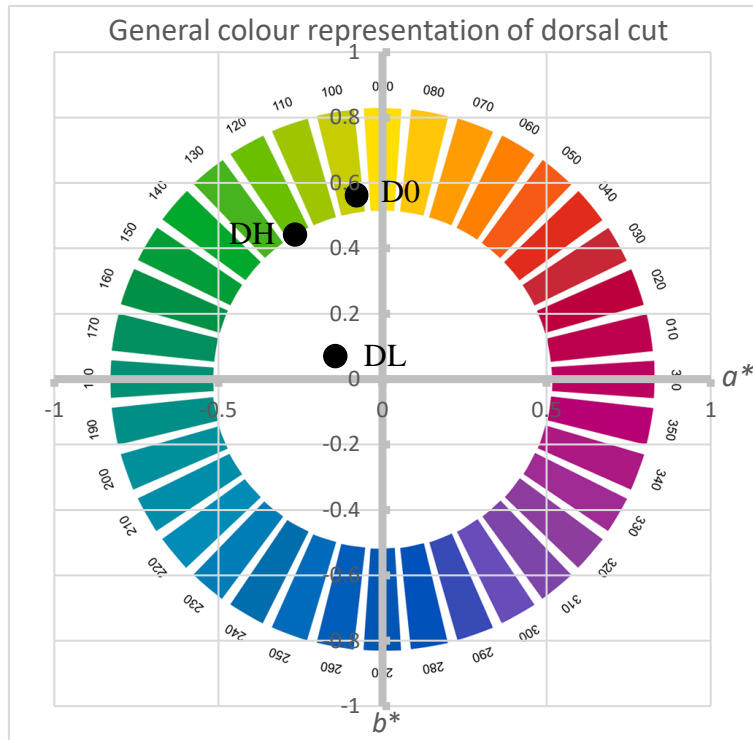


Figure 5.1. General color appearance of the dorsal selections of D0, DL, and DH groups illustrated by a^* b^* dimensions. Color wheel shows the angle of the chroma.

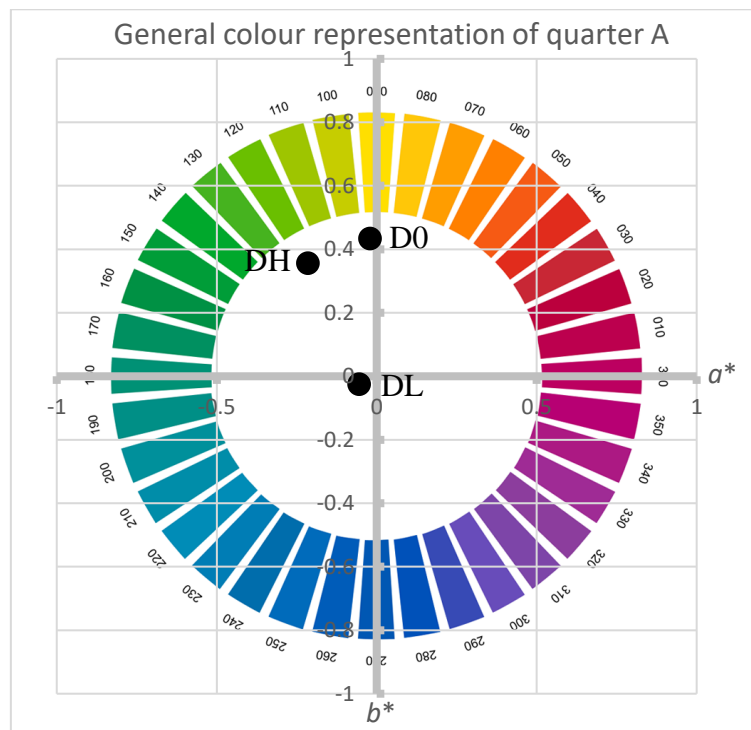


Figure 5.2. General color appearance of the quarter A's of D0, DL, and DH groups illustrated by a^* b^* dimensions. Color wheel shows the angle of the chroma.

The super-dark pixels color appearance had a higher L^* value that differed significantly between the DH group (13.7 ± 0.1) compared to DL (13.4 ± 0.1 ; $P=0.0161$), while D0 (13.51 ± 0.08) units did not significantly differ from DL ($P=0.2779$) and DH ($P=0.1733$) (Table 5.3). The super-dark pixels a^* value in the D0 group (1.1 ± 0.0) was significantly higher compared to DL (1.0 ± 0.0 ; $P=0.0514$) or DH groups (0.9 ± 0.0 ; $P=0.0011$). However, the DL and DH a^* values were not statistically different ($P=0.1557$) (Table 5.3). The approximated dot number in the DL (57 ± 4) was significantly higher of the D0 group (45 ± 3 ; $P=0.0171$), while DH (49 ± 3) did not differ to the D0 ($P=0.5136$) and DL ($P=0.0828$) groups (Table 5.3 and Figure 5.3).

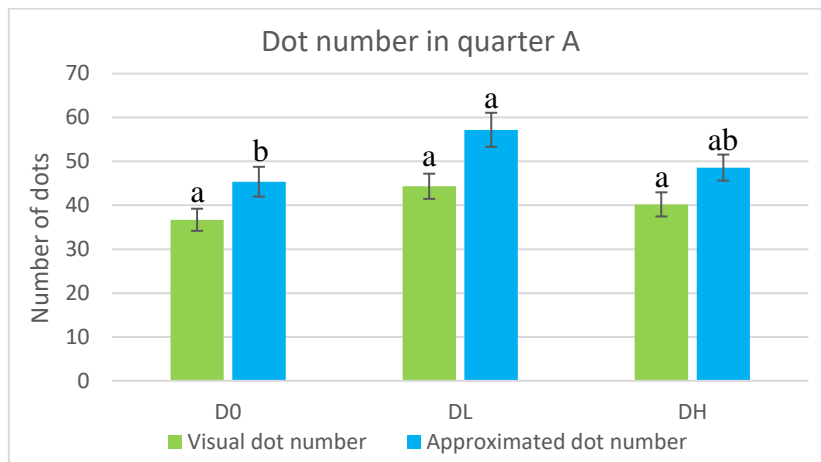


Figure 5.3. Comparison of visual and approximated dot number mean and standard errors in quarter A for the dietary groups: D0, DL, and DH. Different letters above the error bars represent significant differences ($P\leq 0.05$) between groups.

The relative dark pixels area was found significantly higher in the DH group ($9.1\pm 0.7\%$) compared to the D0 group ($7.3\pm 0.6\%$; $P=0.0478$). In contrast, DL ($8.4\pm 0.5\%$) did not vary significantly compared with the D0 ($P=0.2069$) or DH ($P=0.4573$) groups. The dark pixels a^* value of the relatively dark pixels area was found significantly higher in D0 (0.6 ± 0.1) than DH group (0.4 ± 0.1 ; $P=0.0259$). The DL group (0.5 ± 0.05), did not differ significantly from the D0 ($P=0.2585$) and DH ($P=0.2578$) groups (Table 5.3). The background dark pixels a^* value was found significantly higher in the D0 (-0.0 ± 0.0 ; $P=0.0030$), and DL group (-0.0 ± 0.01 ; $P=0.0099$) in comparison to DH (-0.2 ± 0.1) (Table 5.3). The background dark pixels b^* value was significantly higher in the D0 (0.5 ± 0.1 ; $P=0.0210$), and DH groups (0.4 ± 0.2 ; $P=0.0370$) when comparing them with the DL (-0.1 ± 0.2). No statistical differences were found between D0 and DH groups ($P=0.8323$) (Table 5.3).

The a^* value of the light pixels partition was found significantly higher in D0 (-0.4 ± 0.1) than DH group (-0.7 ± 0.1 ; $P=0.0332$). The DL group (-0.6 ± 0.1) did not statistically differ from D0 ($P=0.1897$) or DH groups ($P=0.395$) (Table 5.3).

Significant correlations were found between the visual dot number and the general a^* value (0.29 ; $P=0.0062$), general b^* value (0.24 ; $P=0.0263$), super-dark pixels area (%) (0.52 ; $P<0.0001$), and approximated dot number (0.62 ; $P<0.0001$) (Appendix D). Moreover, the approximated dot number did significantly correlate with the super-dark pixels area (%) (0.80 ; $P<0.0001$) (Appendix D).

Based on observation during sampling, picture collection and other previous studies (Bagnara & Hadley, 1973; Bullock & Roberts, 1974; Fujii, 1993b; Grether et al., 2004; Ito et al., 2000; Kelley & Davies, 2016; Mahalwar et al., 2016; Palazzo et al., 1989), a diagram was created for simplifying the interpretation of the salmon skin appearance described in this chapter (Figure 5.4).

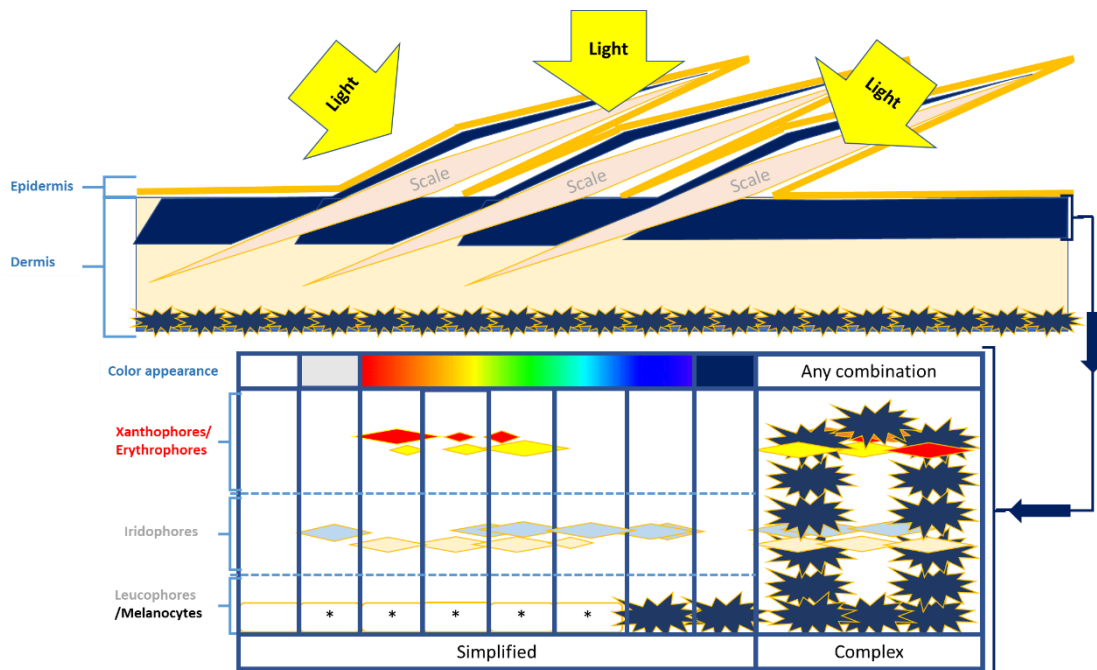


Figure 5.4. Representation of the light-related interaction among pigmentary cells in the salmon skin. These cells are located in the dermis below the basement membrane at the epidermis (dark blue area) and at basal level of the dermis (just melanocytes). They are simplified structured in 3 different layers, from the upper to bottom xanthophores or erythroophores, iridophores and leucophores or melanocytes. Nevertheless, they may follow a different and complex pattern where melanocytes get inversed between iridophores and xanthophores/erythroophores. General color appearance can be described by the combination of these 3 cell types. Notice that the direction of the light source may modify the reflexion of light by the iridophores from silver blue to yellow-like reflex, which may affect the final color appearance (Bagnara & Hadley, 1973; Bullock & Roberts, 1974; Fujii, 1993b; Grether et al., 2004; Ito et al., 2000; Kelley & Davies, 2016; Mahalwar et al., 2016; Palazzo et al., 1989). *The presence of melanocytes would increase the darkness of the resulting color appearance.

5.1.3 Muscle

Information from other authors (Aursand et al., 1994; Bæverfjord & Rye, 1994; Roberts, 2012) and observations from sampling times were used for illustrating and describing the basic anatomy of salmon skeleton and muscle. The ventral selection used for the discoloration analysis of fillets were also represented, which coincided with the highest prevalence area for “dark spots” (Figure 5.5 and Figure 5.6) (Mørkøre, 2012; Mørkøre, 2017).

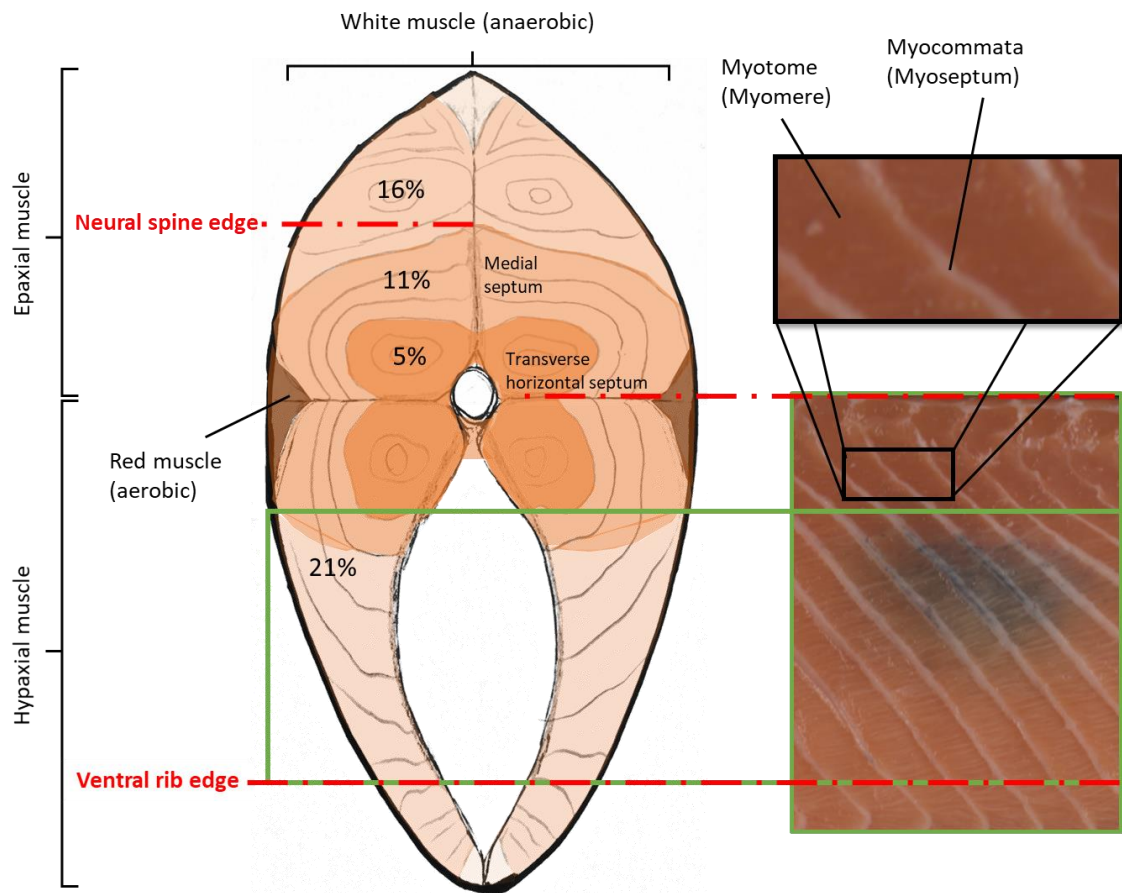


Figure 5.5. Topographic diagram of a transversal cut for a commercial size Atlantic salmon at vertebra number 21 approximately. Main anatomical parts are described as well the ventral hypaxial region where 94% of dark spots occurs (green selection) (Aursand et al., 1994; Bæverfjord & Rye, 1994; Marty-Mahé et al., 2004; Mørkøre, 2012; Mørkøre, 2017).

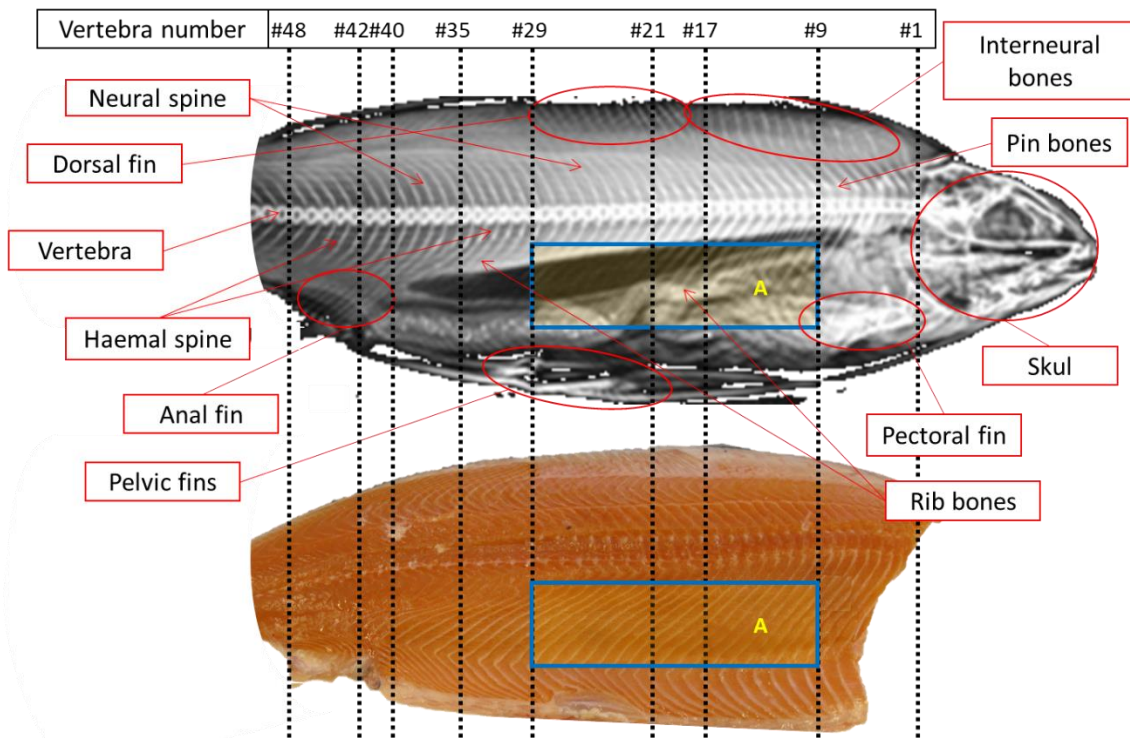


Figure 5.6. Topographic diagram for x-ray picture of an Atlantic salmon fish (top) and fillet (bottom). Main bones are identified on the x-ray diagram, and their topographic location was represented on the fillet. The A selection (blue) represented the area where 94% of dark spots are located (Mørkøre, 2012; Mørkøre, 2017; Roberts, 2012).

Regarding the general descriptive and comparative colorimetric study, a decreasing trend for L^* , a^* , and b^* values were observed affected in small, medium and large black spots areas (Figure 5.7 and Figure 5.8). The larger the discoloration; the larger was this difference. Most of the colorimetric differences from medium to large size were given by a^* and b^* channels (Figure 5.7 and Figure 5.8). The red discoloration was characterized by a smaller a^* value than b^* , and most of the difference was given by a reduction in the L^* and b^* channels, being the a^* value poorly modified. The L^* values remained similar between medium, large dark and red spots (Figure 5.7 and Figure 5.8).

The discoloration analysis showed significantly higher general L^* value of the whole working selection in the DL group (53.8 ± 0.2) than D0 (53.1 ± 0.2 ; $P=0.0338$) or DH (53.0 ± 0.3 ; $P=0.033$) (Table 5.4). No significant differences were observed between the D0 and DH ($P=0.7986$). The b^* was significantly lower value in the DL (22.2 ± 0.2) group about the D0 (22.8 ± 0.2) ($P=0.0271$), but not between DH (22.7 ± 0.2) and D0 ($P=0.7798$) or DL ($P=0.0683$) (Table 5.4).

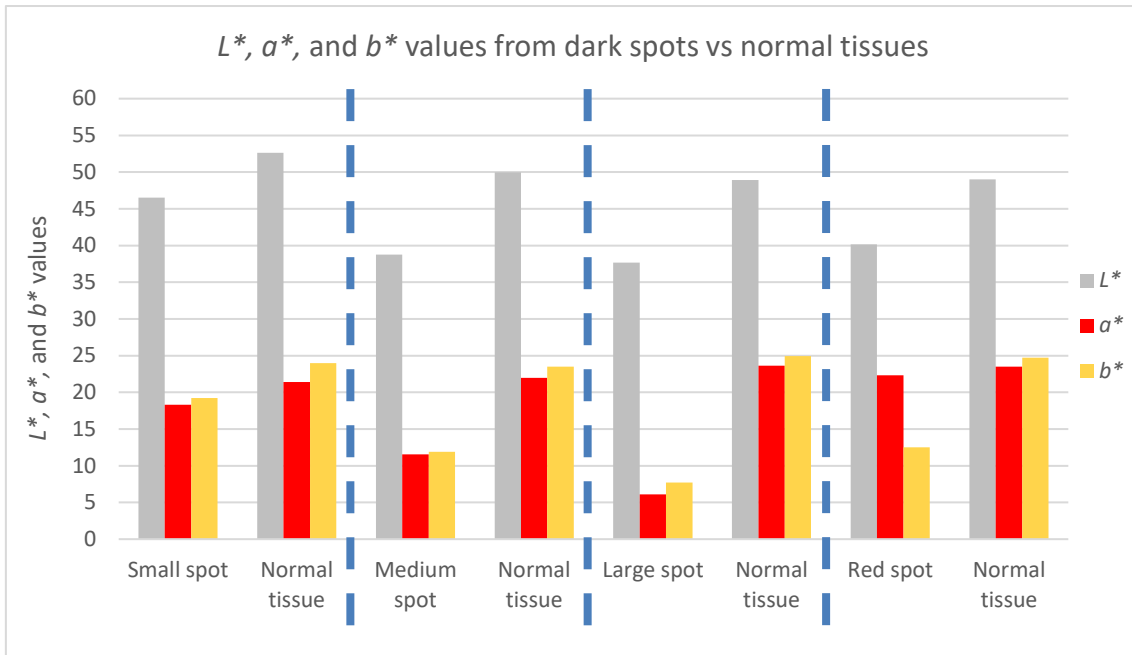


Figure 5.7. Colorimetric L^* , a^* , and b^* values from small, medium, and large black spots and red spot compared to their respective normal tissue in fillets.

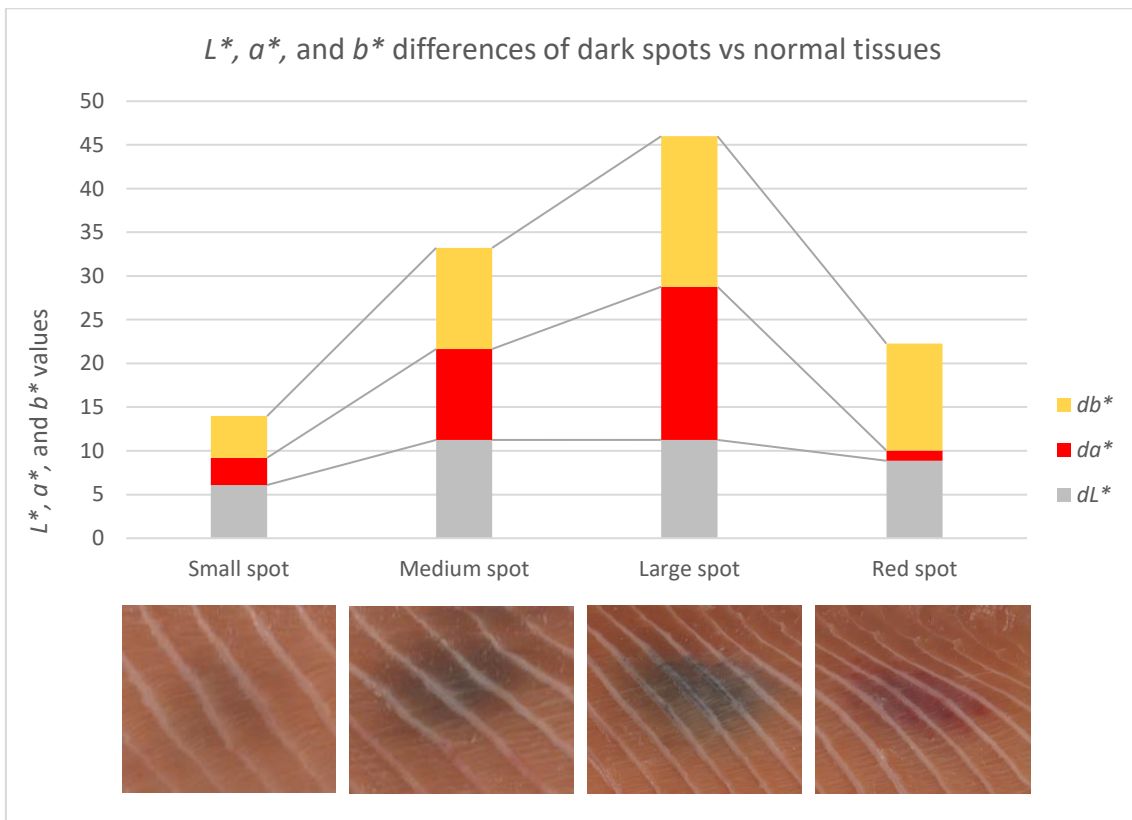


Figure 5.8. Colorimetric L^* , a^* , and b^* differences (d) from small, medium, and large black spots and red spot expressed as reduction compared with their normal tissue areas.

The visual inspection of the discolorations number (P=0.8629) and length (mm; P=0.6165 and %; P=0.7309) did not show any significant differences among treated groups (Table 5.4 and Table 5.5). Significant differences were not observed (P=0.8747) when disclosing the visual discoloration number by the percentage of fish with 0, 1, 2 or 3 spots per treated group. Therefore, the 43%, 50%, and 47% of right fillet from the D0, DL and DH groups respectively were affected by any number of discolored areas or spots (Figure 5.9).

Table 5.4. Means and standard errors for discoloration parameters from ventral selection depending on dietary groups: D0, DL, and DH.

Parameters	D0	DL	DH	P-value	R ²
Colorimetric values					
General L* value	53.1±0.2 ^b	53.8±0.2 ^a	53.0±0.3 ^b	0.0526	0.314
General a* value	20.8±0.2 ^a	20.6±0.2 ^a	20.5±0.3 ^a	0.6415	0.016
General b* value	22.8±0.2 ^a	22.2±0.2 ^b	22.7±0.2 ^{ab}	0.0753	0.042
Light discolored pixels L* value	45.8±0.3 ^a	45.7±0.3 ^a	45.6±0.3 ^a	0.8521	0.06
Light discolored pixels a* value	22.2±0.6 ^a	22.7±0.5 ^a	22.6±0.6 ^a	0.8221	0.097
Light discolored pixels b* value	23.1±0.5 ^a	22.5±0.4 ^a	23.7±0.5 ^a	0.1978	0.003
Dark discolored pixels L* value	43.6±0.4 ^a	43.4±0.5 ^a	44.4±0.4 ^a	0.4032	0.175
Dark discolored pixels a* value	17.3±0.6 ^a	19.3±0.9 ^a	17.7±0.6 ^a	0.3073	0.168
Dark discolored pixels b* value	18.2±0.7 ^a	18.7±0.5 ^a	18.4±0.6 ^a	0.8862	0.111
Low-dark discolored pixels L* value	43.9±0.4 ^a	43.6±0.4 ^a	44.6±0.4 ^a	0.4529	0.042
Low-dark discolored pixels a* value	17.6±0.6 ^a	19.5±0.9 ^a	17.8±0.6 ^a	0.3043	0.153
Low-dark discolored pixels b* value	18.3±0.7 ^a	18.9±0.5 ^a	18.5±0.6 ^a	0.8657	0.131
Medium-dark discolored pixels L* value	37.8±0.1 ^a	37.6±0.3 ^a	37.4±0.2 ^a	0.913	0.061
Medium-dark discolored pixels a* value	15.4±0.3 ^a	12.9±0.3 ^a	13.7±0.2 ^a	0.1504	0.032
Medium-dark discolored pixels b* value	15.6±0.3 ^a	11.8±0.3 ^b	15.0±0.3 ^{ab}	0.0587	0.101
High-dark discolored pixels L* value
High-dark discolored pixels a* value
High-dark discolored pixels b* value
Morphometric values					
Visual discoloration number	1±0 ^a	1±0 ^a	1±0 ^a	0.8629	0.114
Visual discoloration length (mm)	16.7±4.7 ^a	18.6±4.3 ^a	12.9±3.4 ^a	0.6165	0.176
Visual discoloration length (%)	8.9±2.5 ^a	9.4±2.2 ^a	7.1±1.9 ^a	0.7309	0.113
Light discolored pixels area (%)	1.6±0.5 ^a	0.7±0.2 ^a	1.5±0.5 ^a	.	.
Super-light red discolored pixels area (%)	0.2±0.0 ^a	0.4±0.1 ^a	0.2±0.1 ^a	.	.
Super-light red discolored pixels number	6±1 ^b	11±2 ^a	6±1 ^{ab}	0.0495	0.109
Dark discolored pixels area (%)	0.6±0.2 ^a	0.2±0.1 ^a	0.7±0.3 ^a	.	.
Dark discolored pixels circularity ¹	0.8±0.0 ^a	0.5±0.1 ^b	0.6±0.1 ^{ab}	0.0868	0.183
Dark discolored pixels aspect ratio ²	3.3±0.7 ^a	6.4±1.0 ^a	10.8±2.9 ^a	.	.
Dark discolored pixels length (%)	16.0±3.6 ^a	12.2±2.1 ^a	15.8±3.2 ^a	0.7593	0.075
Dark discolored pixels width (%)	0.0±0.0 ^a	0.0±0.0 ^a	0.0±0.0 ^a	0.336	0.103
Dark discolored and light pixels area (%)	2.1±0.7 ^a	0.9±0.3 ^a	2.2±0.7 ^a	.	.
Low-dark discolored pixels area (%)	0.5±0.2 ^a	0.2±0.1 ^a	0.6±0.3 ^a	.	.
Medium-dark discolored pixels area (%)	0.0±0.0 ^a	0.0±0.0 ^a	0.1±0.1 ^a	.	.
High-dark discolored pixels area (%)	0 ^a	0 ^a	0 ^a	.	.
Dark cloudy discolored pixels area (%)	0.1±0.0 ^a	0.0±0.0 ^a	0.1±0.1 ^a	.	.

P-values shows significant levels (P≤0.05). Different superscripts represent significant differences (P≤0.05) between groups. Variation described by the dietary treatment model as the coefficient of determination

$$(R^2). \text{ } ^1 \text{Circularity} = \frac{4 \cdot \pi \cdot \text{Area}}{(\text{Perimeter})^2} \text{ } ^2 \text{Aspect ratio} = \frac{\text{Major axis}}{\text{Minor axis}}$$

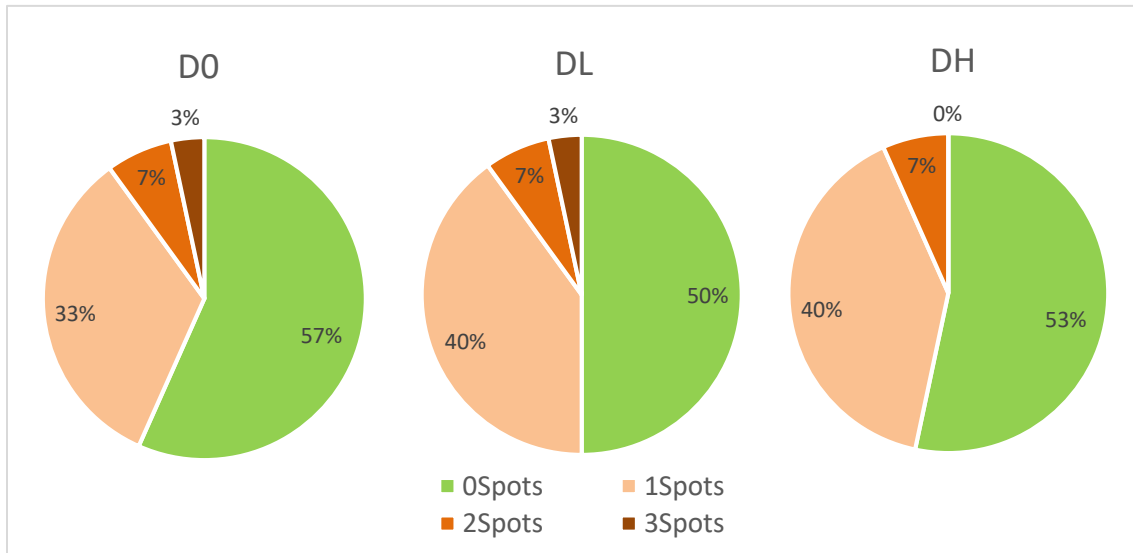


Figure 5.9. Percentage of fish with 0, 1, 2 or 3 visual discolored areas (spots) per treated group: D0, DL, and DH. Notice that differences were not significant ($P \leq 0.05$).

Table 5.5. Skewness for discoloration parameters with challenging data distributions from ventral selection depending on dietary groups: D0, DL, and DH.

Parameters	Skewness			P-value
	D0	DL	DH	
Visual discoloration number	1.4	1.3	0.8	.
Visual discoloration length (mm)	1.8	1.2	1.8	.
Visual discoloration length (%)	1.7	1.1	1.7	.
Light discolored pixels area (%)	2.8	2	2.5	0.2841
Super-light red discolored pixels area (%)	2.7	1.6	2.7	0.2852
Super-light red discolored pixels number	1.5	1.5	1.8	.
Dark discolored pixels area (%)	2.2	3	2.9	0.9631
Dark discolored pixels circularity ¹	-1.5	0	-0.4	.
Dark discolored pixels aspect ratio ²	2.7	0.7	2.4	0.1852
Dark discolored pixels length (%)	1.4	0.9	1.1	.
Dark discolored pixels width (%)	1.3	1.5	1.3	.
Dark discolored and light pixels area (%)	2.3	2	2.2	0.3033
Low-dark discolored pixels area (%)	2.6	3	3	0.9373
Medium-dark discolored pixels area (%)	3.8	3.7	5.1	0.9783
High-dark discolored pixels area (%)
Dark cloudy discolored pixels area (%)	4.2	4.1	3.5	0.9489

P-values were also shown, which prove normally distributed data. ¹ $Circularity = \frac{4 * \pi * Area}{(Perimeter)^2}$

² $Aspect\ ratio = \frac{Major\ axis}{Minor\ axis}$

The super-light discolored pixels number was higher in the DL (11 ± 2) than D0 group (6 ± 1 ; $P=0.0539$). The DH (6 ± 1) did not statistically differ from D0 ($P=0.9408$) or DL groups ($P=0.0584$) (Table 5.5 and Figure 5.10). Regarding the dark discolored pixels (%), its circularity got significantly lower values in the DL group (0.5 ± 0.1) than the D0 (0.8 ± 0.0 ; $P=0.0276$), but no differences were observed between the DH (0.6 ± 0.1) groups and the D0 ($P=0.0752$) or DL ($P=0.8110$) (Table 5.4). The medium-dark discolored b^* value was significantly lower in the DL (11.8 ± 0.4) group than D0 (15.6 ± 0.3 ; $P=0.05$), while the DH (15.0 ± 0.3) compared to D0 or DL groups did not differ significantly ($P=0.6671$ and 0.0651 respectively) (Table 5.4).

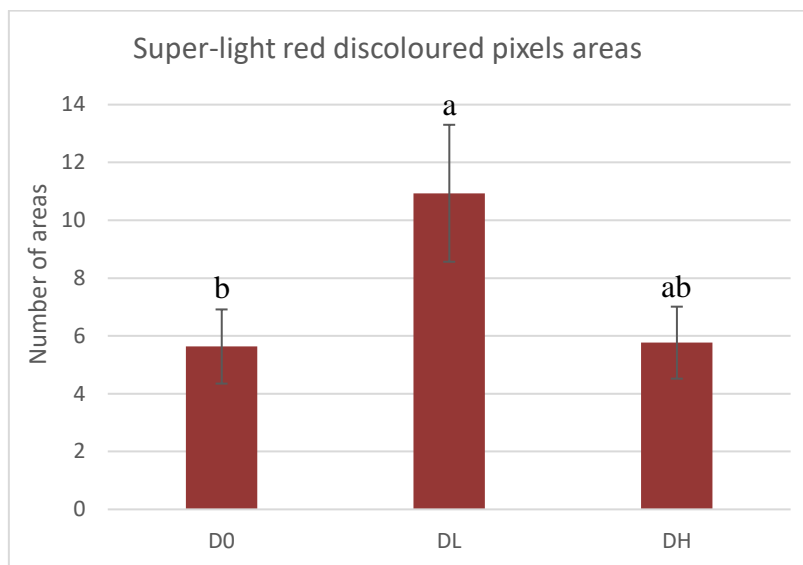


Figure 5.10. Comparison of the number of super-light red discolored pixels formations mean and standard errors in ventral muscle selection in all three groups: D0, DL, and DH. Different letters above the error bars represent significant differences ($P\leq 0.05$) between groups.

The accumulated discoloration area per treated group (Figure 5.11) showed a non-significant decreasing trend ($P=0.3033$) in the DL group in comparison to D0, or DH at four different partition levels; as the light discolored pixels area (%), the low-dark discolored pixels area (%), the medium-dark discoloration pixels area (%) and the super-light red discolored pixels area (%). The accumulation of the main discolored areas may also be represented (Figure 5.12).

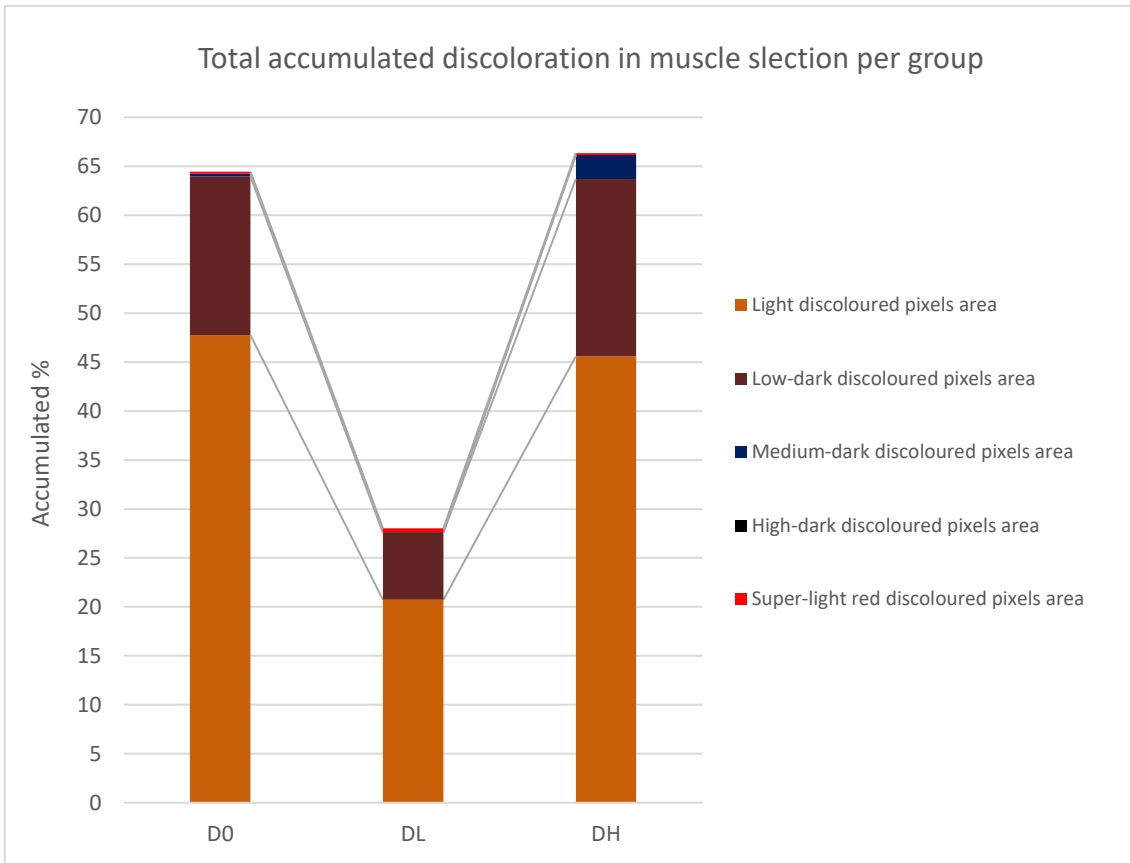


Figure 5.11. Total accumulated discoloration partitions in muscle selection per dietary groups: D0, DL, and DH. Notice that differences were not significant ($P \leq 0.05$). The color-illustrated the type of discoloration, but they did not reflect the original visual perception.

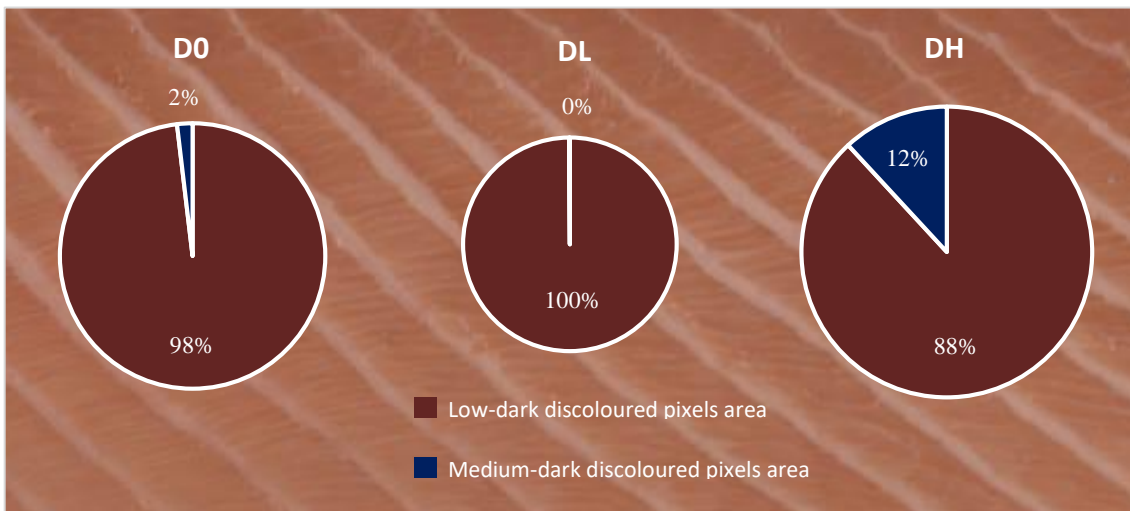


Figure 5.12. The global accumulated composition of dark discolored areas in dietary groups: D0, DL, and DH. As high-dark discolored areas (%) were not detected, they were excluded from the figure. Notice that differences were not significant ($P \leq 0.05$). Color and pie size illustrates the type of discoloration and the size appreciation, but they do not reflect the original visual size or spatial position in the fillet.

Regarding the general spatial position of dark discolorations, the occurrence of these alterations in fillets from all treated groups (D0, DL, and DH) was represented (Figure 5.13). Most of the problematic areas were located following a linear pattern from the cranio-bottom towards caudo-top corner. Therefore, there was a larger number of dark discolored areas (up to 13) between the myocommata #18-20, compared to the rest of myocommatus in the ventral selections (Figure 5.14).

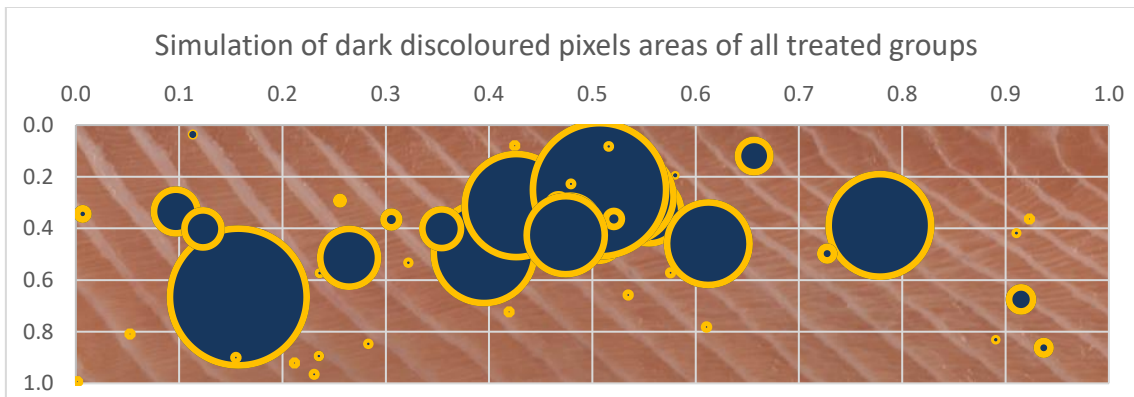


Figure 5.13. Spatial distribution of dark discolorations in the ventral selection of all dietary groups: D0, DL, and DH. Circles represented every discoloration recorded by the system, and their sizes were depending on the area of the respective dark discolored area (%). Notice that figure colors do not represent the original color of every represented discoloration. The transverse horizontal septum was used as a reference for identifying the myocommata number. X-axis [0.0-1.0] belongs to 20 myocommata from #9-29 (Figure 4.2 and Figure 4.5).

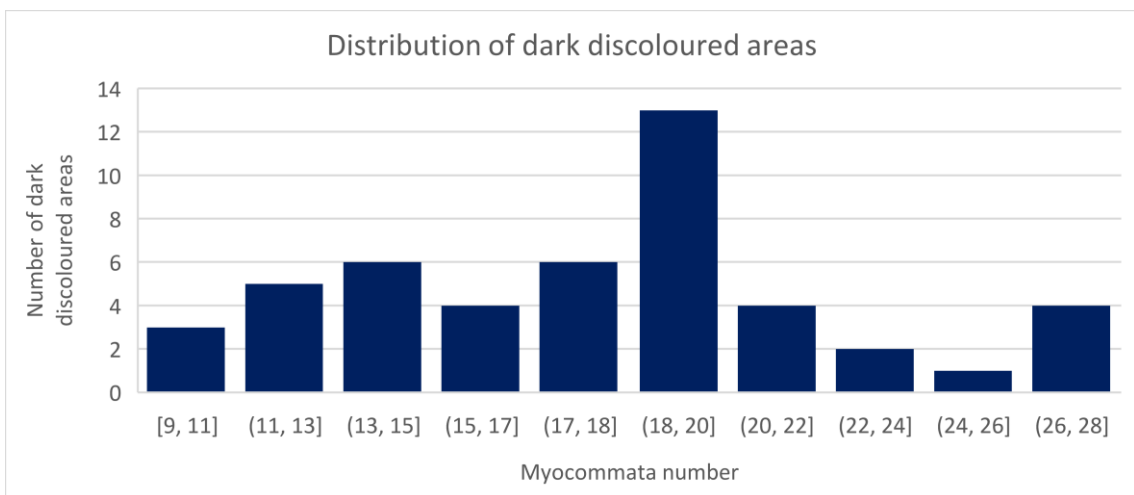


Figure 5.14. Distribution of the number of dark discolored areas for every two myocommata in the ventral selection of all dietary groups: D0, DL, and DH, from myocommata #9-29 (Figure 4.2 and Figure 4.5). Notice that the transverse horizontal septum was used as a reference for identifying the myocommata number.

The visual discoloration length (%) significantly correlated with the general L^* value (-0.36; $P=0.0004$), and the medium-dark discolored pixels area (%) (0.35; $P=0.0008$) (Appendix B). Those correlations were higher between the visual discoloration length (%) and the light discolored pixels area (%) (0.73; $P<0.0001$), the dark discolored pixels area (%) (0.67; $P<0.0001$), the low-dark discolored pixels area (%) (0.68; $P<0.0001$), or the dark discolored pixels length (%) (0.79; $P<0.0001$) (Appendix B).

A significant correlation was found between the visual dot number at quarter A from the salmon skin, and the visual discoloration length (0.25; $P=0.0174$) (Appendix C). Therefore, the visual discoloration length (%), correlated with the general L^* values of quarter A (-0.23; $P=0.0331$), and the visual dot number of quarter A (0.25; $P=0.0174$) (Appendix C). Moreover, a correlation was found between the general b^* value of quarter A, and the ventral selection general b^* value (0.21; $P=0.0464$) (Appendix C).

5.2 In vitro

5.2.1 Microscopy

The stimulation with β -glucans presented the production of floating material at day 8 post-splitting, in all plasmas with an increasing tendency in FBS until day 11 post-splitting. The stimulation with lipopolysaccharides showed no visual effects on SHK-1 cells at any control time.

Salmon plasmas (SP0, SPL, and SPH) had positive effects on cell survival and stability, which was possible to see from day 8 to day 41 post-splitting (Appendix D). Their cells showed viability signs at 41 days post-splitting in contrast to FBS. At 75 days post-splitting, just SPL cells presented apparent alive cells (Appendix D. Black arrows). The FBS status at 8 days post-splitting was not optimum by the swish from stationary phase to floating with low viability. SPL and SPH were confluent at day 8, in contrast to plasma from SP0 group, which had lower growth getting full confluency between day 11 and 21 post splitting. Evident floating dead-cell material (Appendix D. Blue arrows) was observed in all groups excluding SPL. The SPL cells presented a larger self-inhibition of cell growth compared to SPH, SP0, and FBS plasmas, which had more overgrowth (Appendix D. Green arrow).

Regarding cell morphology, at day 8 post-splitting, SPL and SPH cells looked more compact than SP0. At 41 days post-splitting, this compressed appearance differed from previous pictures at 8 or 21 days post splitting (Appendix D. Red arrow). Some small blank circular particles (compatible with melanosomes) were observed in salmon plasmas (Appendix D. Yellow arrows), especially at day 8 post-splitting since the lower the cell concentration, the clearer the appearance (Appendix D).

5.2.2 Image analysis

No significant differences were found by visual counting of melanosomes at day 8 post-splitting ($P=0.8015$) (Table 5.6 and Figure 5.15). Similarly, automatic melanosome counting showed no statistical differences among the groups ($P=0.2202$) (Table 5.6 and Figure 5.15). A smaller standard error was observed in automated than visual counting at day 8 post-splitting (Table 5.6 and Figure 5.15). If we look at day 11 post-splitting, significant differences were found in SP0 (241 ± 20) ($P= 0.0034$) and SPH (224 ± 24) ($P=0.0296$) groups compared to SPL plasmas (161 ± 6). SP0 and SPH pictures did not statistically differ ($P=0.5810$) (Table 5.6 and Figure 5.15). At 21 days post-splitting there was a significantly higher number of melanosomes in SPH (265 ± 16) than SP0 (167 ± 10) ($P=0.0004$) or SPL (170 ± 9) plasmas ($P=0.0004$). SP0 and SPL did not statistically differ ($P=0.8379$) (Table 5.6 and Figure 5.15).

Table 5.6. Means and standard errors for melanosome counting of picture selections from the control SHK-I cells after salmon plasma conditioning; SP0, SPL, and SPH.

Melanosome number	SP0	SPL	SPH	P-value	R ²
At day 8 post-splitting (Visual)	211±20 ^a	195±36 ^a	223±30 ^a	0.8015	0.145
At day 8 post-splitting (Automated)	209±18 ^a	191±12 ^a	236±21 ^a	0.2202	0.086
At day 11 post-splitting (Automated)	241±20 ^a	161±6 ^b	224±24 ^a	0.0185	0.112
At day 21 post-splitting (Automated)	167±10 ^b	170±9 ^b	265±16 ^a	<0.0001	0.067

P-values shows significant levels ($P\leq 0.05$). Different superscripts represent significant differences ($P\leq 0.05$) between groups. Variation described by the dietary treatment model as the coefficient of determination (R^2).

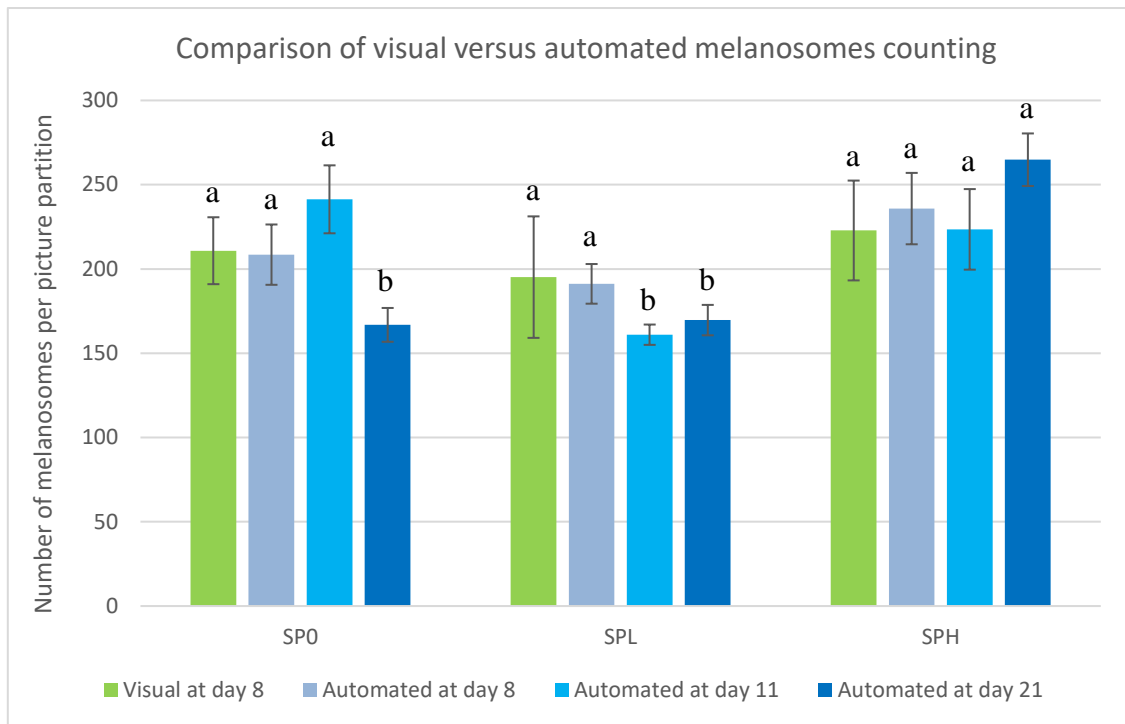


Figure 5.15. Means and standard errors of visual estimation at day 8 and automated melanosomes counting in cell pictures at day 8, 11 and 21 of all three control of the different salmon plasma conditioning; SPO, SPL, and SPH, at day 8, 11 and 21 post-splitting. Fetal bovine plasma are not considered given its cell features. Different letters above the error bars represent significant differences ($P \leq 0.05$) between groups.

5.2.3 RT-PCR

The absolute Tyr mean values showed smaller (<1) Ct (inverse to the amount of nucleic acid) in all salmon plasma groups: SPO, SPL, and SPH, compared to FBS. The SPO gave the lowest value, except its lipopolysaccharides stimulation (Figure 5.16).

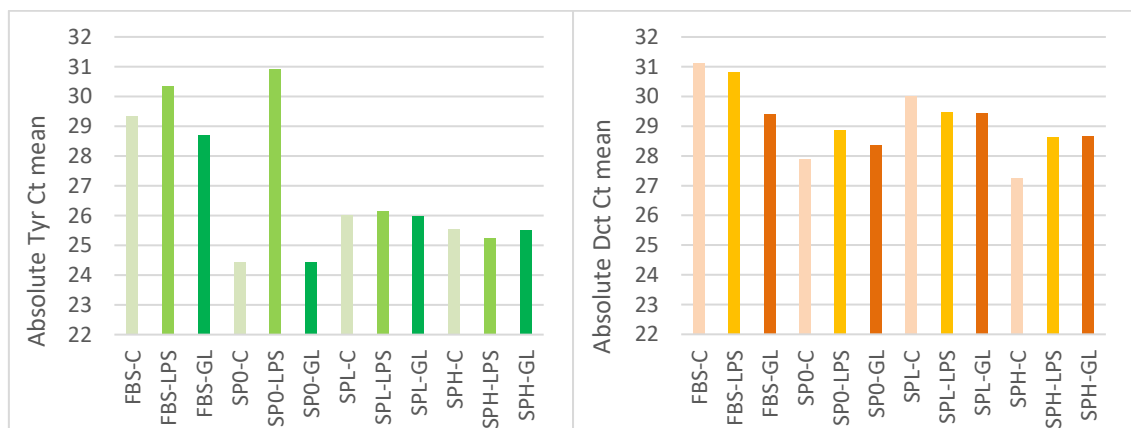


Figure 5.16. Absolute tyrosinase (Tyr; to the left) and dopachrome tautomerase (Dct; to the right) Ct means for SHK-1 cells. The control (C) represents as the palest color, the lipopolysaccharides (LPS) darker, and β -glucans as the darkest color under the FBS, SPO, SPL and SPH conditioning groups. Absolute values are not normalized against the β -actin gene.

Regarding Dct, the absolute mean values followed a similar tendency, with a difference of $>1Ct$ between FBS and salmon plasmas, except for β -glucans. The controls for every plasma gave the most consistent differences, having SP0 and SPH lower $>1Ct$ than SPL (Figure 5.16). Effects of stimulation with lipopolysaccharides and β -glucans can be observed by higher Ct in the SPH group, or lower Ct drop in the FBS cells (Figure 5.16).

The relative Tyr expression showed non-significant differences among FBS, SP0, SPL and SPH plasmas or stimulation with lipopolysaccharides and β -glucans ($P=0.9668$). An upregulation pattern may be observed in the stimulated or conditioned cell with salmon plasmas (SP0, SPL, and SPH) (Figure 5.17). The relative expression of Dct similarly was not significantly different between any plasma or stimulant ($P=0.9999$) (Figure 5.17).

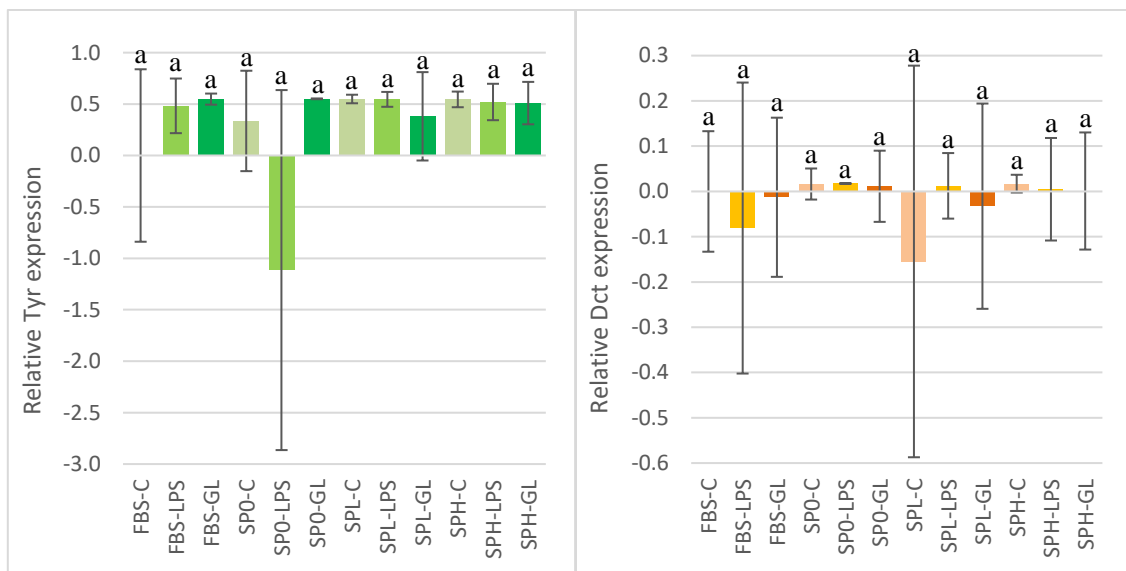


Figure 5.17 Relative tyrosinase (Tyr; to the left) and dopachrome tautomerase (Dct; to the right) genes expression for Control (C) as paler color, lipopolysaccharides (LPS), and β -glucans of SHK-1 cells under the FBS, SP0, SPL and SPH conditioning groups. Each bar represents the standard error of the mean. Different letters above the error bars represent significant differences ($P\leq 0.05$) between cell treatments. The control (C) was represented as the palest color, the lipopolysaccharides (LPS) darker, and β -glucans as the darkest color. Samples are normalized against the β -actin gene according to the $\Delta\Delta Ct$ method, and the up or down-regulation of the normalized values is shown as relative about the mean of the non-stimulated (control) cells under FBS.

6 DISCUSSION

In the present study, three diets with different levels of Antarctic krill meal inclusion (D0, DL, and DH) were used to study the development of dark pigment at three different levels; skin, muscle and *in vitro* cells using plasmas from fish fed similarly (SP0, SPL, and SPH). While for the *in vivo* approach several image analysis methods were developed and used, standard quantification techniques as microscopy evaluation or RT-PCR were used for the *in vitro*.

The status of our population to study was important to understand possible variations in image analysis parameters. Thus, general variables as round body weight, body length, and condition factor were determined. Those fish fed with the DL (5000g;73cm) diet were significantly heavier and bigger than the D0 (4402g;69cm) and DH groups (4030g;68cm). That matched with previous studies, where a moderate inclusion level increased feed palatability, which leads to higher feed intake, and higher growth rates and body weights (Hatlen et al., 2017; Suontama et al., 2007). In contrast to these studies, the condition factor remained statistically similar among the groups. The fact that the DH diet did not show statistical differences compared to the D0 may be explained by a reduction of lipid digestibility, and growth rate as a result of the high levels of chitin, also described in previous researchers (Olsen et al., 2006; Tharanathan & Kittur, 2003). Thus, some compensation between the higher feeding intake and lower lipid digestibility might have given similar round body weight than the S0 diet with none inclusion of krill.

At fish harvesting, some fish presented apparent skeletal deformities by the presence of hocked backs, and when filleting at Nofima fish lab, abnormal vertebrae were observed in the D0 17%, DL 13%, and DH 31% of the sampled fish with non-significant differences qualitatively, and quantitatively among the dietary groups. The position of the abnormal vertebrae of the salmon skeleton ranged approximately from vertebra #11–26, counted from the cranial to the caudal edge of the fillet, with the highest prevalence over vertebrae #20–22. That is an anatomical position located below the dorsal fin of the fish, half-length of the visceral cavity, as can be observed in a presented illustration (Figure 5.6). The corresponding fillet section from the vertebrae #11–26 was also included in the ventral selection used for image analysis on the fillet, ranging from vertebra #9–29 (Figure 4.2 and Figure 5.6).

Since there were no statistical differences on the occurrence of these unexpected results, they were considered equally distributed among our dietary groups with no critical implication in the development of the following measurements.

Regarding the general color muscle appearance, two parameters had statistical differences; the L^* had significantly higher values on DL than D0 or DH, which gave to the DL fillets generally a lighter or less grey appearance in contrast to the D0 and DH groups. Previous studies have shown a positive correlation between L^* values and fat content (Marty-Mahé et al., 2004) or negative with astaxanthin levels on fillets (Bjerkeng et al., 1997a). However, in this master thesis, we focused on its connection with the presence of dark discoloration areas. Therefore, the DL group had a significantly lower b^* value, which meant a lesser yellow appearance, than the D0. Significant correlations were found between visually assessed color intensity and the general L^* value ($r=-0.40$), general a^* value ($r=0.56$), and general b^* value ($r=0.43$), which agrees with previously described patterns (Bjerkeng et al., 1997a). Thus, a higher color fan value, normally focussed on epaxial muscle, negatively correlated with lightness, while positively with red or yellow color dimension at cranio-hypaxial level.

The skin pictures were taken after one week of ice-box storing, which avoided possible initial changes (Erikson & Misimi, 2008). However, in contrast to those authors and saving the differences on the type of treatment, significant colorimetric skin values were described on our dorsal area of interest after 7 days of refrigeration. When it comes to the whole dorsal skin cut, combining all axis (L^* , a^* , and b^*), the DL and DH groups had a general darker blue-green and green-yellow-like appearance respectively than the D0 group. Nevertheless, during filleting it was observed a visible side-effect of the ice over the skin during refrigeration, getting a paler color probably because of the melanocyte dendritic contraction at low temperatures (Bagnara & Hadley, 1973; Gesto et al., 2017; Ito et al., 2000). That must be taken into consideration, even considering the similar storing condition for all groups. As a result, the cranio-bottom quarter A got more focus since it was relatively less exposed to ice than other dorsal areas. The same area has also been focused in other skin colorimetric studies (Erikson & Misimi, 2008; Gesto et al., 2017; Kittilsen et al., 2009; Pavlidis et al., 2006).

While our fish material was not specially designed for producing a variation among the skin dot number (Khan et al., 2016; Kittilsen et al., 2009), a visual and automated estimation of it was carried out for complementing our skin color features on quarter A's. Thus, the DL group had a significantly higher approximated dot number than the D0 group. It did significantly correlate with their non-significant visual counting of sampled fish ($r=0.62$), which was not a very high correlation coefficient if we compare it with the correlation that we got at the calibration of the method with 8 fish ($r=0.83$). Additionally, the approximated number strongly correlated with the super-dark area (%) ($r=0.80$), which suggest an easier and strong indirect parameter. Although when comparing the correlation between the super-dark pixels area (%), and the visual dot number it gave a moderate but lower value ($r=0.52$) than between the approximated and visual dot number. The counting of skin dots was challenging to threshold since a big fraction of them had a lower dark appearance, which may carry and overestimation of them by automated methods while an underestimation if a visual counting is performed with high discrimination rules, normally necessary for highlining dots from micro pigmented areas. On the top of that, the super-dark pixels area (%) objective nature should also be taken into consideration, when comparing with visual results. The visual dot number also had week significant correlations with the general a^* value ($r=0.29$), and the general b^* value ($r=0.24$), which disagreed with the global color profiles where the DL with the largest dot counting generally had the lowest a^* and b^* values.

Salmon skin of DL and DH diets generally gave a darker appearance while those differences were not evident at quarter A level. Also, the D0 group showed significantly less, bigger and redder skin dots in their quarter A. Lower numbers of skin dots or generally darker areas have been previously related to highly responsive rainbow trout to stressors (Khan et al., 2016; Kittilsen et al., 2009). That may point to more stressed fish in the D0 group or less stressed fish at the DL and DH groups since cortisol increases the production of MC1R antagonists, agouti signaling protein (ASIP) and agouti-related protein (AGRP) (Cal et al., 2017; Cone et al., 1996). Additionally, considering the self-inhibition for the hypothalamic-pituitary-adrenal axis, the production of melanin may drop (Khan et al., 2016; Kittilsen et al., 2009; Smith et al., 2003). However, not all studies have similar conclusions (Gesto et al., 2017) likely by the type of stress.

Another aspect to consider about the skin color from those group were the a^* and b^* axis. Since fish from all treated groups belonged to the same families, and they were raised under similar farming conditions, lineage or site effects lost weight as the possible cause of this skin color plasticity, in contrast to what was performed in other studies (Costa et al., 2017; Horth, 2003; Marie-Orleach et al., 2014; Wedekind et al., 2008). As a result, we formulated another hypothesis to explain those differences between colors of the D0, DL and DH groups based on the skin color diagram (Figure 5.4). Normally, during on-growing farming conditions at sea level, the dorsal salmon skin had a dark-blue appearance given by the combination of melanocytes and blue position iridophores (like the DL group). Then, by sexual maturation or other factors, fish start to move carotenoids to xanthophores/erythrophores (Grether et al., 1999; Hardy et al., 1990; Wedekind et al., 1998; Wedekind et al., 2008), generating a combination of yellow-red and dark blue colors resulting in a growing greener appearance (the DH group). On the other hand, if the process continues, the increasing number of carotenoids moves the angle of the a^* and b^* axis to a yellower position. This process also may carry a drop of the general dark appearance with a reduction or hiding of melanocytes by leucophores or iridocytes. Those melanocytes may be aggregated into bigger dots, which would explain the reduction in their number in the D0 compared to the other groups. However, the redder color of those bigger skin dots together with the general dysmorphism between the DH and D0 may indicate gender relate differences. Further studies comparing these findings with sexual maturation markers as gonads development, could help to understand these facts better.

Regarding the colorimetric study of discolorations in ventral selections, as a result of the general descriptive and comparative colorimetric study on cranio-hypaxial muscle in salmon fillets, we saw that any type of discoloration on muscle was characterised by a drop in L^* , a^* and b^* values, that depended on the type or grade of the alteration. Generally, if we talk about “black spots”, the larger was the discoloration, the larger was this difference, which agreed with previous descriptive studies (Weizhi, 2016). However, “red spots” were characterized by a lower a^* than b^* value, and most of the difference was given by a reduction in the L^* and b^* channels. The pattern of the general colorimetric value from ventral selections had high similarities with normal tissues profiles. Since non-significant variations were observed in both a^* and b^* axis, the higher L^* value of the DL group may confirm a possible higher fat content in those fish fillets (Marty-Mahé et al., 2004).

Astaxanthin levels in fish fillets should also be considered (Bjerkeng et al., 1997a), especially by the significant drop of a^* or b^* , with an increase of L^* . Future studies comparing those values with fat and carotenoid content of the same fillet may help to understand better this connexion already studied (Bjerkeng et al., 1997a; Marty-Mahé et al., 2004).

The common methodology for evaluation “dark spots” on salmon fillets based on visual inspection (Mørkøre, 2012) was hybridized with image analysis techniques to maximize its capacities, especially at changing the scoring system of the discoloration by length values. Relativizing this visual length data allowed its comparison with the novel image analysis method for discoloration.

None significant differences were observed when using the hybrid system either number, fish (%) with 0, 1, 2 or 3 spots, or length (mm). If we look at the segmentation of the image analysis method, not many statistical differences were described between dietary groups; the super-light discolored pixels number or “micro red dots” were found significantly higher in the DL group. Regarding the color profile of the dark discolored pixels areas (%), the inversion of the a^* and b^* means pattern indicated discolorations towards “red spots” in the DL group, while the D0 and DH matched with small “dark spots” features, generally less pigmented. This is commercially interesting since small and poorly pigmented spots have a relatively low economic impact (Färber, 2017). Moreover, if we look closer, the medium-dark discolored b^* value was significantly lower in the DL group, which suggested a reduction of the yellowness. That matched with the significantly lower b^* values of the general color appearance from ventral selections, being probably the origin of this general variation. The non-significant means of the whole color profile from the medium-dark discolored pixels partitions also followed the inversion of the a^* and b^* pattern previously described, compatible with “red spots which may explain the significantly larger number of “micro red dots”. Additionally, the circularity of the dark discolored pixels (%) got significantly lower values in the DL group compared to D0, which suggested more irregular edges in “dark spots” given none differences with their aspect ratio. When comparing the hybrid with the novel method. The main relative values of segmented areas followed a non-significant inverse pattern, when comparing them with the visual length (%), being the DL diet the least affected group, and the most affected respectively.

If we look at the affected:non-affected visual fish ratio by discoloration, the 43%, 50%, and 47% of right fillets from the D0, DL, and DH groups respectively were affected by any number of spots which is more than twice the prevalence described in previous reports (Mørkøre, 2012; Mørkøre et al., 2015). Since these differences were not significant, they may be given by random chance. Nevertheless, strong correlations were found between both parameters from both systems, even considering that length and area do not necessarily must be fully correlated given by different spot morphologies. Thus, the visual discoloration length (%) significantly correlated with the general L^* value (-0.36), the light discolored pixels area (%) (0.73), the dark discolored pixels area (%) (0.67), the dark discolored pixels length (%) with the highest correlation as expected because geometric similarities (0.79), the low-dark discolored pixels area (%) (0.68), or the medium-dark discolored pixels area (%) (0.35). Factors as more than one “dark spots”, or deviated center of mass respect the centroid of the selection, may disturb the correlation with the dark discolored pixels length (%). It seemed that the more specific or selective we go on the segmentation level, the larger is the reduction of the determination coefficient. These high correlations could confirm the random chance effect on different mean patterns between both methods, which is a positive indicator but did not confirm the veracity of the novel tool. Performing this system in further studies, where the group discoloration differences are more evident may be determinant. Additionally, weak but significant correlations were observed between parameters from muscle discoloration as the visual discoloration length (%), and at skin quarter A data as the visual dot number (0.25) or the general L^* value (-0.23). These might be evidences of a possible positive link between “dark spots” and skin melanin, as was hypothesised at the beginning from possible common regulators as ACTH (Lerner & McGuire, 1961; Levine et al., 1991), or because of a systemic inflammation status (Bologna et al., 1989; Chakraborty et al., 1995; Corre et al., 2004) by the omega-3:6 fatty acids ratio (Sissener et al., 2016), and triggered by chemicals (Haugarvoll et al., 2010), or biologicals agents (Bjørger et al., 2015; Nylund et al., 2011). Another skin and muscle correlation was described between the general b^* value of quarter A, and the ventral selection general b^* value (0.21), which suggested a weak positive relationship between carotenoids levels (Bjerkeng et al., 1997b; Herring, 1994; Wedekind et al., 1998).

One of the most interesting reasons for developing a novel method for measuring the discoloration on salmon fillets based on image analysis was to harvest quantitative values. As a result, other ways of illustrating data can be used despite significant differences were not observed; as the accumulation of the different picture fragmentations per group; the light discolored pixels area (%), the low-dark discolored pixels area (%), the medium-dark discoloration pixels area (%) and the super-light red discolored pixels area (%). In this case, the DL group got the lowest amount of this problem in comparison to D0, or DH. The digital nature of the novel method allowed to relativize the two-dimensional position of every single centroid of discoloration detected. Thus, transferring those values from all three groups into a global position matrix to have considerable positive discolored areas, their position was visualized and studied. We observed most of the problematic areas were located following a linear pattern from the cranio-bottom towards caudo-top corner. Therefore, there was a larger number of dark discolored areas (up to 13) between the myocommata #18-20. This was very different from the highest peak reported by other authors around myocommata #18, but it did coincide with the second peak (Mørkøre et al., 2015; Weizhi, 2016). Unexpectedly, this highest frequency of discoloration problems in our salmon fillet was very close topographically to the highest frequency of the abnormal vertebrae at #20–22.

The fact that most of the dark spots are located cranially on the hypaxial muscle of salmon fillets (Mørkøre, 2012; Mørkøre, 2017), gave us reasons to compile which anatomical factors make that zone special (Figure 5.6 and Figure 5.5) as visceral and rib bones proximity, or a thinner white muscle wall with higher fat content, that differ from other fillet anatomical areas, specially epaxial. Therefore, these factors may be linked together; we know that elevated temperatures may increase the production of radicals (Dittmar et al., 2014), and they could easily react in those fatty areas with polyunsaturated fatty acids giving oxidation-induced compounds (Lauritzsen et al., 1999; Peng et al., 2009; Sahoo & Mukherjee, 2002). A proinflammatory activity, related to omega-6 family fatty acids (Sissener et al., 2016), may be locally more intense in these fatty areas, being “overreactive” under infectious or physical stressors. It has also been a reported temperature-dependent activity of the tyrosinase gene family in salmon leukocytes from the SHK-1 cell line (Larsen et al., 2013). Thus, temperature, membrane lipids profile, and oxidative activity could potentially play an important role explaining all these facts.

Despite dark spots are normally measured on salmon fillets after slaughtering (Mørkøre, 2012), the conditioning of primary cells with specific salmon plasma (Seierstad et al., 2009) gave us reasons enough for trying to replicate those results *in vitro*. In our *in vitro* study, the SHK-1 cell line, with melanogenesis machinery (Haugarvoll et al., 2006) and theoretically more stable than primary the isolated cells (Seierstad et al., 2009), was used for performing some basic cells stimulation assignment with lipopolysaccharides and β -glucans under four different conditionings; FBS, SP0, SPL and SLH. Similarly than our reference studies (Larsen et al., 2013; Seierstad et al., 2009), the RT-PCR did not give any significant differences on tyrosinase gene family genes or immune-related activity if we consider the melanogenic response as a part of the innate immune system.

If we look at the absolute Ct value, the absolute Tyr expression was higher in all salmon plasma groups; SP0, SPL, and SPH, compared to the FBS. Moreover, the SP0 conditioning gave the highest overall mean, except its lipopolysaccharides stimulation, which had very different parallel Ct values. It seems that salmon Tyr absolute values followed a similar pattern than our microscopy observations, probably as a result of the number or functionality of the cells. The absolute Dct mean values followed a similar tendency except for the β -glucans stimulation, being easily observed in the controls of every conditioning. In this case, the stimulation effects with lipopolysaccharides and β -glucans can be observed in the SPH group and FBS cells with opposite tendencies.

The stimulation effects of β -glucans presented and additional production of floating material at day 8 post-splitting, in all conditionings with an increasing tendency in the FBS until the day 11 post-splitting. These visual findings have not been described in similar studies (Larsen et al., 2013; Seierstad et al., 2009; Skår-Ulvestad, 2017). However, if we look at the cell appearance, positive effects on cell survival and stability were found in salmon plasmas from day 8 to day 41 post-splitting (Appendix D). Normally with conventional FBS conditioning, the cell status at 8 days post-splitting is not optimum by the switch from stationary to floating phase with low viability, but unexpectedly, at 75 days post-splitting the SPL cells still presented apparent alive cells. The later confluency of the SP0 cells between day 11 and 21 post splitting revealed lower growth than other salmon conditionings. Moreover, on the last control points evident floating dead-cell material was observed except the SPL cells.

That may be explained by a larger self-inhibition of cell growth, preventing overgrowth, which agrees with the fact that the SPL cells remain partially viable at day 75 post-splitting. Regarding cell morphology, at 41 days post-splitting the side-by-side compressed appearance because of confluency differed from previous pictures at 8 or 21 days post splitting.

As we see in the pictures, melanosomes were observed in all conditioned plasma cells, especially at day 8 post-splitting since the lower the cell concentration, the easier it was to visualize them. Given that observations a method for quantifying them was tested, where none significant differences were found by visual and automated counting of melanosomes at day 8 post-splitting. Applying the already calibrated system to the same control plates in the following respective pictures, at day 11 post-splitting, the SP0 and SPH cells had significantly more melanosomes, while at 21 days post-splitting there was a significantly higher number in the SPH than the SP0 or SPL plasma conditioning. It may look that the automated number of melanosomes per control decreased, but it may be due to hiding because of cell overgrowth. Consequently, we did not focus on this self-comparison over the time. The fact that we found a significantly higher number of melanosomes in the SPH cells with non-significant expression of melanogenic genes may indicate a time-accumulation off those pigments and low relative or absolute melanogenesis inactivity at the time of cell harvesting. However, possible errors by the system must be taken into consideration given the nature of the automatic quantification method for melanosomes. Longer conditioning prior final splitting or different plasma concentrations can be tested in future studies for validating and standardizing the *in vitro* method.

7 CONCLUSION

When it comes to the *in vivo* study, a novel method was developed for Atlantic salmon skin colorimetric appearance, which has shown the capacity for detecting dietary-related variations of different skin components. Dietary inclusion of krill meal significantly altered the skin color. At low inclusion level, fish were darker with bluer appearance. On the other hand, at high inclusion, they got a darker and greener appearance. The showed novel muscle discoloration method did not have a good context for testing its usability in an experiment, given the low variability among the groups. Although high correlations have been found between the “dark spot” length using the hybridized method and several of the homolog parameters given by image analysis. If the novel discoloration method resulted validly, discoloration in salmon fillets could be relatively quantified by colorimetric, morphology and spatial features. There was a high prevalence of “dark spots” on fillets, which were generally low pigmented on all groups of this experiment. Moreover, the inclusion of krill meal had no apparent effects on the development of “dark spots” in this trial. However, the low krill inclusion showed “dark spots” more towards red type. We have evidences of a positive correlation between “dark spots” from fillets and skin melanin as was hypothesized. Another positive correlation was described between the general b^* value of salmon skin, and the b^* value of the cranio-hypaxial muscle, which suggested a relationship between carotenoids levels in both structures. We have compiled anatomical factors that make the cranio-hypaxial zone of salmon fillets different from another part of the body, as visceral and rib bones proximity, or a thinner white muscle wall with higher fat content.

Regarding the *in vitro* study, the absolute expression of the tyrosinase relate family genes was higher in all salmon plasma groups, compared to the FBS, although no significant differences in their relative expression were observed. Moreover, salmon plasmas showed positive effects on cell growth and survival, especially the plasma from groups fed with low krill meal inclusion.

8 REFERENCES

- Acton, R. T., Weinheimer, P. F., Hall, S. J., Niedermeier, W., Shelton, E. & Bennett, J. C. (1971). Tetrameric immune macroglobulins in three orders of bony fishes. *Proc Natl Acad Sci U S A*, 68 (1): 107-11.
- Agius, C. (1979). The role of melano-macrophage centres in iron storage in normal and diseased fish. *Journal of Fish Diseases*, 2 (4): 337-343. doi: doi:10.1111/j.1365-2761.1979.tb00175.x.
- Agius, C. (1980). Phylogenetic development of melano-macrophage centres in fish. *Journal of Zoology*, 191 (1): 11-31. doi: doi:10.1111/j.1469-7998.1980.tb01446.x.
- Agius, C. (1981). Preliminary Studies on the Ontogeny of the Melano-Macrophages of Teleost Haemopoietic Tissues and Age-Related Changes. *Developmental & Comparative Immunology*, 5 (4): 597-606. doi: [https://doi.org/10.1016/S0145-305X\(81\)80034-1](https://doi.org/10.1016/S0145-305X(81)80034-1).
- Agius, C. & Agbede, S. A. (1984). An electron microscopical study on the genesis of lipofuscin, melanin and haemosiderin in the haemopoietic tissues of fish. *Journal of Fish Biology*, 24 (4): 471-488. doi: doi:10.1111/j.1095-8649.1984.tb04818.x.
- Agius, C. (1985). The melano-macrophage centres in fish: a review. In Manning, M. J. & Tatner, M. F. (eds) *Fish Immunology*, pp. 85-105. London, UK: Academic Press.
- Agius, C. & Roberts, R. J. (2003). Melano-macrophage centres and their role in fish pathology. *J Fish Dis*, 26 (9): 499-509.
- Ainsworth, A. J., Dexiang, C. & Waterstrat, P. R. (1991). Changes in Peripheral Blood Leukocyte Percentages and Function of Neutrophils in Stressed Channel Catfish. *Journal of Aquatic Animal Health*, 3 (1): 41-47. doi: 10.1577/1548-8667(1991)003<0041:CIPBLP>2.3.CO;2.
- Albers, J. (1963). *Interaction of Color*. New Haven, Connecticut: Yale University Press.
- Alexander, J. B. & Ingram, G. A. (1992). Noncellular nonspecific defence mechanisms of fish. *Annual Review of Fish Diseases*, 2: 249-279. doi: [https://doi.org/10.1016/0959-8030\(92\)90066-7](https://doi.org/10.1016/0959-8030(92)90066-7).
- Alfnes, F., Guttormsen, A. G., Steine, G. & Kolstad, K. (2006). Consumers' Willingness to Pay for the Color of Salmon: A Choice Experiment with Real Economic Incentives. *American Journal of Agricultural Economics*, 88 (4): 1050-1061. doi: 10.1111/j.1467-8276.2006.00915.x.
- Anderson, S. (2001, 2012-12-04). *Salmon Color and the Consumer*: International Institute of Fisheries Economics and Trade.
- Ando, H., Niki, Y., Ito, M., Akiyama, K., Matsui, M. S., Yarosh, D. B. & Ichihashi, M. (2012). Melanosomes are transferred from melanocytes to keratinocytes through the processes of packaging, release, uptake, and dispersion. *J Invest Dermatol*, 132 (4): 1222-9. doi: 10.1038/jid.2011.413.
- Andrew. (15/04/2018). *Color models*.
- Arciuli, M., Fiocco, D., Cicero, R., Maida, I., Zanna, P. T., Guida, G., Horsberg, T. E., Koppang, E. O. & Gallone, A. (2012). Melanogenesis in visceral tissues of *Salmo salar*. A link between immunity and pigment production? *Biochem Cell Biol*, 90 (6): 769-78. doi: 10.1139/o2012-033.
- Arkoosh, M. R. & Kaattari, S. L. (1991). Development of immunological memory in rainbow trout (*Oncorhynchus mykiss*). I. An immunochemical and cellular analysis of the B cell response. *Dev Comp Immunol*, 15 (4): 279-93.

- Aroca, P., Solano, F., Salinas, C., Garcia-Borron, J. C. & Lozano, J. A. (1992). Regulation of the final phase of mammalian melanogenesis. The role of dopachrome tautomerase and the ratio between 5,6-dihydroxyindole-2-carboxylic acid and 5,6-dihydroxyindole. *Eur J Biochem*, 208 (1): 155-63.
- Aursand, M., Bleivik, B., Rainuzzo, J. R., Leif, J. & Mohr, V. (1994). Lipid distribution and composition of commercially farmed atlantic salmon (salmosalar). *Journal of the Science of Food and Agriculture*, 64 (2): 239-248. doi: doi:10.1002/jsfa.2740640214.
- Baeverfjord, G. & Rye, M. (1994). *Hvor lagrer laksen fettet?: NorskFiskeoppdrett*.
- Bagnara, J. T. & Hadley, M. E. (1973). *Chromatophores and Color Change*, Englewood Cliffs: Prentice-Hall.
- Bagnara, J. T. & Matsumoto, J. (2006). Comparative anatomy and physiology of pigment cells in nonmammalian tissues. In Nordlund, J. J., Boissy, R. E., Hearing, V. J., King, R. A. & Ortonne, J.-P. (eds) *The pigmentary system: physiology and pathophysiology*, pp. 9-40. New York: Oxford University Press.
- Berg, A., Yurtseva, A., Hansen, T., Lajus, D. & Fjellidal, P. G. (2012). Vaccinated farmed Atlantic salmon are susceptible to spinal and skull deformities. *Journal of Applied Ichthyology*, 28 (3): 446-452. doi: 10.1111/j.1439-0426.2012.01988.x.
- Bjerkeng, B., Følling, M., Lagocki, S., Storebakken, T., Olli, J. J. & Alsted, N. (1997a). Bioavailability of all-E-astaxanthin and Z-isomers of astaxanthin in rainbow trout (*Oncorhynchus mykiss*). *Aquaculture*, 157 (1): 63-82. doi: https://doi.org/10.1016/S0044-8486(97)00146-4.
- Bjerkeng, B., Refstie, S., Fjalestad, K. T., Storebakken, T., Rødbotten, M. & Roem, A. J. (1997b). Quality parameters of the flesh of Atlantic salmon (*Salmo salar*) as affected by fat content and full-fat soybean meal as a partial substitute for fish meal in the diet. *Aquaculture*, 157: 295-307.
- Bjørngen, H., Wessel, Ø., Fjellidal, P. G., Hansen, T., Sveier, H., Sæbø, H. R., Enger, K. B., Monsen, E., Kvellestad, A., Rimstad, E., et al. (2015). Piscine orthoreovirus (PRV) in red and melanised foci in white muscle of Atlantic salmon (*Salmo salar*). *Veterinary Research*, 46 (1): 89. doi: 10.1186/s13567-015-0244-6.
- Blazer, V. S. (1991). Piscine Macrophage Function and Nutritional Influences: A Review. *Journal of Aquatic Animal Health*, 3 (2): 77-86. doi: 10.1577/1548-8667(1991)003<0077:PMFANI>2.3.CO;2.
- Boes, M. (2000). Role of natural and immune IgM antibodies in immune responses. *Mol Immunol*, 37 (18): 1141-9.
- Boissy, R. E. & Hornyak, T. J. (2007). Extracutaneous Melanocytes. In *The Pigmentary System*, pp. 91-107: Blackwell Publishing Ltd.
- Bologna, J., Murray, M. & Pawelek, J. (1989). UVB-induced melanogenesis may be mediated through the MSH-receptor system. *J Invest Dermatol*, 92 (5): 651-6.
- Boonanuntanasarn, S., Yoshizaki, G., Iwai, K. & Takeuchi, T. (2004). Molecular cloning, gene expression in albino mutants and gene knockdown studies of tyrosinase mRNA in rainbow trout. *Pigment Cell Res*, 17 (4): 413-21. doi: 10.1111/j.1600-0749.2004.00166.x.
- Borovansky, J. (1994). Zinc in pigmented cells and structures, interactions and possible roles. *Sb Lek*, 95 (4): 309-320.
- Børresen, T. (2008). Part II Health benefits. In vol. 10 *Improving seafood products for the consumer*, pp. 165-166: Woodhead Publishing.
- Bowness, J. M., Morton, R. A., Shakir, M. H. & Stubbs, A. L. (1952). Distribution of copper and zinc in mammalian eyes. Occurrence of metals in melanin fractions from eye tissues. *Biochem J*, 51 (4): 521-30.

- Braasch, I., Scharfl, M. & Volff, J. N. (2007). Evolution of pigment synthesis pathways by gene and genome duplication in fish. *BMC Evol Biol*, 7: 74. doi: 10.1186/1471-2148-7-74.
- Braasch, I., Volff, J. N. & Scharfl, M. (2008). The evolution of teleost pigmentation and the fish-specific genome duplication. *Journal of Fish Biology*, 73: 1891-1918.
- Brattgjerd, S. & Evensen, O. (1996). A sequential light microscopic and ultrastructural study on the uptake and handling of *Vibrio salmonicida* in phagocytes of the head kidney in experimentally infected Atlantic salmon (*Salmo salar* L.). *Vet Pathol*, 33 (1): 55-65. doi: 10.1177/030098589603300106.
- Brown, C. L. & George, C. J. (1985). Age-dependent accumulation of macrophage aggregates in the yellow perch, *Perca flavescens* (Mitchill). *Journal of Fish Diseases*, 8 (1): 135-138. doi: doi:10.1111/j.1365-2761.1985.tb01195.x.
- Browne, R. & Deegan, B. (2005). *Status of Irish Aquaculture 2005*.
- Bullock, A. M. & Roberts, R. J. (1974). The normal integument. In vol. 13 *The dermatology of marine teleost fish. I. An Annual Review*, pp. 383-411: Oceanography and Marine Biology.
- Burgoyne, T., O'Connor, M. N., Seabra, M. C., Cutler, D. F. & Futter, C. E. (2015). Regulation of melanosome number, shape and movement in the zebrafish retinal pigment epithelium by OA1 and PMEL. *Journal of Cell Science*, 128 (7): 1400-1407. doi: 10.1242/jcs.164400.
- Cal, L., Suarez-Bregua, P., Cerdá-Reverter, J. M., Braasch, I. & Rotllant, J. (2017). Fish pigmentation and the melanocortin system. *Comparative Biochemistry and Physiology Part A: Molecular & Integrative Physiology*, 211: 26-33. doi: <https://doi.org/10.1016/j.cbpa.2017.06.001>.
- Camacho-Hubner, A., Rossier, A. & Beermann, F. (2000). The Fugu rubripes tyrosinase gene promoter targets transgene expression to pigment cells in the mouse. *Genesis*, 28 (3-4): 99-105.
- Camacho-Hubner, A., Richard, C. & Beermann, F. (2002). Genomic structure and evolutionary conservation of the tyrosinase gene family from Fugu. *Gene*, 285 (1-2): 59-68.
- Cato, A. C. B. & Wade, E. (1996). Molecular mechanisms of anti-inflammatory action of glucocorticoids. *BioEssays*, 18 (5): 371-378. doi: 10.1002/bies.950180507.
- Chakraborty, A., Slominski, A., Ermak, G., Hwang, J. & Pawelek, J. (1995). Ultraviolet B and Melanocyte-Stimulating Hormone (MSH) Stimulate mRNA Production for α MSH Receptors and Proopiomelanocortin-Derived Peptides in Mouse Melanoma Cells and Transformed Keratinocytes. *Journal of Investigative Dermatology*, 105 (5): 655-659. doi: <https://doi.org/10.1111/1523-1747.ep12324134>.
- Chantanachookhin, C., Seikai, T. & Tanaka, M. (1991). Comparative study of the ontogeny of the lymphoid organs in three species of marine fish. *Aquaculture*, 99 (1): 143-155. doi: [https://doi.org/10.1016/0044-8486\(91\)90294-H](https://doi.org/10.1016/0044-8486(91)90294-H).
- CIE. (1976). *L*a*b* colour space*.
- Clark, A. J. & Weber, A. (1998). Adrenocorticotropin insensitivity syndromes. *Endocr Rev*, 19 (6): 828-43. doi: 10.1210/edrv.19.6.0351.
- Clydesdale, G. J., Dandie, G. W. & Muller, H. K. (2001). Ultraviolet light induced injury: Immunological and inflammatory effects. *Immunology And Cell Biology*, 79: 547. doi: 10.1046/j.1440-1711.2001.01047.x.

- Cone, R. D., Lu, D., Koppula, S., Vage, D. I., Klungland, H., Boston, B., Chen, W., Orth, D. N., Pouton, C. & Kesterson, R. A. (1996). The melanocortin receptors: agonists, antagonists, and the hormonal control of pigmentation. *Recent Prog Horm Res*, 51: 287-317; discussion 318.
- Corre, S., Primot, A., Sviderskaya, E., Bennett, D. C., Vaulont, S., Goding, C. R. & Galibert, M. D. (2004). UV-induced expression of key component of the tanning process, the POMC and MC1R genes, is dependent on the p-38-activated upstream stimulating factor-1 (USF-1). *J Biol Chem*, 279 (49): 51226-33. doi: 10.1074/jbc.M409768200.
- Costa, D. C., Mattioli, C. C., Silva, W. S., Takata, R., Leme, F. O. P., Oliveira, A. L. & Luz, R. K. (2017). The effect of environmental colour on the growth, metabolism, physiology and skin pigmentation of the carnivorous freshwater catfish *Lophiosilurus alexandri*. *Journal of Fish Biology*, 90 (3): 922-935. doi: 10.1111/jfb.13208.
- Couillard, C. M. & Hodson, P. V. (1996). Pigmented macrophage aggregates: A toxic response in fish exposed to bleached-kraft mill effluent? *Environmental Toxicology and Chemistry*, 15 (10): 1844-1854. doi: 10.1002/etc.5620151027.
- Crook, A. C. (1997). Colour patterns in a coral reef fish is background complexity important? *Journal of Experimental Marine Biology and Ecology*, 217 (2): 237-252. doi: [https://doi.org/10.1016/S0022-0981\(97\)00059-2](https://doi.org/10.1016/S0022-0981(97)00059-2).
- Dalmo, R. A. & Seljelid, R. (1995). The immunomodulatory effect of LPS, laminaran and sulphated laminaran [β (1,3)-D-glucan] on Atlantic salmon, *Salmo salar* L., macrophages in vitro. *Journal of Fish Diseases*, 18 (2): 175-185. doi: 10.1111/j.1365-2761.1995.tb00275.x.
- Danilova, N., Bussmann, J., Jekosch, K. & Steiner, L. A. (2005). The immunoglobulin heavy-chain locus in zebrafish: identification and expression of a previously unknown isotype, immunoglobulin Z. *Nat Immunol*, 6 (3): 295-302. doi: 10.1038/ni1166.
- Dannevig, B. H., Falk, K. & Namork, E. (1995). Isolation of the causal virus of infectious salmon anaemia (ISA) in a long-term cell line from Atlantic salmon head kidney. *J Gen Virol*, 76 (Pt 6): 1353-9. doi: 10.1099/0022-1317-76-6-1353.
- Dannevig, B. H., Brudeseth, B. E., Gjoen, T., Rode, M., Wergeland, H. I., Evensen, Ø. & Press, C. M. (1997). Characterisation of a long-term cell line (SHK-1) developed from the head kidney of Atlantic salmon (*Salmo salar* L.). *Fish & Shellfish Immunology*, 7: 213-226.
- De Bosscher, K., Vanden Berghe, W. & Haegeman, G. (2000). Mechanisms of anti-inflammatory action and of immunosuppression by glucocorticoids: negative interference of activated glucocorticoid receptor with transcription factors. *Journal of Neuroimmunology*, 109 (1): 16-22. doi: [https://doi.org/10.1016/S0165-5728\(00\)00297-6](https://doi.org/10.1016/S0165-5728(00)00297-6).
- de Cassia, R. G. R. & Pombeiro-Sponchiado, S. R. (2005). Antioxidant activity of the melanin pigment extracted from *Aspergillus nidulans*. *Biol Pharm Bull*, 28 (6): 1129-31.
- de Gruijl, F. R. (2000). Photocarcinogenesis: UVA vs UVB. *Methods Enzymol*, 319: 359-66.
- de Kinkelin, P. & Dorson, M. (1973). Interferon production in rainbow trout (*Salmo gairdneri*) experimentally infected with Egtved virus. *J Gen Virol*, 19 (1): 125-7. doi: 10.1099/0022-1317-19-1-125.

- Dittmar, J., Janssen, H., Kuske, A., Kurtz, J. & Scharsack, J. P. (2014). Heat and immunity: an experimental heat wave alters immune functions in three-spined sticklebacks (*Gasterosteus aculeatus*). *J Anim Ecol*, 83 (4): 744-57. doi: 10.1111/1365-2656.12175.
- dos Santos, N. M. S., Romano, N., de Sousa, M., Ellis, A. E. & Rombout, J. H. W. M. (2000). Ontogeny of B and T cells in sea bass (*Dicentrarchus labrax*, L.). *Fish & Shellfish Immunology*, 10 (7): 583-596. doi: <https://doi.org/10.1006/fsim.2000.0273>.
- Double, K. L., Ben-Shachar, D., Youdim, M. B. H., Zecca, L., Riederer, P. & Gerlach, M. (2002). Influence of neuromelanin on oxidative pathways within the human substantia nigra. *Neurotoxicology and Teratology*, 24 (5): 621-628. doi: [https://doi.org/10.1016/S0892-0362\(02\)00218-0](https://doi.org/10.1016/S0892-0362(02)00218-0).
- Ducrest, A.-L., Keller, L. & Roulin, A. (2008). Pleiotropy in the melanocortin system, coloration and behavioural syndromes. *Trends in Ecology & Evolution*, 23 (9): 502-510. doi: <https://doi.org/10.1016/j.tree.2008.06.001>.
- Dunford, R., Land, E. J., Rozanowska, M., Sarna, T. & Truscott, T. G. (1995). Interaction of melanin with carbon- and oxygen-centered radicals from methanol and ethanol. *Free Radical Biology and Medicine*, 19 (6): 735-740. doi: [https://doi.org/10.1016/0891-5849\(95\)00059-7](https://doi.org/10.1016/0891-5849(95)00059-7).
- Edelstein, L. M. (1971). *Melanin: a unique biopolymer*. In Pathobiology Annual, New York, pp. 309–324: Appleton-Century-Crofts.
- Einstein, A. (1905). "Über einen die Erzeugung und Verwandlung des Lichtes betreffenden heuristischen Gesichtspunkt". *Annalen der Physik*, 17 (6): 132-148.
- Ellis, A. E. & Sousa, M. d. (1974). Phylogeny of the lymphoid system. I. A study of the fate of circulating lymphocytes in plaice. *European Journal of Immunology*, 4 (5): 338-343. doi: doi:10.1002/eji.1830040505.
- Ellis, A. E. (1980). Antigen-trapping in the spleen and kidney of the plaice *Pleuronectes platessa* L. *Journal of Fish Diseases*, 3 (5): 413-426. doi: doi:10.1111/j.1365-2761.1980.tb00425.x.
- Ellis, A. E. (2001). Innate host defense mechanisms of fish against viruses and bacteria. *Dev Comp Immunol*, 25 (8-9): 827-39.
- Engelsma, M. Y., Hougee, S., Nap, D., Hofenk, M., Rombout, J. H. W. M., van Muiswinkel, W. B. & Lidy Verburg-van Kemenade, B. M. (2003). Multiple acute temperature stress affects leucocyte populations and antibody responses in common carp, *Cyprinus carpio* L. *Fish & Shellfish Immunology*, 15 (5): 397-410. doi: [https://doi.org/10.1016/S1050-4648\(03\)00006-8](https://doi.org/10.1016/S1050-4648(03)00006-8).
- Erikson, U. & Misimi, E. (2008). Atlantic salmon skin and fillet color changes effected by perimortem handling stress, rigor mortis, and ice storage. *J Food Sci*, 73 (2): C50-9. doi: 10.1111/j.1750-3841.2007.00617.x.
- Fänge, R., Lundblad, G. & Lind, J. (1976). Lysozyme and chitinase in blood and lymphomyeloid tissues of marine fish. *Marine Biology*, 36 (3): 277-282. doi: 10.1007/BF00389289.
- FAO. (2016). *The State of World Fisheries and Aquaculture 2016*. Rome.
- Färber, F. (2017). *Melanin spots in Atlantic salmon fillets - An investigation of the general problem, the frequency and the economic implication based on an online survey*. Ås: Norwegian University of Life Sciences (NMBU).
- Fast, M. D., Hosoya, S., Johnson, S. C. & Afonso, L. O. B. (2008). Cortisol response and immune-related effects of Atlantic salmon (*Salmo salar* Linnaeus) subjected to short- and long-term stress. *Fish & Shellfish Immunology*, 24 (2): 194-204. doi: <https://doi.org/10.1016/j.fsi.2007.10.009>.

- Ferguson, H. W. (1976). *The reticulo-endothelial system of teleost fish with special reference to the plaice (Pleuronectes platessa L.)*: University of Stirling.
- Ferguson, H. W. (1989). *Systemic Pathology of Fish: A text and atlas comparative tissue response in diseases of teleost*. 1st ed. Transactions of the American Fisheries Society. Iowa, USA: Taylor & Francis.
- Fletcher, T. C. & White, A. (1976). The lysozyme of the plaice *Pleuronectes platessa L.* *Comparative Biochemistry and Physiology Part B: Comparative Biochemistry*, 55 (2): 207-210. doi: [https://doi.org/10.1016/0305-0491\(76\)90231-5](https://doi.org/10.1016/0305-0491(76)90231-5).
- Folkestad, A., Wold, J. P., Rørvik, K.-A., Tschudi, J., Haugholt, K. H., Kolstad, K. & Mørkøre, T. (2008). Rapid and non-invasive measurements of fat and pigment concentrations in live and slaughtered Atlantic salmon (*Salmo salar L.*). *Aquaculture*, 280 (1): 129-135. doi: <https://doi.org/10.1016/j.aquaculture.2008.04.037>.
- Fraser, T. W., Hansen, T., Fleming, M. S. & Fjellidal, P. G. (2015). The prevalence of vertebral deformities is increased with higher egg incubation temperatures and triploidy in Atlantic salmon *Salmo salar L.* *J Fish Dis*, 38 (1): 75-89.
- Fujii, R. (1993a). Coloration and chromatophores. In Evans, D. H. (ed.) *The physiology of fishes*, pp. 535-562. Boca Raton: CRC Press.
- Fujii, R. (1993b). Cytophysiology of fish chromatophores. *International Review of Cytology* 143: 191-255.
- Gallo, V. P. & Civinini, A. (2003). Survey of the adrenal homolog in teleosts. *Int Rev Cytol*, 230: 89-187.
- Gemballa, S. (1995). *Vergleichend-anatomische Untersuchungen am Lokomotionsapparat der Actinopterygii. Phylogenetische Rekonstruktion und funktionelle Hypothesen*. Tübingen: Eberhard-Karls Universität.
- Gesto, M., Skov, P. V. & Jokumsen, A. (2017). Emergence Time and Skin Melanin Spot Patterns Do Not Correlate with Growth Performance, Social Competitive Ability or Stress Response in Farmed Rainbow Trout. *Frontiers in Neuroscience*, 11: 311-319.
- Giese, J. (1995). Measuring physical properties of foods. *Food Technology*.
- Godoy G, M. (2015). *Melanosis muscular en Salmón del Atlántico (Salmo salar): Patología macroscópica*. Patología en acuicultura. Available at: <http://goo.gl/P9D0NF> (accessed: 12/04/2018).
- Gray, J. (1968). *Animal Locomotion*. 1st ed. London: Littlehampton Book Services Ltd.
- Green, A., Martin, N., McKenzie, G., Pfitzner, J., Quintarelli, F., Thomas, B. W., O'Rourke, M. & Knight, N. (1991). Computer image analysis of pigmented skin lesions. *Melanoma Res*, 1 (4): 231-6.
- Grether, G. F., Hudon, J. & Millie, D. F. (1999). Carotenoid limitation of sexual coloration along an environmental gradient in guppies. *Proceedings of the Royal Society B: Biological Sciences*, 266 (1426): 1317-1317. doi: 10.1098/rspb.1999.0781.
- Grether, G. F., Kolluru, G. R. & Nersissian, K. (2004). Individual colour patches as multicomponent signals. *Biol Rev Camb Philos Soc*, 79 (3): 583-610.
- Griffith, S. C., Parker, T. H. & Olson, V. A. (2006). Melanin- versus carotenoid-based sexual signals: is the difference really so black and red? *Animal Behaviour*, 71 (4): 749-763. doi: <https://doi.org/10.1016/j.anbehav.2005.07.016>.
- Hancock, R. E. & Lehrer, R. (1998). Cationic peptides: a new source of antibiotics. *Trends Biotechnol*, 16 (2): 82-8.

- Hansen, J. D., Landis, E. D. & Phillips, R. B. (2005). Discovery of a unique Ig heavy-chain isotype (IgT) in rainbow trout: Implications for a distinctive B cell developmental pathway in teleost fish. *Proc Natl Acad Sci U S A*, 102 (19): 6919-24. doi: 10.1073/pnas.0500027102.
- Hardy, R. W., Torrissen, O. J. & Scott, T. M. (1990). Absorption and distribution of ¹⁴C-labeled canthaxanthin in rainbow trout (*Oncorhynchus mykiss*). *Aquaculture*, 87 (3): 331-340. doi: [https://doi.org/10.1016/0044-8486\(90\)90070-4](https://doi.org/10.1016/0044-8486(90)90070-4).
- Harrell, L. W., Etlinger, H. M. & Hodgins, H. O. (1976). Humoral factors important in resistance of salmonid fish to bacterial disease. II. Anti-*Vibrio anguillarum* activity in mucus and observations on complement. *Aquaculture*, 7 (4): 363-370. doi: [https://doi.org/10.1016/0044-8486\(76\)90133-2](https://doi.org/10.1016/0044-8486(76)90133-2).
- Hatlen, B., Berge, K., Nordrum, S., Johnsen, K., Kolstad, K. & Mørkøre, T. (2017). The effect of low inclusion levels of Antarctic krill (*Euphausia superba*) meal on growth performance, apparent digestibility and slaughter quality of Atlantic salmon (*Salmo salar*). *Aquaculture Nutrition*, 23 (4): 721-729. doi: 10.1111/anu.12439.
- Hatten, F., Fredriksen, A., Hordvik, I. & Endresen, C. (2001). Presence of IgM in cutaneous mucus, but not in gut mucus of Atlantic salmon, *Salmo salar*. Serum IgM is rapidly degraded when added to gut mucus. *Fish Shellfish Immunol*, 11 (3): 257-68. doi: 10.1006/fsim.2000.0313.
- Haugarvoll, E., Thorsen, J., Laane, M., Huang, Q. & Koppang, E. O. (2006). Melanogenesis and evidence for melanosome transport to the plasma membrane in a CD83+ teleost leukocyte cell line. *Pigment Cell Research*, 19 (3): 214-225. doi: 10.1111/j.1600-0749.2006.00297.x.
- Haugarvoll, E., Bjerkas, I., Szabo, N. J., Satoh, M. & Koppang, E. O. (2010). Manifestations of systemic autoimmunity in vaccinated salmon. *Vaccine*, 28 (31): 4961-9. doi: 10.1016/j.vaccine.2010.05.032.
- Hearing, V. J. (1993). Unraveling the melanocyte. *Am J Hum Genet*, 52 (1): 1-7.
- Heia, K., Sivertsen, A. H. & Birkeland, S. (2009). *Automated Quality Control of Salmon Fillets - Hyperspectral imaging for on-line inspection*. NIR 2009, Bangkok.
- Helen, N.-S., Aspengren, S. & Wallin, M. (2013). Rapid color change in fish and amphibians – function, regulation, and emerging applications. *Pigment Cell & Melanoma Research*, 26 (1): 29-38. doi: 10.1111/pcmr.12040.
- Hennessy, A., Oh, C., Diffey, B., Wakamatsu, K., Ito, S. & Rees, J. (2005). Eumelanin and pheomelanin concentrations in human epidermis before and after UVB irradiation. *Pigment Cell Res*, 18 (3): 220-3. doi: 10.1111/j.1600-0749.2005.00233.x.
- Herraez, M. P. & Zapata, A. G. (1986). Structure and function of the melano-macrophage centres of the goldfish *Carassius auratus*. *Veterinary Immunology and Immunopathology*, 12 (1): 117-126. doi: [https://doi.org/10.1016/0165-2427\(86\)90116-9](https://doi.org/10.1016/0165-2427(86)90116-9).
- Herring, P. J. (1994). Reflective systems in aquatic animals. *Comparative Biochemistry and Physiology*, 109 (A): 513-546.
- Herrling, T., Jung, K. & Fuchs, J. (2008). The role of melanin as protector against free radicals in skin and its role as free radical indicator in hair. *Spectrochimica Acta Part A: Molecular and Biomolecular Spectroscopy*, 69 (5): 1429-1435. doi: <https://doi.org/10.1016/j.saa.2007.09.030>.
- Hikima, J., Jung, T. S. & Aoki, T. (2011). Immunoglobulin genes and their transcriptional control in teleosts. *Dev Comp Immunol*, 35 (9): 924-36. doi: 10.1016/j.dci.2010.10.011.

- Hill, H. Z. (1992). The function of melanin or six blind people examine an elephant. *BioEssays*, 14 (1): 49-56. doi: 10.1002/bies.950140111.
- Hjelmeland, K., Christie, M. & Raa, J. (1983). Skin mucus protease from rainbow trout, *Salmo gairdneri* Richardson, and its biological significance. *Journal of Fish Biology*, 23 (1): 13-22. doi: 10.1111/j.1095-8649.1983.tb02878.x.
- Horcicko, J., Borovansky, J., Duchon, J. & Prochazkova, B. (1973). Distribution of zinc and copper in pigmented tissues. *Hoppe Seylers Z Physiol Chem*, 354 (2): 203-4.
- Hordvik, I. (2015). Immunoglobulin Isotypes in Atlantic Salmon, *Salmo Salar*. *Biomolecules*, 5 (1): 166-177. doi: 10.3390/biom5010166.
- Horth, L. (2003). Melanic body colour and aggressive mating behaviour are correlated traits in male mosquitofish (*Gambusia holbrooki*). *Proceedings of the Royal Society B: Biological Sciences*, 270 (1519): 1033-1040. doi: 10.1098/rspb.2003.2348.
- Hullo, M. F., Moszer, I., Danchin, A. & Martin-Verstraete, I. (2001). CotA of *Bacillus subtilis* is a copper-dependent laccase. *J Bacteriol*, 183 (18): 5426-30.
- Iger, Y., Abraham, M., Zhang, L., Stoumboudi, M., Alexis, M., Tsangaris, K., Wendelaar Bonga, S. & van Ham, E. (2001). *Fish skin alterations as indicators for stress in fresh- and seawater aquaculture*. European Aquaculture Society, pp. 109-110.
- Ilie, A. & Welch, G. (2005). *Ensuring color consistency across multiple cameras*. Proceedings of the tenth IEEE international conference on computer vision, pp. 1368-1275.
- Ingram, G. A. (1980). Substances involved in the natural resistance of fish to infection—A review. *Journal of Fish Biology*, 16 (1): 23-60. doi: 10.1111/j.1095-8649.1980.tb03685.x.
- Isaksson, T., Tøgersen, G., Iversen, A. & Hildrum, K. I. (1995). Non-destructive determination of fat, moisture and protein in salmon fillets by use of near-infrared diffuse spectroscopy. *Journal of the Science of Food and Agriculture*, 69: 95-100.
- Ito, S. (1986). Reexamination of the structure of eumelanin. *Biochim Biophys Acta*, 883 (1): 155-61.
- Ito, S., Wakamatsu, K. & Ozeki, H. (2000). Chemical analysis of melanins and its application to the study of the regulation of melanogenesis. *Pigment Cell Res*, 13 Suppl 8: 103-9.
- Ito, S. (2003). The IFPCS presidential lecture: a chemist's view of melanogenesis. *Pigment Cell Res*, 16 (3): 230-6.
- Jackson, I. J., Chambers, D. M., Tsukamoto, K., Copeland, N. G., Gilbert, D. J., Jenkins, N. A. & Hearing, V. (1992). A second tyrosinase-related protein, TRP-2, maps to and is mutated at the mouse slaty locus. *Embo j*, 11 (2): 527-35.
- Jain, S., Jagtap, V. & Pise, N. (2015). Computer Aided Melanoma Skin Cancer Detection Using Image Processing. *Procedia Computer Science*, 48: 735-740. doi: <https://doi.org/10.1016/j.procs.2015.04.209>.
- Janeway, C. A., Travers, P., Walport, M. & Capra, J. D. (1999). Basic Concepts in Immunology. In Woof, R. (ed.) *Immuno biology. The immune system in health and disease*, pp. 10-31: Elsevier Science Ltd/Garland Publishing.
- Jenkins, P. G., Wrathmell, A. B., Harris, J. E. & Pulsford, A. L. (1994). Systemic and mucosal immune responses to enterically delivered antigen in *Oreochromis mossambicus*. *Fish & Shellfish Immunology*, 4 (4): 255-271. doi: <https://doi.org/10.1006/fsim.1994.1023>.
- Jia, X., Patrzykat, A., Devlin, R. H., Ackerman, P. A., Iwama, G. K. & Hancock, R. E. W. (2000). Antimicrobial Peptides Protect Coho Salmon from *Vibrio anguillarum* Infections. *Applied and Environmental Microbiology*, 66 (5): 1928-1932.

- Jimenez-Cervantes, C., Solano, F., Lozano, J. A. & Garcia-Borrón, J. C. (1994). The DHICA oxidase activity of the melanosomal tyrosinases LEMT and HEMT. *Pigment Cell Res*, 7 (5): 298-304.
- Kelley, J. L. & Davies, W. I. L. (2016). The Biological Mechanisms and Behavioral Functions of Opsin-Based Light Detection by the Skin. *Frontiers in Ecology and Evolution*, 4 (106): 1-13.
- Kelsh, R. N., Schmid, B. & Eisen, J. S. (2000). Genetic Analysis of Melanophore Development in Zebrafish Embryos. *Developmental Biology*, 225 (2): 277-293. doi: <https://doi.org/10.1006/dbio.2000.9840>.
- Khan, U. W., Overli, O., Hinkle, P. M., Pasha, F. A., Johansen, I. B., Berget, I., Silva, P. I., Kittilsen, S., Høglund, E., Omholt, S. W., et al. (2016). A novel role for pigment genes in the stress response in rainbow trout (*Oncorhynchus mykiss*). *Sci Rep*, 6: 28969. doi: 10.1038/srep28969.
- Kittilsen, S., Schjolden, J., Beitnes-Johansen, I., Shaw, J. C., Pottinger, T. G., Sørensen, C., Braastad, B. O., Bakken, M. & Overli, O. (2009). Melanin-based skin spots reflect stress responsiveness in salmonid fish. *Horm Behav*, 56 (3): 292-8. doi: 10.1016/j.yhbeh.2009.06.006.
- Kobayashi, T., Urabe, K., Winder, A., Jiménez-Cervantes, C., Imokawa, G., Brewington, T., Solano, F., García-Borrón, J. C. & Hearing, V. J. (1994). Tyrosinase related protein 1 (TRP1) functions as a DHICA oxidase in melanin biosynthesis. *The EMBO Journal*, 13 (24): 5818-5825.
- Kollias, N., Sayre, R. M., Zeise, L. & Chedekel, M. R. (1991). New trends in photobiology: Photoprotection by melanin. *Journal of Photochemistry and Photobiology B: Biology*, 9 (2): 135-160. doi: [https://doi.org/10.1016/1011-1344\(91\)80147-A](https://doi.org/10.1016/1011-1344(91)80147-A).
- Koppang, E. O., Haugarvoll, E., Hordvik, I., Aune, L. & Poppe, T. T. (2005). Vaccine-associated granulomatous inflammation and melanin accumulation in Atlantic salmon, *Salmo salar* L., white muscle. *J Fish Dis*, 28 (1): 13-22. doi: 10.1111/j.1365-2761.2004.00583.x.
- Korzan, W. J. & Fernald, R. D. (2007). Territorial male color predicts agonistic behavior of conspecifics in a color polymorphic species. *Behavioral Ecology*, 18 (2): 318-323. doi: 10.1093/beheco/arl093.
- Koteng, D. F. (1992). *Markedsundersøkelse, norsk laks: Fiskerinaeringsens Landsforening*.
- Kottler, V. A., Kunstner, A. & Scharl, M. (2015). Pheomelanin in fish? *Pigment Cell Melanoma Res*, 28 (3): 355-6. doi: 10.1111/pcmr.12359.
- Kripke, M. L. (1984). Immunological unresponsiveness induced by ultraviolet radiation. *Immunol Rev*, 80: 87-102.
- Kroumpouzou, G., Urabe, K., Kobayashi, T., Sakai, C. & Hearing, V. J. (1994). Functional analysis of the slaty gene product (TRP2) as dopachrome tautomerase and the effect of a point mutation on its catalytic function. *Biochem Biophys Res Commun*, 202 (2): 1060-8. doi: 10.1006/bbrc.1994.2036.
- Kuo, M. J. & Alexander, M. (1967). Inhibition of the lysis of fungi by melanins. *J Bacteriol*, 94 (3): 624-9.
- Kuznetsov, V. D., Filippova, S. N. & Rybakova, A. M. (1984). [Nature of the brown pigment and the composition of the phenol oxidases of *Streptomyces galbus*]. *Mikrobiologiya*, 53 (2): 251-256.

- Lam, C., Schutze, E., Hildebrandt, J., Aschauer, H., Liehl, E., Macher, I. & Stutz, P. (1991). SDZ MRL 953, a novel immunostimulatory monosaccharidic lipid A analog with an improved therapeutic window in experimental sepsis. *Antimicrob Agents Chemother*, 35 (3): 500-5.
- Lamers, C. H. & De Haas, M. J. (1985). Antigen localization in the lymphoid organs of carp (*Cyprinus carpio*). *Cell Tissue Res*, 242 (3): 491-8.
- Lange, S. & Magnadóttir, B. (2003). Spontaneous haemolytic activity of Atlantic halibut (*Hippoglossus hippoglossus* L.) and sea bass (*Dicentrarchus labrax*) serum. *Comparative Biochemistry and Physiology Part B: Biochemistry and Molecular Biology*, 136 (1): 99-106. doi: [https://doi.org/10.1016/S1096-4959\(03\)00173-8](https://doi.org/10.1016/S1096-4959(03)00173-8).
- Larsen, H. A., Austbo, L., Morkore, T., Thorsen, J., Hordvik, I., Fischer, U., Jirillo, E., Rimstad, E. & Koppang, E. O. (2012). Pigment-producing granulomatous myopathy in Atlantic salmon: a novel inflammatory response. *Fish Shellfish Immunol*, 33 (2): 277-85. doi: 10.1016/j.fsi.2012.05.012.
- Larsen, H. A., Austbo, L., Konig, M., Sorum, H., Rimstad, E. & Koppang, E. O. (2013). Transcription of the tyrosinase gene family in an Atlantic salmon leukocyte cell line (SHK-1) is influenced by temperature, but not by virus infection or bacterin stimulation. *Dev Comp Immunol*, 41 (1): 50-8. doi: 10.1016/j.dci.2013.03.019.
- Lauritzsen, K., Martinsen, G. & Olsen, R. L. (1999). Copper induced lipid oxidation during salting of cod (*Gadus morhua* L.). *Journal of Food Lipids*, 6 (4): 299-315. doi: 10.1111/j.1745-4522.1999.tb00152.x.
- Lerner, A. B. & McGuire, J. S. (1961). Effect of alpha- and betamelanocyte stimulating hormones on the skin colour of man. *Nature*, 189: 176-9.
- Levine, N., Sheftel, S. N., Eytan, T., Dorr, R. T., Hadley, M. E., Weinrach, J. C., Ertl, G. A., Toth, K., McGee, D. L. & Hruby, V. J. (1991). Induction of skin tanning by subcutaneous administration of a potent synthetic melanotropin. *Jama*, 266 (19): 2730-6.
- Liu, Y., Hong, L., Wakamatsu, K., Ito, S., Adhyaru, B., Cheng, C.-Y., Bowers, C. R. & Simon, J. D. (2005). Comparison of Structural and Chemical Properties of Black and Red Human Hair Melanosomes. *Photochemistry and Photobiology*, 81 (1): 135-144. doi: 10.1562/2004-08-03-RA-259.1.
- Liu, Y., Hong, L., Wakamatsu, K., Ito, S., Adhyaru, B. B., Cheng, C. Y., Bowers, C. R. & Simon, J. D. (2005). Comparisons of the structural and chemical properties of melanosomes isolated from retinal pigment epithelium, iris and choroid of newborn and mature bovine eyes. *Photochem Photobiol*, 81 (3): 510-6. doi: 10.1562/2004-10-19-ra-345.1.
- Livak, K. J. & Schmittgen, T. D. (2001). Analysis of Relative Gene Expression Data Using Real-Time Quantitative PCR and the $2^{-\Delta\Delta CT}$ Method. *Methods*, 25 (4): 402-408. doi: <https://doi.org/10.1006/meth.2001.1262>.
- Long, E. R., Macdonald, D. D., Smith, S. L. & Calder, F. D. (1995). Incidence of adverse biological effects within ranges of chemical concentrations in marine and estuarine sediments. *Environmental Management*, 19 (1): 81-97. doi: 10.1007/BF02472006.
- Lumsden, J. S., Ostland, V. E., Byrne, P. J. & Ferguson, H. W. (1993). Detection of a distinct gill-surface antibody response following horizontal infection and bath challenge of brook trout *Salvelinus fontinalis* with *Flavobacterium branchiophilum*, the causative agent of bacterial gill disease. *Diseases of Aquatic Organisms*, 16 (1): 21-27. doi: 10.3354/dao016021.

- Magnadottir, B., Lange, S., Gudmundsdottir, S., Bogwald, J. & Dalmo, R. A. (2005). Ontogeny of humoral immune parameters in fish. *Fish Shellfish Immunol*, 19 (5): 429-39. doi: 10.1016/j.fsi.2005.03.010.
- Magnadottir, B. (2006). Innate immunity of fish (overview). *Fish Shellfish Immunol*, 20 (2): 137-51. doi: 10.1016/j.fsi.2004.09.006.
- Magnadottir, B. (2010). Immunological control of fish diseases. *Mar Biotechnol (NY)*, 12 (4): 361-79. doi: 10.1007/s10126-010-9279-x.
- Mahalwar, P., Singh, A. P., Fadeev, A., Nüsslein-Volhard, C. & Irion, U. (2016). Heterotypic interactions regulate cell shape and density during color pattern formation in zebrafish. *Biology Open*, 5 (11): 1680-1690. doi: 10.1242/bio.022251.
- Malik, S., Dolan, T. M., Maben, Z. J. & Hinkle, P. M. (2015). Adrenocorticotrophic Hormone (ACTH) Responses Require Actions of the Melanocortin-2 Receptor Accessory Protein on the Extracellular Surface of the Plasma Membrane. *J Biol Chem*, 290 (46): 27972-85. doi: 10.1074/jbc.M115.668491.
- Marie-Orleach, L., Roussel, J.-M., Bugeon, J., Tremblay, J., Ombredane, D. & Evanno, G. (2014). Melanin-based coloration of sneaker male Atlantic salmon is linked to viability and emergence timing of their offspring. *Biological Journal of the Linnean Society*, 111 (1): 126-135. doi: 10.1111/bij.12187.
- Marks, M. S., Theos, A. C. & Raposo, G. (2003). Melanosomes and MHC class II antigen-processing compartments: a tinted view of intracellular trafficking and immunity. *Immunol Res*, 27 (2-3): 409-26. doi: 10.1385/ir:27:2-3:409.
- Marty-Mahé, P., Loisel, P., Fauconneau, B. t., Haffray, P., Brossard, D. & Davenel, A. (2004). Quality traits of brown trouts (*Salmo trutta*) cutlets described by automated color image analysis. *Aquaculture*, 232 (1): 225-240. doi: [https://doi.org/10.1016/S0044-8486\(03\)00458-7](https://doi.org/10.1016/S0044-8486(03)00458-7).
- Mathiassen, J. R. & Misimi, E. (2007). *A Simple Computer Vision Method for Automatic Detection of Melanin Spots in Atlantic Salmon Fillets*. International Machine Vision and Image Processing Conference, Maynooth, pp. 192-200.
- Maule, A. G. & Schreck, C. B. (1990). Changes in numbers of leukocytes in immune organs of juvenile coho salmon after acute stress or cortisol treatment. *Journal of Aquatic Animal Health*, 2 (4): 298-304. doi: 10.1577/1548-8667(1990)002<0298:CINOLI>2.3.CO;2.
- Meinelt, T., Krüger, R., Pietrock, M., Osten, R. & Steinberg, C. (1997). Mercury pollution and macrophage centres in pike (*Esox lucius*) tissues. *Environmental Science and Pollution Research*, 4 (1): 32-36. doi: 10.1007/bf02986262.
- Mellgren, E. M. & Johnson, S. L. (2002). The evolution of morphological complexity in zebrafish stripes. *Trends Genet*, 18 (3): 128-34.
- Menzies, F. D., Wheatley, S. B., McLoughlin, F. M. & Gooall, E. A. (1996). Development of a computerized information retrieval system for Atlantic salmon, *Salmo salar* L., production. *Aquaculture Research*, 27: 183-190.
- Meyskens Jr, F. L., Farmer, P. & Fruehauf, J. P. (2001). Redox Regulation in Human Melanocytes and Melanoma. *Pigment Cell Research*, 14 (3): 148-154. doi: 10.1034/j.1600-0749.2001.140303.x.
- Michelsen, O. J. (2000). *Effect of different lipid sources on the non-specific immune system of Atlantic salmon (Salmo salar)*. Bergen, Norway: University of Bergen.
- Mishra, N. K. & Emre Celebi, M. (2016). An Overview of Melanoma Detection in Dermoscopy Images Using Image Processing and Machine Learning.
- Mørkøre, T. (2012). *Mørke flekker i laksefilet – Kunnskapsstatus og tiltak for å begrense omfanget*. Nofima.

- Mørkøre, T., Larsson, T., Kvellestad, A. S., Koppang, E. O., Åsli, M., Krasnov, A., Dessen, J.-E., Moreno, H. M., Rørvik, K. A., Valen, E., et al. (2015). *Mørke flekker i laksefilet – Kunnskapsstatus og tiltak for å begrense omfanget*: Nofima.
- Mørkøre, T. (2017). *Mørke flekker i laksefilet - kunnskapsstatus*: Nofima.
- Napolitano, A., Crescenzi, O. & Prota, G. (1993). Copolymerisation of 5,6-dihydroxyindole and 5,6-dihydroxyindole-2-carboxylic acid in melanogenesis: Isolation of a cross-coupling product. *Tetrahedron Letters*, 34 (5): 885-888. doi: [https://doi.org/10.1016/0040-4039\(93\)89040-W](https://doi.org/10.1016/0040-4039(93)89040-W).
- Nassau, K. (1998). *Color for science, art and technology*. Amsterdam, The Netherlands: Elsevier Science B.V.
- Newton, I. (1672). 'A Letter of Mr. Isaac Newton containing his New Theory about Light and Colors'. *Philosophical Transactions of the Royal Society*, 80: 3075-3087.
- Nickell, D. C. & Springate, J. R. (2001). Pigmentation of farmed salmonids. In Kestin, S. C. & Warris, P. D. (eds) *Fish Farmed Quality*, pp. 58-75.
- Nonaka, M., Yamaguchi, N., Natsuume-Sakai, S. & Takahashi, M. (1981). The complement system of rainbow trout (*Salmo gairdneri*). I. Identification of the serum lytic system homologous to mammalian complement. *J Immunol*, 126 (4): 1489-94.
- Nortvedt, R., Espe, M., Gribbestad, I. S., Jørgensen, L., Karlsen, C. & Otterå, H. (2007). High-quality Seafood Products based on Ethical and Sustainable Production. In Consumption, A. R. F. C. t. (ed.), pp. 28-44: The Research Council of Norway.
- Nylund, S., Andersen, L., Saevareid, I., Plarre, H., Watanabe, K., Arnesen, C. E., Karlsbakk, E. & Nylund, A. (2011). Diseases of farmed Atlantic salmon *Salmo salar* associated with infections by the microsporidian *Paranucleospora theridion*. *Dis Aquat Organ*, 94 (1): 41-57. doi: 10.3354/dao02313.
- Olsen, R. E., Suontama, J., Langmyhr, E., Mundheim, H., Ringø, E., Melle, W., Malde, M. K. & Hemre, G. I. (2006). The replacement of fish meal with Antarctic krill, *Euphausia superba* in diets for Atlantic salmon, *Salmo salar*. *Aquaculture Nutrition*, 12 (4): 280-290. doi: doi:10.1111/j.1365-2095.2006.00400.x.
- Orazio, J., Jarrett, S., Amaro-Ortiz, A. & Scott, T. (2013). UV Radiation and the Skin. *International Journal of Molecular Sciences*, 14 (6): 12222.
- Orlow, S. J. (1995). Melanosomes are specialized members of the lysosomal lineage of organelles. *J Invest Dermatol*, 105 (1): 3-7.
- Ozeki, H., Wakamatsu, K., Ito, S. & Ishiguro, I. (1997). Chemical characterization of eumelanins with special emphasis on 5,6-dihydroxyindole-2-carboxylic acid content and molecular size. *Anal Biochem*, 248 (1): 149-57. doi: 10.1006/abio.1997.2079.
- Palazzo, R. E., Lynch, T. J., Lo, S. J., Taylor, J. D. & Tchen, T. T. (1989). Rearrangements of pterinosomes and cytoskeleton accompanying pigment dispersion in goldfish xanthophores. *Cell Motility and the Cytoskeleton*, 13 (1): 9-20. doi: 10.1002/cm.970130103.
- Pasquier, L. D. (1982). Antibody diversity in lower vertebrates—why is it so restricted? *Nature*, 296: 311. doi: 10.1038/296311a0.
- Patel, K. R., Wyman, J. A., Patel, K. A. & Burden, B. J. (1996). A Mutant of *Bacillus thuringiensis* Producing a Dark-Brown Pigment with Increased UV Resistance and Insecticidal Activity. *Journal of Invertebrate Pathology*, 67 (2): 120-124. doi: <https://doi.org/10.1006/jipa.1996.0018>.
- Pathak, M. A., Jimbow, K. & Fitzpatrick, T. (1980). Photobiology of pigment cell. In Seiji, M. (ed.) *Phenotypic Expression in Pigment Cells*, pp. 655-670. Tokyo, Japan: University of Tokyo Press.

- Paulsen, S. M., Lunde, H., Engstad, R. E. & Robertsen, B. (2003). In vivo effects of beta-glucan and LPS on regulation of lysozyme activity and mRNA expression in Atlantic salmon (*Salmo salar* L.). *Fish Shellfish Immunol*, 14 (1): 39-54.
- Pavlidis, M., Papandroulakis, N. & Divanach, P. (2006). A method for the comparison of chromaticity parameters in fish skin: Preliminary results for coloration pattern of red skin Sparidae. *Aquaculture*, 258 (1): 211-219. doi: <https://doi.org/10.1016/j.aquaculture.2006.05.028>.
- Peng, G., Taylor, J. D. & Tchen, T. T. (1994). Goldfish tyrosinase related protein I (TRP-1): deduced amino acid sequence from cDNA and comments on structural features. *Pigment Cell Res*, 7 (1): 9-16.
- Peng, S., Chen, L., Qin, J. G., Hou, J., Yu, N., Long, Z., Li, E. & Ye, J. (2009). Effects of dietary vitamin E supplementation on growth performance, lipid peroxidation and tissue fatty acid composition of black sea bream (*Acanthopagrus schlegelii*) fed oxidized fish oil. *Aquaculture Nutrition*, 15 (3): 329-337. doi: 10.1111/j.1365-2095.2009.00657.x.
- Perceptually uniform color spaces*. (17/04/2018). Programming Design Systems. Available at: <https://programmingdesignsystems.com/color/perceptually-uniform-color-spaces/>.
- Pfeifer, G. P., You, Y.-H. & Besaratinia, A. (2005). Mutations induced by ultraviolet light. *Mutation Research/Fundamental and Molecular Mechanisms of Mutagenesis*, 571 (1): 19-31. doi: <https://doi.org/10.1016/j.mrfmmm.2004.06.057>.
- Pickering, A. D. & Pottinger, T. G. (1985). Cortisol can increase the susceptibility of brown trout, *Salmo trutta* L., to disease without reducing the white blood cell count. *Journal of Fish Biology*, 27 (5): 611-619. doi: 10.1111/j.1095-8649.1985.tb03206.x.
- Pickering, A. D. & Pottinger, T. G. (1987). Crowding causes prolonged leucopenia in salmonid fish, despite interrenal acclimation. *Journal of Fish Biology*, 30 (6): 701-712. doi: 10.1111/j.1095-8649.1987.tb05799.x.
- Potaman, V. N., Alfeeva, L. Y., Kamensky, A. A. & Nezavibatko, V. N. (1993). Degradation of ACTH/MSH(4-10) and its synthetic analog semax by rat serum enzymes: an inhibitor study. *Peptides*, 14 (3): 491-5.
- Poynton, C. & Funt, B. (2014). Perceptual uniformity in digital image representation and display. *Color Research & Application*, 39 (1): 6-15. doi: doi:10.1002/col.21768.
- Press, C. M., Evensen, Ø., Reitan, L. J. & Landsverk, T. (1996). Retention of furunculosis vaccine components in Atlantic salmon, *Salmo salar* L., following different routes of vaccine administration. *Journal of Fish Diseases*, 19 (3): 215-224. doi: doi:10.1111/j.1365-2761.1996.tb00128.x.
- Rafiq, M. B. (2015). *Dietary Impact of Feed on Performance, Health and Tissue Melanization of Atlantic Salmon (Salmo salar L.)*. 1432 Ås, Norway: Norwegian University of Life Sciences and Faculty of Veterinary Medicine and Biosciences.
- Randhawa, M., Huff, T., Valencia, J. C., Younossi, Z., Chandhoke, V., Hearing, V. J. & Baranova, A. (2009). Evidence for the ectopic synthesis of melanin in human adipose tissue. *Faseb j*, 23 (3): 835-43. doi: 10.1096/fj.08-116327.
- Raposo, G., Fevrier, B., Stoorvogel, W. & Marks, M. S. (2002). Lysosome-related organelles: a view from immunity and pigmentation. *Cell Struct Funct*, 27 (6): 443-56.
- Rasband, W. S. (1997). *ImageJ*. Bethesda, Maryland, USA: U. S. National Institutes of Health.

- Roberts, R. J. (1975). Melanin-containing cells of the teleost fish and their relation to disease. In Ribelin, W. E. & Migaki, G. (eds) *The Pathology of Fishes*, pp. 399-428. Madison, USA: University of Wisconsin Press.
- Roberts, R. J. (1976). Experimental Pathogenesis of Lymphocystis in the Plaice (*Pleuronectes Platessa*). In Page, L. A. (ed.) *Wildlife Diseases*, pp. 431-441. Boston, MA: Springer US.
- Roberts, R. J. (2012). *Fish pathology*. 4th ed. Oxford, UK: Wiley-Blackwell.
- Rodger, H., Graham, D., Foyle, L., Norris, A., Ratcliff, J., Murphy, K., Mitchell, S., Staples, C., Jewhurst, H., Todd, D., et al. (2005). Research on Pancreas Disease in Irish Farmed Salmon 2004/2005 – Current and Future Initiatives. *Marine Environment and Health Series*, 22: 49.
- Rombout, J. W., Blok, L. J., Lamers, C. H. & Egberts, E. (1986). Immunization of carp (*Cyprinus carpio*) with a *Vibrio anguillarum* bacterin: indications for a common mucosal immune system. *Dev Comp Immunol*, 10 (3): 341-51.
- Rouzaud, F., Costin, G.-E., Yamaguchi, Y., Valencia, J. C., Berens, W. F., Chen, K. G., Hoashi, T., Böhm, M., Abdel-Malek, Z. A. & Hearing, V. J. (2006). Regulation of constitutive and UVR-induced skin pigmentation by melanocortin 1 receptor isoforms. *The FASEB Journal*, 20 (11): 1927-1929. doi: 10.1096/fj.06-5922fje.
- Rózanowska, M., Sarna, T., Land, E. J. & Truscott, T. G. (1999). Free radical scavenging properties of melanin: Interaction of eu- and pheo-melanin models with reducing and oxidising radicals. *Free Radical Biology and Medicine*, 26 (5): 518-525. doi: [https://doi.org/10.1016/S0891-5849\(98\)00234-2](https://doi.org/10.1016/S0891-5849(98)00234-2).
- Rye, M. (1991). Prediction of carcass composition in Atlantic salmon by computerized tomography. *Aquaculture*, 99: 35-48.
- Saberioon, M., Cisar, P., Labbe, L., Soucek, P., Pelissier, P. & Kerneis, T. (2018). Comparative Performance Analysis of Support Vector Machine, Random Forest, Logistic Regression and k-Nearest Neighbours in Rainbow Trout (*Oncorhynchus Mykiss*) Classification Using Image-Based Features. *Sensors (Basel)*, 18 (4). doi: 10.3390/s18041027.
- Sahoo, P. K. & Mukherjee, S. C. (2002). Influence of high dietary α -tocopherol intakes on specific immune response, nonspecific resistance factors and disease resistance of healthy and aflatoxin B1-induced immunocompromised Indian major carp, *Labeo rohita* (Hamilton). *Aquaculture Nutrition*, 8 (3): 159-167. doi: 10.1046/j.1365-2095.2002.00189.x.
- Salinas, I., Lockhart, K., Bowden, T. J., Collet, B., Secombes, C. J. & Ellis, A. E. (2004). An assessment of immunostimulants as Mx inducers in Atlantic salmon (*Salmo salar* L.) parr and the effect of temperature on the kinetics of Mx responses. *Fish & Shellfish Immunology*, 17 (2): 159-170. doi: <https://doi.org/10.1016/j.fsi.2004.01.003>.
- Sarna, T., Menon, I. A. & Sealy, R. C. (1985). Photosensitization of melanins: a comparative study. *Photochem Photobiol*, 42 (5): 529-32.
- Scott, T. L., Christian, P. A., Kesler, M. V., Donohue, K. M., Shelton, B., Wakamatsu, K., Ito, S. & D'Orazio, J. (2012). Pigment-independent cAMP-mediated epidermal thickening protects against cutaneous UV injury by keratinocyte proliferation. *Experimental Dermatology*, 21 (10): 771-777. doi: 10.1111/exd.12012.
- Sealy, R. C. (1984). Free radicals in melanin Formation, Structure and reactions. In Armstrong, D. (ed.) *Free Radicals in Molecular Biology, Aging and Disease*, pp. 67-76. New York, USA: Raven Press.

- Sealy, R. C., Sarna, T., Wanner, E. J. & Reszka, K. (1984). Photosensitization of melanin: an electron spin resonance study of sensitized radical production and oxygen consumption. *Photochem Photobiol*, 40 (4): 453-9.
- Secombes, C. J. & Fletcher, T. C. (1992). The role of phagocytes in the protective mechanisms of fish. *Annual Review of Fish Diseases*, 2: 53-71. doi: [https://doi.org/10.1016/0959-8030\(92\)90056-4](https://doi.org/10.1016/0959-8030(92)90056-4).
- Seierstad, S. L., Haugland, Ø., Larsen, S., Waagbø, R. & Evensen, Ø. (2009). Pro-inflammatory cytokine expression and respiratory burst activity following replacement of fish oil with rapeseed oil in the feed for Atlantic salmon (*Salmo salar* L.). *Aquaculture*, 289 (3): 212-218. doi: <https://doi.org/10.1016/j.aquaculture.2008.12.004>.
- Shephard, K. L. (1994). Functions for fish mucus. *Reviews in Fish Biology Fisheries*, 4: 401-429.
- Sichel, G., Scalia, M., Mondio, F. & Corsaro, C. (1997). The Amphibian Kupffer Cells Build and Demolish Melanosomes: An Ultrastructural Point of View. *Pigment Cell Research*, 10 (5): 271-287. doi: 10.1111/j.1600-0749.1997.tb00687.x.
- Sissener, N. H., Waagbø, R., Rosenlund, G., Tvenning, L., Susort, S., Lea, T. B., Oaland, Ø., Chen, L. & Breck, O. (2016). Reduced n-3 long chain fatty acid levels in feed for Atlantic salmon (*Salmo salar* L.) do not reduce growth, robustness or product quality through an entire full scale commercial production cycle in seawater. *Aquaculture*, 464: 236-245. doi: <https://doi.org/10.1016/j.aquaculture.2016.06.034>.
- Skår-Ulvestad, J. (2017). *Studies on the stimulation of Atlantic salmon macrophage-like cells with emphasis on respiratory burst*. 60: The Arctic university of Norway.
- Slominski, A., Tobin, D. J., Shibahara, S. & Wortsman, J. (2004). Melanin pigmentation in mammalian skin and its hormonal regulation. *Physiol Rev*, 84 (4): 1155-228. doi: 10.1152/physrev.00044.2003.
- Slominski, A. (2009). Neuroendocrine activity of the melanocyte. *Experimental Dermatology*, 18 (9): 760-763. doi: 10.1111/j.1600-0625.2009.00892.x.
- Smith, S. R., Gawronska-Kozak, B., Janderova, L., Nguyen, T., Murrell, A., Stephens, J. M. & Mynatt, R. L. (2003). Agouti expression in human adipose tissue: functional consequences and increased expression in type 2 diabetes. *Diabetes*, 52 (12): 2914-22.
- Solem, S. T., Jørgensen, J. B. & Robertsen, B. (1995). Stimulation of respiratory burst and phagocytic activity in Atlantic salmon (*Salmo salar* L.) macrophages by lipopolysaccharide. *Fish & Shellfish Immunology*, 5 (7): 475-491. doi: [https://doi.org/10.1016/S1050-4648\(95\)80049-2](https://doi.org/10.1016/S1050-4648(95)80049-2).
- Sono, K., Lye, D., Moore, C. A., Boyd, W. C., Gorlin, T. A. & Belitsky, J. M. (2012). Melanin-Based Coatings as Lead-Binding Agents. *Bioinorganic Chemistry and Applications*, 2012: 361803. doi: 10.1155/2012/361803.
- Stien, L. H., Amundsen, A. H., Mørkøre, T., Økland, S. N. & Nortvedt, R. (2006). Instrumental colour analyses of Atlantic salmon (*Salmo salar* L.) muscle. In Luten, J. B., Jacobsen, C., Bakaert, K. & Sæbø, A. (eds) *Seafood research from fish to dish – Quality, safety and processing of wild and farmed fish*, pp. 525-539.
- Suontama, J., Kiessling, A., Melle, W., Waagbø, R. & Olsen, R. E. (2007). Protein from Northern krill (*Thysanoessa inermis*), Antarctic krill (*Euphausia superba*) and the Arctic amphipod (*Themisto libellula*) can partially replace fish meal in diets to Atlantic salmon (*Salmo salar*) without affecting product quality. *Aquaculture Nutrition*, 13 (1): 50-58. doi: doi:10.1111/j.1365-2095.2007.00453.x.

- Tadiso, T. M., Lie, K. K. & Hordvik, I. (2011). Molecular cloning of IgT from Atlantic salmon, and analysis of the relative expression of tau, mu, and delta in different tissues. *Vet Immunol Immunopathol*, 139 (1): 17-26. doi: 10.1016/j.vetimm.2010.07.024.
- Takeuchi, I. K. (1976). Electron microscopy of two types of reflecting chromatophores (iridophores and leucophores) in the guppy, *Lebistes reticulatus* Peters. *Cell Tissue Res*, 173 (1): 17-27.
- Tews, D. S. & Pongratz, D. E. (1995). Immunohistological analysis of sarcoid myopathy. *Journal of Neurology, Neurosurgery, and Psychiatry*, 59 (3): 322-325.
- Tharanathan, R. N. & Kittur, F. S. (2003). Chitin--the undisputed biomolecule of great potential. *Crit Rev Food Sci Nutr*, 43 (1): 61-87. doi: 10.1080/10408690390826455.
- Thorsen, J., Høyheim, B. & Koppang, E. O. (2006). Isolation of the Atlantic salmon tyrosinase gene family reveals heterogenous transcripts in a leukocyte cell line. *Pigment Cell Research*, 19 (4): 327-336. doi: 10.1111/j.1600-0749.2006.00319.x.
- Tripathi, R. K., Hearing, V. J., Urabe, K., Aroca, P. & Spritz, R. A. (1992). Mutational mapping of the catalytic activities of human tyrosinase. *J Biol Chem*, 267 (33): 23707-12.
- Tsukamoto, K., Jackson, I. J., Urabe, K., Montague, P. M. & Hearing, V. J. (1992a). A second tyrosinase-related protein, TRP-2, is a melanogenic enzyme termed DOPachrome tautomerase. *Embo j*, 11 (2): 519-26.
- Tsukamoto, K., Palumbo, A., D'Ischia, M., Hearing, V. J. & Prota, G. (1992b). 5,6-Dihydroxyindole-2-carboxylic acid is incorporated in mammalian melanin. *Biochem J*, 286 (Pt 2): 491-5.
- Turan, S., Hughes, C., Atay, Z., Guran, T., Haliloglu, B., Clark, A. J., Bereket, A. & Metherell, L. A. (2012). An atypical case of familial glucocorticoid deficiency without pigmentation caused by coexistent homozygous mutations in MC2R (T152K) and MC1R (R160W). *J Clin Endocrinol Metab*, 97 (5): E771-4. doi: 10.1210/jc.2011-2414.
- Turner, W. A., Taylor, J. D. & Tchen, T. T. (1975). Melanosome formation in the goldfish: the role of multivesicular bodies. *J Ultrastruct Res*, 51 (1): 16-31.
- Tyrrell, R. M. (1995). Ultraviolet radiation and free radical damage to skin. *Biochemical Society Symposium*, 61: 47-53. doi: 10.1042/bss0610047.
- Uribe, C., Folch, H., Enriquez, R. & Moran, G. (2011). Innate and adaptive immunity in teleost fish: a review. *Veterinárni Medicina*, 56 (10): 486-503.
- Veliyulin, E., Van der Zwaag, C., Burk, W. & Erikson, U. (2005). In vivo determination of fat content in Atlantic salmon (*Salmo salar*) with a mobile NMR spectrometer. *Journal of the Science of Food and Agriculture*, 85: 1299-1304.
- Videler, J. J. (1993). Fish swimming. In Chapman & Hall (eds) *Fish and Fisheries*. London.
- Wang, Z., Dillon, J. & Gaillard, E. R. (2006). Antioxidant properties of melanin in retinal pigment epithelial cells. *Photochem Photobiol*, 82 (2): 474-9. doi: 10.1562/2005-10-21-ra-725.
- Ward, W. C. & Simon, J. D. (2007). The differing embryonic origins of retinal and uveal (iris/ciliary body and choroid) melanosomes are mirrored by their phospholipid composition. *Pigment Cell Res*, 20 (1): 61-9. doi: 10.1111/j.1600-0749.2006.00357.x.

- Wedekind, C., Meyer, P., Frischknecht, M., Niggli, U. A. & Pfander, H. (1998). Different Carotenoids and Potential Information Content of Red Coloration of Male Three-Spined Stickleback. *Journal of Chemical Ecology*, 24 (5): 787-801. doi: 10.1023/a:1022365315836.
- Wedekind, C., Jacob, A., Evanno, G., Nusslé, S. & Müller, R. (2008). Viability of brown trout embryos positively linked to melanin-based but negatively to carotenoid-based colours of their fathers. *Proceedings of the Royal Society B: Biological Sciences*, 275 (1644): 1737-1744. doi: 10.1098/rspb.2008.0072.
- Weizhi, W. (2016). *The effect of dietary antioxidants on hyperpigmented fillet spots of Atlantic salmon (Salmo salar L.)*. 1432 Ås, Norway: Norwegian University of Life Sciences (NMBU).
- Westneat, M. W., Hoese, W., Pell, C. A. & Wainwright, S. A. (1993). The horizontal septum: Mechanisms of force transfer in locomotion of scombrid fishes (Scombridae, Perciformes). *Journal of Morphology*, 217 (2): 183-204. doi: doi:10.1002/jmor.1052170207.
- Whittington, R. J., Munday, B. L., Akhlaghi, M., Reddacliff, G. L. & Carson, J. (1994). Humoral and peritoneal cell responses of rainbow trout (*Oncorhynchus mykiss*) to ovalbumin, *Vibrio anguillarum* and Freund's complete adjuvant following intraperitoneal and bath immunisation. *Fish & Shellfish Immunology*, 4 (7): 475-488. doi: <https://doi.org/10.1006/fsim.1994.1042>.
- Whyte, S. K. (2007). The innate immune response of finfish--a review of current knowledge. *Fish Shellfish Immunol*, 23 (6): 1127-51. doi: 10.1016/j.fsi.2007.06.005.
- Widlund, H. R. & Fisher, D. E. (2003). Microphthalmia-associated transcription factor: a critical regulator of pigment cell development and survival. *Oncogene*, 22: 3035. doi: 10.1038/sj.onc.1206443.
- Wilson, M. R. & Warr, G. W. (1992). Fish immunoglobulins and the genes that encode them. *Annual Review of Fish Diseases*, 2: 201-221. doi: [https://doi.org/10.1016/0959-8030\(92\)90064-5](https://doi.org/10.1016/0959-8030(92)90064-5).
- Wold, J. P., Jakobsen, T. & Krane, L. (1996). Atlantic salmon average fat content estimated by near-infrared transmittance spectroscopy. *Journal of Food Science*, 61: 74-77.
- Wolke, R. E., Murchelano, R. A., Dickstein, C. D. & George, C. J. (1985). Preliminary evaluation of the use of macrophage aggregates (MA) as fish health monitors. *Bull Environ Contam Toxicol*, 35 (2): 222-7.
- Wootton, R., Springall, D. R. & Polak, J. M. (1995). *Image Analysis in Histology: Conventional and Confocal Microscopy*: Cambridge University Press.
- Wu, Y., Shan, L., Yang, S. & Ma, A. (2008). Identification and antioxidant activity of melanin isolated from *Hypoxyylon archeri*, a companion fungus of *Tremella fuciformis*. *J Basic Microbiol*, 48 (3): 217-21. doi: 10.1002/jobm.200700366.
- Xu, H. G., Zhao, M., Zheng, K. K., Wei, Y. L., Yan, L. & Liang, M. Q. (2017). Antarctic krill (*Euphausia superba*) meal in the diets improved the reproductive performance of tongue sole (*Cynoglossus semilaevis*) broodstock. *Aquaculture Nutrition*, 23 (6): 1287-1295. doi: doi:10.1111/anu.12503.
- Yamaguchi, Y., Brenner, M. & Hearing, V. J. (2007). The regulation of skin pigmentation. *J Biol Chem*, 282 (38): 27557-61. doi: 10.1074/jbc.R700026200.
- Zapata, A., Diez, B., Cejalvo, T., Gutierrez-de Frias, C. & Cortes, A. (2006). Ontogeny of the immune system of fish. *Fish Shellfish Immunol*, 20 (2): 126-36. doi: 10.1016/j.fsi.2004.09.005.

- Zhang, Y. A., Salinas, I., Li, J., Parra, D., Bjork, S., Xu, Z., LaPatra, S. E., Bartholomew, J. & Sunyer, J. O. (2010). IgT, a primitive immunoglobulin class specialized in mucosal immunity. *Nat Immunol*, 11 (9): 827-35. doi: 10.1038/ni.1913.
- Zuasti, A., Jara, J. R., Ferrer, C. & Solano, F. (1989). Occurrence of melanin granules and melanosynthesis in the kidney of *Sparus auratus*. *Pigment Cell Res*, 2 (2): 93-9.
- Zuasti, A., Ferrer, C., Aroca, P. & Solano, F. (1990). Distribution of Extracutaneous Melanin Pigment in *Sparus auratus*, *Mugil cephalus*, and *Dicertranchus labrax* (Pisces, Teleostei). *Pigment Cell Research*, 3 (3): 126-131. doi: doi:10.1111/j.1600-0749.1990.tb00276.x.

9 APPENDICES

9.1 Appendix A

Correlation table for general slaughtering and image data number from dorsal selections (DS) and quarter A parameters of all fish groups: D0, DL, and DH.

	General L* value DS	General L* value	General a* value	General b* value	Super-dark area (%)	Super-dark L* value	Super-dark a* value	Visual dot number	Approximated dot number	Dot circularity ¹	Total darkest area (%)
General L* value DS	1 89	0.73933 <0.0001 89	0.31425 0.0027 89	0.32787 0.0017 89	-0.51617 <0.0001 89	0.39913 0.0001 89	0.28384 0.0070 89	-0.11853 0.2686 89	-0.43148 <0.0001 89	-0.22674 0.0630 68	-0.58090 <0.0001 89
General L* value	0.73933 <0.0001 89	1 89	0.17573 0.0995 89	0.26349 0.0126 89	-0.64067 <0.0001 89	0.44007 <0.0001 89	0.07848 0.4648 89	-0.16276 0.1275 89	-0.59459 <0.0001 89	-0.00157 0.9899 68	-0.78439 <0.0001 89
General a* value	0.31425 0.0027 89	0.17573 0.0995 89	1 89	0.35094 0.0007 89	0.02522 0.8145 89	0.01149 0.9149 89	0.47989 <0.0001 89	0.28822 0.0062 89	0.11370 0.2887 89	0.05370 0.6636 68	-0.06162 0.5662 89
General b* value	0.32787 0.0017 89	0.26349 0.0126 89	0.35094 0.0007 89	1 89	-0.00208 0.9846 89	0.11038 0.3031 89	0.15291 0.1526 89	0.23550 0.0263 89	-0.00187 0.9861 89	0.09729 0.4299 68	-0.08172 0.4464 89
Super-dark area (%)	-0.51617 <0.0001 89	-0.64067 <0.0001 89	0.02522 0.8145 89	-0.00208 0.9846 89	1 89	-0.66883 <0.0001 89	-0.13156 0.2191 89	0.52125 <0.0001 89	0.80157 <0.0001 89	0.15881 0.1958 68	0.84136 <0.0001 89
Super-dark L* value	0.39913 0.0001 89	0.44007 <0.0001 89	0.01149 0.9149 89	0.11038 0.3031 89	-0.66883 <0.0001 89	1 89	-0.10951 0.3070 89	-0.19998 0.0602 89	-0.48781 <0.0001 89	-0.33606 0.0051 68	-0.47658 <0.0001 89
Super-dark a* value	0.28384 0.0070 89	0.07848 0.4648 89	0.47989 <0.0001 89	0.15291 0.1526 89	-0.13156 0.2191 89	-0.10951 0.3070 89	1 89	0.14830 0.1655 89	0.01258 0.9069 89	-0.00231 0.9851 68	-0.24542 0.0204 89
Visual dot number	-0.11853 0.2686 89	-0.16276 0.1275 89	0.28822 0.0062 89	0.23550 0.0263 89	0.52125 <0.0001 89	-0.19998 0.0602 89	0.14830 0.1655 89	1 89	0.61793 <0.0001 89	0.26670 0.0279 68	0.22068 0.0377 89
Approximated dot number	-0.43148 <0.0001 89	-0.59459 <0.0001 89	0.11370 0.2887 89	-0.00187 0.9861 89	0.80157 <0.0001 89	-0.48781 <0.0001 89	0.01258 0.9069 89	0.61793 <0.0001 89	1 89	0.04300 0.7277 68	0.69643 <0.0001 89
Dot circularity ¹	-0.22674 0.0630 68	-0.00157 0.9899 68	0.05370 0.6636 68	0.09729 0.4299 68	0.15881 0.1958 68	-0.33606 0.0051 68	-0.00231 0.9851 68	0.26670 0.0279 68	0.04300 0.7277 68	1 68	-0.00573 0.9630 68
Total darkest area (%)	-0.58090 <0.0001 89	-0.78439 <0.0001 89	-0.06162 0.5662 89	-0.08172 0.4464 89	0.84136 <0.0001 89	-0.47658 <0.0001 89	-0.24542 0.0204 89	0.22068 0.0377 89	0.69643 <0.0001 89	-0.00573 0.9630 68	1 89

Those parameters belonging to DS are indicated. Top, middle and bottom position in every square represent the Pearson correlation coefficient (r), P-value (P≤0.05) and the total number of observations respectively. Green colors show 0.0001<P≤0.05, while red P<0.0001.

$$^1 \text{Circularity} = \frac{4*\pi*Area}{(Perimeter)^2}$$

9.2 Appendix B

Correlation table for discoloration parameters from ventral selections of all fish groups: D0, DL, and DH.

	General L* value	General b* value	Light discolored pixels area (%)	Super-light red discolored pixels area (%)	Dark discolored pixels area (%)	Low-dark discolored pixels area (%)	Medium-dark discolored pixels area (%)	Medium-dark discolored pixels b* value	Visual discoloration length (%)	Dark discolored pixels length (%)	Dark discolored pixels circularity ¹	Dark discolored pixels aspect ratio ²
General L* value	1 90	-0.50164 <0.0001 90	-0.56567 <0.0001 90	-0.33850 0.0011 90	-0.37409 0.0003 90	-0.36593 0.0004 90	-0.27700 0.0082 90	-0.44968 0.1425 12	-0.36265 0.0004 90	-0.42166 0.0025 49	0.12462 0.3936 49	-0.02853 0.8457 49
General b* value	-0.50164 <0.0001 90	1 90	-0.12068 0.2572 90	0.12781 0.2299 90	-0.18843 0.0753 90	-0.20073 0.0578 90	-0.0447 0.6757 90	0.2315 0.4691 12	-0.20222 0.0560 90	-0.37361 0.0082 49	-0.194346 0.1809 49	0.18955 0.1921 49
Light discolored pixels area (%)	-0.56567 <0.0001 90	-0.12068 0.2572 90	1 90	0.00888 0.9338 90	0.69114 <0.0001 90	0.70312 <0.0001 90	0.35529 0.0006 90	0.61224 0.0343 12	0.72891 <0.0001 90	0.83112 <0.0001 49	-0.01187 0.9355 49	-0.11253 0.4414 49
Super-light red discolored pixels area (%)	-0.33850 0.0011 90	0.12781 0.2299 90	0.00888 0.9338 90	1 90	-0.01121 0.9165 90	-0.02234 0.8344 90	0.05746 0.5906 90	-0.22362 0.4848 12	0.15881 0.1349 90	-0.05932 0.6856 49	-0.32146 0.0243 49	0.26031 0.0709 49
Dark discolored pixels area (%)	-0.37409 0.0003 90	-0.18843 0.0753 90	0.69114 <0.0001 90	-0.01121 0.9165 90	1 90	0.99158 <0.0001 90	0.66297 <0.0001 90	0.34354 0.2743 12	0.67281 <0.0001 90	0.83958 <0.0001 49	0.22175 0.12568 49	-0.20784 0.15185 49
Low-dark discolored pixels area (%)	-0.36593 0.0004 90	-0.20073 0.0578 90	0.70312 <0.0001 90	-0.02234 0.8344 90	0.99158 <0.0001 90	1 90	0.56044 <0.0001 90	0.39833 0.1997 12	0.684 <0.0001 90	0.85557 <0.0001 49	0.22340 0.1228 49	-0.21325 0.1412 49
Medium-dark discolored pixels area (%)	-0.277 0.0082 90	-0.0447 0.6757 90	0.35529 0.0006 90	0.05746 0.5906 90	0.66297 <0.0001 90	0.56044 <0.0001 90	1 90	-0.00778 0.9809 12	0.34862 0.0008 90	0.42502 0.0023 49	0.12633 0.3871 49	-0.09729 0.5060 49
Medium-dark discolored pixels b* value	-0.44968 0.1425 12	0.2315 0.4691 12	0.61224 0.0343 12	-0.22362 0.4848 12	0.34354 0.2743 12	0.39833 0.1997 12	-0.00778 0.9809 12	1 12	0.38497 0.2166 12	0.43387 0.1588 12	0.15076 0.6400 12	-0.18484 0.5652 12
Visual discoloration length (%)	-0.36265 0.0004 90	-0.20222 0.0560 90	0.72891 <0.0001 90	0.15881 0.1349 90	0.67281 <0.0001 90	0.684 <0.0001 90	0.34862 0.0008 90	0.38497 0.2166 12	1 90	0.79197 <0.0001 49	-0.04911 0.7375 49	-0.15314 0.2935 49
Dark discolored pixels length (%)	-0.42166 0.0025 49	-0.37361 0.0082 49	0.83112 <0.0001 49	-0.05932 0.6856 49	0.83958 <0.0001 49	0.85557 <0.0001 49	0.42502 0.0023 49	0.43387 0.1588 12	0.79197 <0.0001 49	1 49	-0.03914 0.7895 49	-0.06595 0.6526 49
Dark discolored pixels circularity ¹	0.12462 0.3936 49	-0.19435 0.1809 49	-0.01187 0.9355 49	-0.32146 0.0243 49	0.22175 0.1257 49	0.2234 0.1228 49	0.12633 0.3871 49	0.15076 0.6400 12	-0.04911 0.7375 49	-0.03914 0.7895 49	1 49	-0.7337 <0.0001 49
Dark discolored pixels aspect ratio ²	-0.02853 0.8457 49	0.18955 0.1921 49	-0.11253 0.4414 49	0.26031 0.0709 49	-0.20784 0.1518 49	-0.21325 0.1412 49	-0.09729 0.5060 49	-0.18484 0.5652 12	-0.15314 0.2935 49	-0.06595 0.6526 49	-0.7337 <0.0001 49	1 49

Top, middle and bottom position in every square represent the Pearson correlation coefficient (r), P-value (P≤0.05) and the total number of observations respectively. Green colors show 0.0001<P≤0.05, while red P<0.0001.

$$^1 \text{Circularity} = \frac{4 \cdot \pi \cdot \text{Area}}{(\text{Perimeter})^2}$$

$$^2 \text{Aspect ratio} = \frac{\text{Major axis}}{\text{Minor axis}}$$

9.3 Appendix C

Global correlation table for the *in vivo* experiment. Most important slaughter, skin and muscle parameters of all fish groups: D0, DL, and DH, are compared.

	Quarter A general L* value	Quarter A general a* value	Quarter A general b* value	Visual dot number	Ventral selection general L* value	Ventral selection general a* value	Ventral selection general b* value	Light discolored pixels area (%)	Super-light red discolored pixels area (%)	Dark discolored pixels area (%)	Visual discoloration length (%)
Quarter A general L* value	1 0.0995 89	0.17573 0.0995 89	0.26349 0.0126 89	-0.16276 0.1275 89	0.09594 0.3711 89	0.10802 0.3137 89	0.04528 0.6735 89	-0.19943 0.0610 89	-0.03293 0.7593 89	-0.07876 0.4632 89	-0.22608 0.0331 89
Quarter A general a* value	0.17573 0.0995 89	1 0.0007 89	0.35094 0.0007 89	0.28822 0.0062 89	-0.04059 0.7057 89	0.14803 0.1662 89	0.10431 0.3307 89	-0.01962 0.8552 89	-0.03611 0.7369 89	-0.00155 0.9885 89	-0.01757 0.8701 89
Quarter A general b* value	0.26349 0.0126 89	0.35094 0.0007 89	1 0.0263 89	0.23550 0.0263 89	-0.16917 0.1130 89	0.15993 0.1344 89	0.21174 0.0464 89	-0.00339 0.9748 89	0.12149 0.2567 89	-0.04984 0.6428 89	-0.07018 0.5134 89
Visual dot number	-0.16276 0.1275 89	0.28822 0.0062 89	0.23550 0.0263 89	1 0.0263 89	-0.05830 0.5873 89	-0.00876 0.9351 89	-0.09967 0.3527 89	0.16865 0.1141 89	0.00266 0.9802 89	0.10714 0.3176 89	0.25164 0.0174 89
Ventral selection general L* value	0.09594 0.3711 89	-0.04059 0.7057 89	-0.16917 0.1130 89	-0.05830 0.5873 89	1 0.90	-0.60255 <0.0001 90	-0.50164 <0.0001 90	-0.56567 <0.0001 90	-0.33850 0.0011 90	-0.37409 0.0003 90	-0.36265 0.0004 90
Ventral selection general a* value	0.10802 0.3137 89	0.14803 0.1662 89	0.15993 0.1344 89	-0.00876 0.9351 89	-0.60255 <0.0001 90	1 0.90	0.84008 <0.0001 90	-0.04267 0.6897 90	0.45123 <0.0001 90	-0.14978 0.1588 90	-0.13241 0.2135 90
Ventral selection general b* value	0.04528 0.6735 89	0.10431 0.3307 89	0.21174 0.0464 89	-0.09967 0.3527 89	-0.50164 <0.0001 90	0.84008 <0.0001 90	1 0.90	-0.12068 0.2572 90	0.12781 0.2299 90	-0.18843 0.0753 90	-0.20222 0.0560 90
Light discolored pixels area (%)	-0.19943 0.0610 89	-0.01962 0.8552 89	-0.00339 0.9748 89	0.16865 0.1141 89	-0.56567 <0.0001 90	-0.04267 0.6897 90	-0.12068 0.2572 90	1 0.90	0.00888 0.9338 90	0.69114 <0.0001 90	0.72891 <0.0001 90
Super-light red discolored pixels area (%)	-0.03293 0.7593 89	-0.03611 0.7369 89	0.12149 0.2567 89	0.00266 0.9802 89	-0.33850 0.0011 90	0.45123 <0.0001 90	0.12781 0.2299 90	0.00888 0.9338 90	1 0.90	-0.01121 0.9165 90	0.15881 0.1349 90
Dark discolored pixels area (%)	-0.07876 0.4632 89	-0.00155 0.9885 89	-0.04984 0.6428 89	0.10714 0.3176 89	-0.37409 0.0003 90	-0.14978 0.1588 90	-0.18843 0.0753 90	0.69114 <0.0001 90	-0.01121 0.9165 90	1 0.90	0.67281 <0.0001 90
Visual discoloration length (%)	-0.22608 0.0331 89	-0.01757 0.8701 89	-0.07018 0.5134 89	0.25164 0.0174 89	-0.36265 0.0004 90	-0.13241 0.2135 90	-0.20222 0.0560 90	0.72891 <0.0001 90	0.15881 0.1349 90	0.67281 <0.0001 90	1 0.90

Top, middle and bottom position in every square represent the Pearson correlation coefficient (r), P-value (P≤0.05) and the total number of observations respectively. Green colors show 0.0001<P≤0.05, while red P<0.0001.

9.4 Appendix D

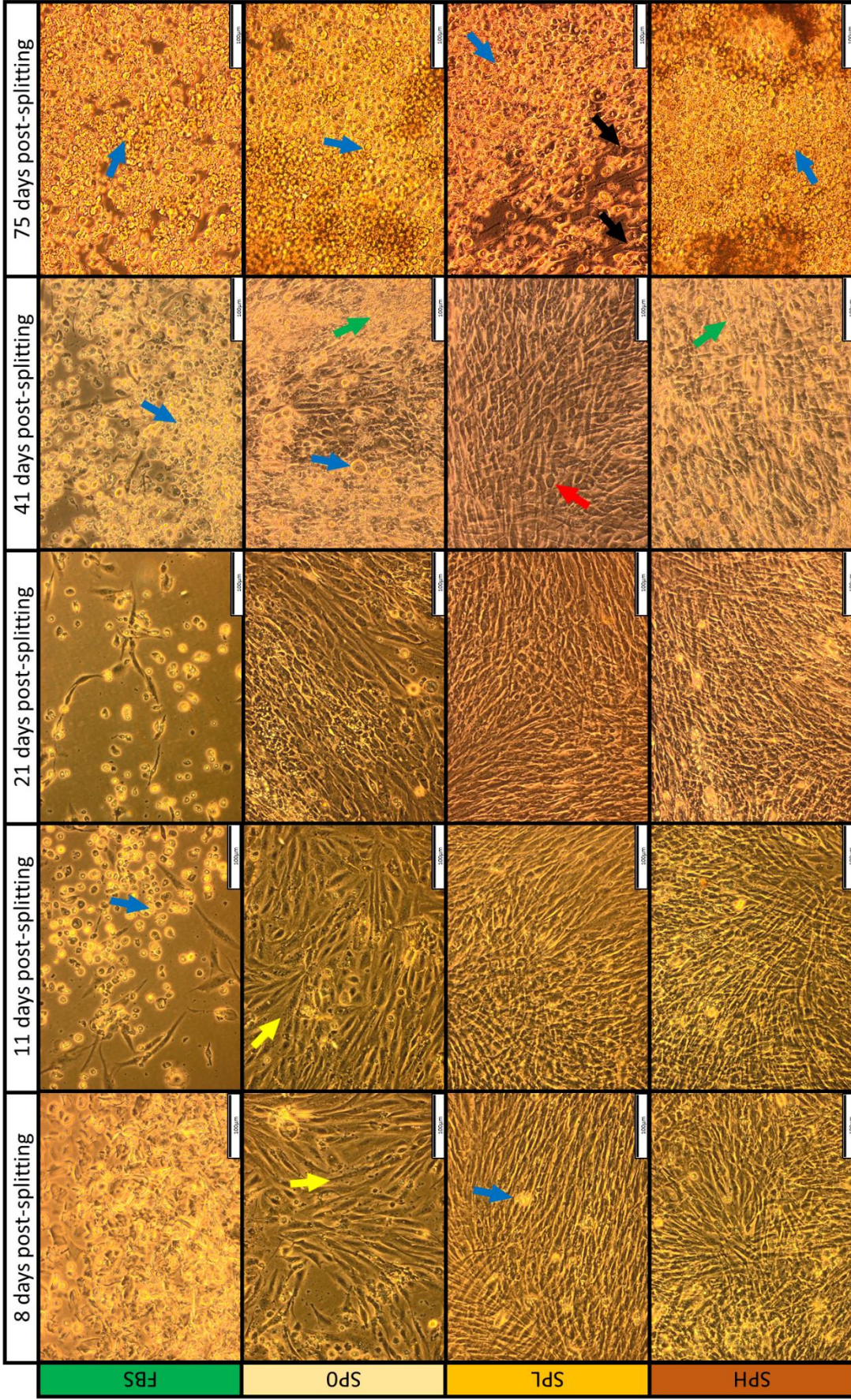


Illustration of FBS (fetal bovine plasma), SP0, SPL and SPH plasma effects in SHK-I cells at 8, 11, 21, 41 and 75 days post-splitting.

Yellow arrows indicate melanosomes, red abnormal cell shape, green overgrown cell shape, blue flouting dead-cell material, and black surviving cells. Pictures are taken by an inverted microscope at 10x magnification. The scale box represents 100µm.